MICROCOPY RESOLUTION TEST CHART
NATIONAL BUREAU OF STANDARDS-1963-A

SRI International

November 4, 1982

Final Report

STUDY OF METASTABLE RARE GAS COLLISIONS WITH MOLECULES

By: Keith T. Gillen

Approved:

*Donald C. Lorents*

Donald C. Lorents, Director
Molecular Physics Laboratory

George R. Abrahamson
Vice President
Physical Sciences Division

DTIC
ELECTE
DEC 16 1982

A

333 Ravenswood Ave. • Menlo Park, CA 94025
(415) 859-6200 • TWX: 910-373-2046 • Telex: 334 486

82 12 16 091

| REPORT DOCUMENTATION PAGE | | READ INSTRUCTIONS BEFORE COMPLETING FORM |
|---|---|---|
| 1. REPORT NUMBER | 2. GOVT ACCESSION NO. AD-A122 544 | 3. RECIPIENT'S CATALOG NUMBER |
| 4. TITLE (and Subtitle) Metastable Rare Gas Collisions with Molecules | | 5. TYPE OF REPORT & PERIOD COVERED FINAL REPORT JULY 1976 - AUGUST 1982 |
| | | 6. PERFORMING ORG. REPORT NUMBER MP 82-133 |
| 7. AUTHOR(s) Keith T. Gillen | | 8. CONTRACT OR GRANT NUMBER(s) N00014-76-C-0734 |
| 9. PERFORMING ORGANIZATION NAME AND ADDRESS SRI International 333 Ravenswood Avenue Menlo Park, CA 94025 | | 10. PROGRAM ELEMENT, PROJECT, TASK AREA & WORK UNIT NUMBERS |
| 11. CONTROLLING OFFICE NAME AND ADDRESS Office of Naval Research 800 N. Quincy Street Arlington, VA 22217 | | 12. REPORT DATE November 4, 1982 |
| | | 13. NUMBER OF PAGES 81 Pages |
| 14. MONITORING AGENCY NAME & ADDRESS(if different from Controlling Office) | | 15. SECURITY CLASS. (of this report) Unclassified |
| | | 15a. DECLASSIFICATION/DOWNGRADING SCHEDULE |

16. DISTRIBUTION STATEMENT (of this Report)

Approved for public release; distribution unlimited

17. DISTRIBUTION STATEMENT (of the abstract entered in Block 20, if different from Report)

18. SUPPLEMENTARY NOTES

19. KEY WORDS (Continue on reverse side if necessary and identify by block number)

Metastable rare gas collisions; metastable helium; excited atom collisions; metastable argon; excited state collisions; ion-pair formation; inelastic scattering; collisional excitation; Penning ionization; rainbow scattering.

20. ABSTRACT (Continue on reverse side if necessary and identify by block number)

This report summarizes an experimental and computer-modeling investigation of reactive and inelastic scattering of fast metastable rare gas atoms [He$^*$ ($2^1$S), He$^*$ ($2^3$S), and Ar$^*$] by O$_2$ and I$_2$ target molecules. Similarities to (and difference from) analogous alkali atom interactions with halogen and oxygen molecules were probed. Processes investigated and characterized included ion-pair formation, ion-pair mediated vibrational excitation, and Penning ionization. Coincidence techniques were developed that allowed the first double-differential cross section measurements of a Penning process in a triatomic system.

DD FORM 1473 EDITION OF 1 NOV 68 IS OBSOLETE
1 JAN 73

# CONTENTS

APPENDICES

1

# INTRODUCTION

Our primary objective in this research program was to use experimental atomic beam scattering techniques on carefully selected systems to increase our understanding of the detailed collisional processes occurring in three-body (atomic plus diatomic) systems involving multiple electronic states with many competing product channels. We have used a sophisticated atomic beam scattering apparatus[1] to study and characterize various important reactive and inelastic channels in collision systems that are complex enough to challenge the most advanced experimental and theoretical techniques available. By systematically varying the projectile, the target molecule, the collision energy, and the process investigated, we have been exploring a wide variety of interactions, searching for insight into the competition between various reaction pathways in relatively complex systems.

Earlier work on two different classes of problems had laid a foundation on which to build our efforts. First, numerous molecular beam experiments[2] at energies near thermal, accompanied by theoretical studies ranging from classical trajectory calculations to quantum close-coupling techniques, had provided a great deal of insight into both reactive and nonreactive collisions of an atom with a diatomic molecule in the special (and important) case where the predominant interactions were confined to a single electronic potential energy surface. Second, a large body of knowledge[3] had been acquired, both experimentally and theoretically, regarding electronic excitation processes, energy transfer, and ionization in colliding systems composed of two atoms (or

an atomic ion and an atom) where two or more electronic states were involved. Systems that combined these two features (three or more atoms and multiple, competing product electronic states) had received little attention.

Although many complex triatomic systems are amenable to detailed investigation, most would yield results so complicated as to be completely intractable. Only a carefully selected set of reactions could be expected to yield any true insight into the processes occurring on multiple and competing potential energy surfaces. When our work began, the greatest success[4] in characterizing a complex triatomic system had been achieved for the interaction of fast alkali atoms (M) with halogen molecules ($X_2$). A detailed examination of ion-pair formation in this group of reactions had produced a generally clear picture of the dynamic properties important for describing the interaction on the two relevant intersecting electronic surfaces.

We intended to build on this work by choosing systems (rare gas metastable atoms, $R_g^*$, colliding with halogen molecule targets) that had analogous ion-pair formation channels as well as a competing set of processes. One major competing process in these systems, Penning ionization, involved an ionization continuum; such continua had not been studied in any great detail, and they were a challenging research frontier both experimentally and theoretically.

Initially, we investigated[5] ion-pair formation in $Ar^* + I_2$ collisions and searched for similarities and differences in ion-pair formation relative to analogous $M + X_2$ systems. The similarities were striking and suggested a very strong analogy in ion-pair formation for $M + X_2$ and $R_g^* + X_2$ systems. The differences[6] were minor and yielded little insight into the interesting continuum channel.

The direction of our work then changed, as we began to examine systems ($R_g^*$ + $O_2$ in particular) and product channels where competition from continuum processes was expected to be more easily observed. We worked closely with Professor Joop Los and Dr. Aart Kleyn (at the FOM Institute in Amsterdam), who were simultaneously investigating M + $O_2$ collisions. In these systems, we observed[7] some fascinating consequences of the rapid (subpicosecond) vibrational motion of the trasient $O_2^-$ ion formed at the instant of ion-pair formation. Again, the $R_g^*$ and M projectiles gave very similar ion-pair formation and inelastic scattering results. There were no obvious modifications of these channels in $R_g^*$ + $O_2$ caused by the competing continuum processes.

It became apparent that the continuum channel, even when it was the dominant inelastic process, was not easy to observe indirectly through its effects on the product distributions for other channels.

The last major goal of our work, therefore, was to develop a method for examining the continuum processes directly. To do this, we developed and tested a delayed coincidence technique that allows for the separation of Penning processes from other inelastic and elastic scattering events. First results for $He^*(2^3S)$ + $O_2$ are presented here.

The collision systems we have studied are typical of collisional interactions important in a wide area of gas phase physics (e.g., discharges, lasers, excited atmospheres) that require improved characterization and understanding. As more detailed reaction rate information is generated and understood for a few relatively simple and carefully chosen model systems, comparison and extrapolation should yield increasing insight into the mechanisms important in the most general cases.

# RESULTS

### $\underline{Ar^* + I_2}$

At collision energies above several eV, the interaction of a rare gas metastable $(R_g^*)$ with halogen target molecules $(X_2)$ has an important reaction channel, ion-pair formation,

$$R_g^* + X_2 \rightarrow R_g^+ + X_2^- \text{ (or } X + X^-). \tag{1}$$
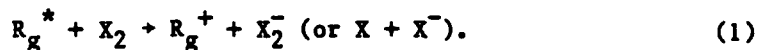
This channel results from an electron jump occurring at the surface crossing between the relatively flat incoming covalent potential surface and an (asymptotically higher) attractive coulombic $R_g^+ + X_2^-$ surface that cuts through the initial covalent state at intermediate or large internuclear separation. A similar channel, involving analogous surfaces, is important in collisions involving alkali atoms M with the same targets,

$$M + X_2 \rightarrow M^+ + X_2^-. \tag{2}$$

For alkali projectiles, this surface crossing dominates the reaction dynamics and initiates the prototype harpooning chemical reaction long studied at thermal energies[8]

$$M + X_2 \rightarrow M^+ + X_2^- \rightarrow M^+X^- + X. \tag{3}$$
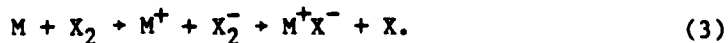
The second step rapidly follows the initial electron jump because the strong ionic $M^+X^-$ bond can form at the expense of dissociating the much weaker transiently formed $X_2^-$ bond. Even at higher energies,[4] when the projectile's velocity precludes new bond formation, the single-surface crossing continues to dominate the dynamics, and the major inelastic channel evolves to ion-pair formation.

Similarities in electronic configuration, ionization potentials, and reaction properties of M and $R_g^*$ have often been noted.[9] The alkali analogy is a useful one, at least as a first approximation, for understanding both the ion-pair formation [reaction (1)] and certain collisional excitation channels for $R_g^* + X_2$ collisions. This analogy is an important starting point because the $M + X_2$ reactions have been studied experimentally in great detail and because the existing theoretical models for alkali reactions can be used to predict the corresponding $R_g^*$ interactions.

However, the differences between the two systems are also fascinating. Most significant is the large $R_g^*$ excitation energy. If this energy is larger than the ionization energy of $X_2$, the Penning ionization reaction

$$R_g^* + X_2 \rightarrow R_g + X_2^+ + e^-$$
(4)
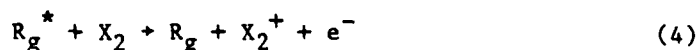
can occur. In this case the original covalent $R_g^* + X_2$ potential surface and the interacting $R_g^+ + X_2^-$ surface are imbedded in an ionization continuum that can deplete intensity from the two alkali-like surfaces during the collision. This extra channel and the manner in which it modifies and competes with ion-pair formation add an extra dimension to the $R_g^* + X_2$ systems.

Our original investigation of ion-pair formation in $Ar^* + I_2$ was initiated with the expectation of testing the alkali analogy and probing for possible effects caused by the ion-pair formation process occurring completely within an ionization continuum. In the original publication (Appendix A) supported by this contract, we showed[5] the striking overall similarity between the ion-pair formation differential cross sections for the reactions

$$Ar^* + I_2 \rightarrow Ar^+ + I_2^- \tag{5}$$

and

$$K + I_2 \rightarrow K^+ + I_2^- \tag{6}$$

at center-of-mass energies of $\sim$ 25-130 eV. This similarity occurred despite both the competing Penning channel [reaction (1) of Appendix A] and the fact that the inner-shell vacancy in the $Ar^*$ projectile implied multiple sets of interacting covalent and ion-pair surfaces in contrast to the single surface crossing in the alkali interaction. We explain this result with reference to the very large $Ar-I_2$ distance at which the electron transfer occurs. As noted in Appendix A, the ion-pair cross section is so large that the most important contributions occur at impact parameters much larger than those that would be expected for a Penning process. Also, at the large surface crossing distances important to ion-pair formation, the core electron vacancy should have only a very minor effect on the potential shapes and surface coupling matrix elements; deviations from alkali-like properties should only occur at smaller distances where core overlap becomes significant (see Appendix B).

6

More quantitative comparisons, with appraisals of the effects on the distributions of reaction (5) caused by the competing Penning ionization and excitation transfer channels, were initially hampered by the lack of a computational model. A simple classical trajectory, surface-hopping model had been used previously by Los and coworkers[10] to treat ion-pair formation in reaction (2). We modified and extended their model to include the effects of depletion by a competing continuum channel. Our calculations[6] treated the continuum process as an absorption width that was assumed to be important only along the original covalent surface, not the ion-pair surface. The calculations demonstrated the small differences between reactions (5) and (6), as well as the most reasonable explanations for the observed differences. This work is summarized in Appendix B.

The overriding utility of the alkali analogy cannot be overemphasized, because the results for one reaction ($Ar^* + I_2$) led us to conclude that the essential features of the ion-pair formation product distributions in all $R_g^* + X_2$ systems can be predicted from comparisons with suitably chosen $M + X_2$ data. Since a large body of systematic data already exist for $M + X_2$ interactions, our conclusion vastly expands the impact of the work on $Ar^* + I_2$. The extrapolation to other $R_g^* + X_2$ systems was consistent with our general desire to achieve predictive insight from studying carefully chosen representative triatomic systems. It also induced us to direct our subsequent effort into collision systems with somewhat different properties, especially those with ion-pair formation cross sections that are not so dominant relative to other processes.

Before turning to other systems, we should comment on the structure observed (see Figure 1 of Appendix A) in the angular distribution for reaction (5). At high energies, two peaks are evident. The "ionic" peak at large

angles is a rainbow feature derived from trajectories that transfer to the strongly attractive coulombic (ionic) surface as the incoming system first crosses the intersection region (see Figure 2 of Appendix A). The smaller angle "covalent" peak contains trajectories that remain on the covalent surface until they become ion-pairs on the second (outward) crossing of the two surfaces.

At lower energies, the dominant ionic rainbow peak develops additional structure, a shoulder on its bright (low-angle) side. In many other recent measurements of ion-pair formation differential cross sections, a similar shoulder appears on the bright side of the main ionic rainbow peak. Although this feature also appears in trajectory calculations on these systems, its essential cause defied explanation until we derived an analytical description of the differential cross section for a very simple model two-state system. The derivation, an explanation, and a sample calculation for the Na + I system are given[11] in Appendix C.

## $Ar^* + O_2$ Ion-Pair Formation

The large vertical electron affinity ($EA_v$) of the $I_2$ molecule (and other halogens) is the major cause of the large ion-pair cross section because the asymptotic energy separation between the covalent and coulombic surfaces is

$$\Delta E = IP - EA_v \qquad (7)$$

and the surfaces cross at a distance

$$R_c = 1/\Delta E, \qquad (8)$$

where IP is the ionization potential of the projectile and Eq. (8) is in atomic units; $R_c$ is 10.6 a.u. for $Ar^* + I_2$. Significantly smaller crossing distances would imply smaller ion-pair formation cross sections. Oxygen molecules have a much smaller electron affinity than $I_2$ and, therefore, yield much smaller ion-pair cross sections in collisions with M or $R_g^*$. Hence competing processes might be expected to have more pronounced effects on the observed distributions.

We have, therefore, investigated ion-pair formation in the $Ar^* + O_2$ system,

$$Ar^* + O_2 \rightarrow Ar^+ + O_2^-. \tag{9}$$
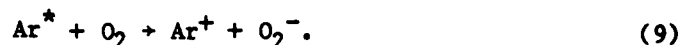
Differential cross section measurements for this reaction are given in Figure 1. Our efforts on this system were closely coordinated with simultaneous measurements of ion-pair formation in the analogous reaction

$$K + O_2 \rightarrow K^+ + O_2^- \tag{10}$$

by Kleyn et al.[12] at FOM. Additional data on reaction (10) were obtained by Young et al.[13] at Argonne. The available data for reaction (10) are shown in Figure 2.

The excitation energy of $Ar^*$ is slightly lower than the ionization energy of $O_2$. Hence the continuum $Ar + O_2^+ + e^-$ is asymptotically slightly above our incoming channel (see Figure 3). However, we still expected a large cross section for excitation transfer to the near-resonant Rydberg states of $O_2$,

$$Ar^* + O_2 \rightarrow Ar + O_2^{**}, \tag{11}$$

9
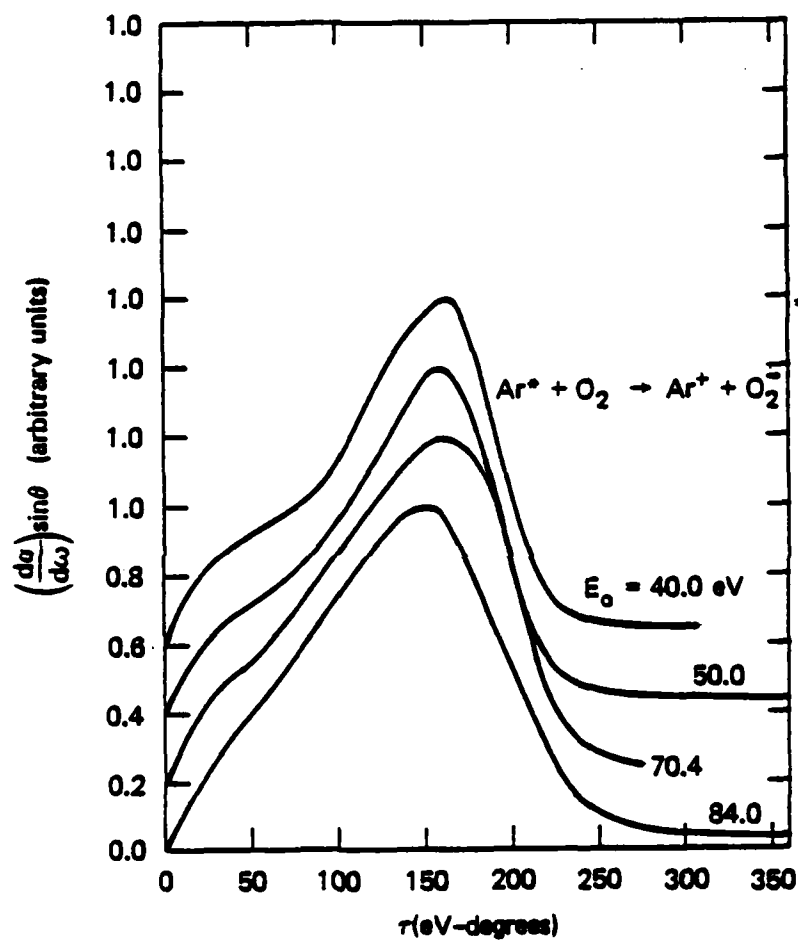
Figure 1. Experimental Ar* + O₂ ion-pair formation differential cross section data from our laboratory. Each curve is labeled with the energy ($E_o$) of the Ar* beam.

10
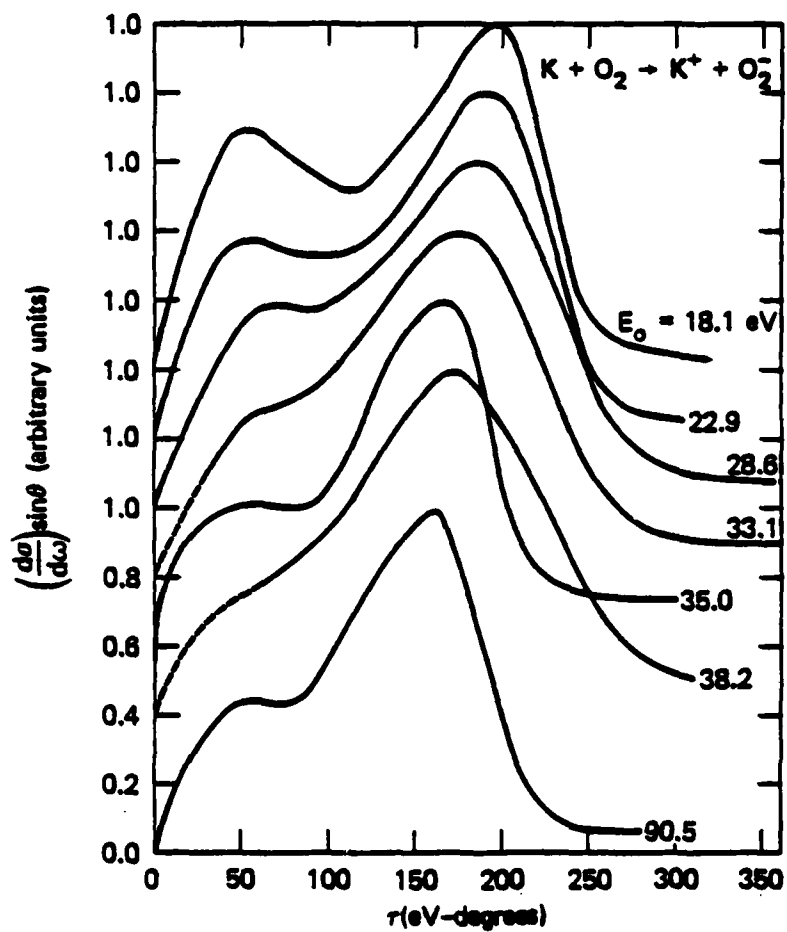
Figure 2. Experimental K + $O_2$ ion-pair formation differential cross section data from FOM ($E_o$ = 35.0 and 90.5 eV) and Argonne (all others).
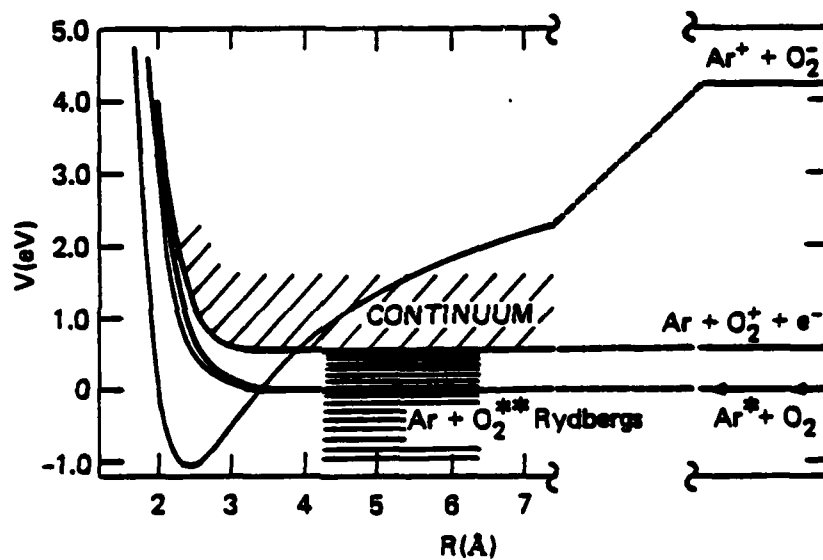
11

Figure 3. Schematic $Ar^* + O_2$ potentials plotted vs. the $Ar^*-O_2$ separation. The incoming $Ar^* + O_2$ surface is imbedded in a Rydberg series converging on $Ar + O_2^+ + e^-$.

a pseudo-continuum process, as discussed by Miller and Morgner.[14]  In fact, we have used attenuation techniques to show that reaction (9) is less than 3.)% of the measured total (20-25 $A^2$) destruction cross section for $Ar^*$ in collisions with $O_2$.

Recently, using approximate formulas of Miller and Morgner,[14] we have estimated the pseudo-continuum coupling due to reaction (11) and have completed a classical trajectory study of the pair of reactions (9) and (10). Although the estimated cross section for reaction (11) ($\sim$ 15-20 $A^2$) is substantially larger than the cross sections (5-7 $A^2$) for reactions (9) and (10), it surprisingly causes only a small difference in the shape of the calculated differential cross section.  Since the differences in shape between our $Ar^* + O_2$ data (e.g., Figure 1, 40 eV) and the $K + O_2$ data are less than the differences between the FOM data[12] (e.g., Figure 2, 35 eV) and the Argonne data[13] (e.g., Figure 2, 38.2 eV), one could hardly expect to extract any information on the pseudo-continuum reaction from a comparison of Figures 1 and 2, and the trajectory calculations indeed confirm this observation.  Once again, the ion-pair formation process in $Ar^* + O_2$ is not significantly different from expectations based on an analogy to alkali systems.  A manuscript detailing this work will be prepared.


## Vibrational Timing in Transient $O_2^-$

The importance of the ion-pair surface is not, however, limited to reactions involving ion-pair formation.  In fact, the ion-pair surface can act as a transient intermediate that profoundly affects inelastic scattering as well (both vibrationally and electronically).[7]  Since the equilibrium bond length

13

of $O_2^-$ is larger than that of $O_2$, the electron transfer from $Ar^*$ to $O_2$ at the surface crossing generates an initially compressed $O_2^-$ (see Figure 4) that then expands and begins to vibrate as the collision evolves.

For $Ar^* + O_2$ collisions in the energy range that we investigate, the vibrational period of the transient $O_2^-$ ion, formed after the initial (incoming) transfer to the ion-pair surface, is comparable to the collision time. The path chosen by the system at the second (outgoing) crossing of the ionic and covalent surfaces will depend profoundly on the state of the transiently formed $O_2^-$ ion at the instant of that second crossing. This is because the vertical electron affinity $EA_v$ changes dramatically with $O_2^-$ bond length (see Figure 4), and $EA_v$ determines the crossing distance [from Eqs. (7) and (8)] on the outgoing trajectory, which in turn profoundly alters the matrix element coupling the two interacting surfaces.

Appendix D explains these effects in more detail, while describing[15] the first observations of large internal excitation of neutral products mediated by $O_2^-$ expansion on a transiently formed ion-pair surface. Similar results have also been reported[16] for alkali-oxygen collisions.

Our efforts in the past few years have convinced us that these previously neglected transient timing effects, caused by bond expansions and vibrations in fleeting collision intermediates, should be important to the dynamics of many other collision systems. Appendix E reviews[7] the considerable range of observations on transiently formed $O_2^-$ and mentions results for several other systems. Of particular note is the process of covalent reneutralization[17] (see Figures 7 and 8 of Appendix E), where expansion of a transiently formed $I_2^-$ induces a third surface crossing and reneutralization of $Ar^+ + I_2^-$ in the $Ar^* + I_2$ collision.
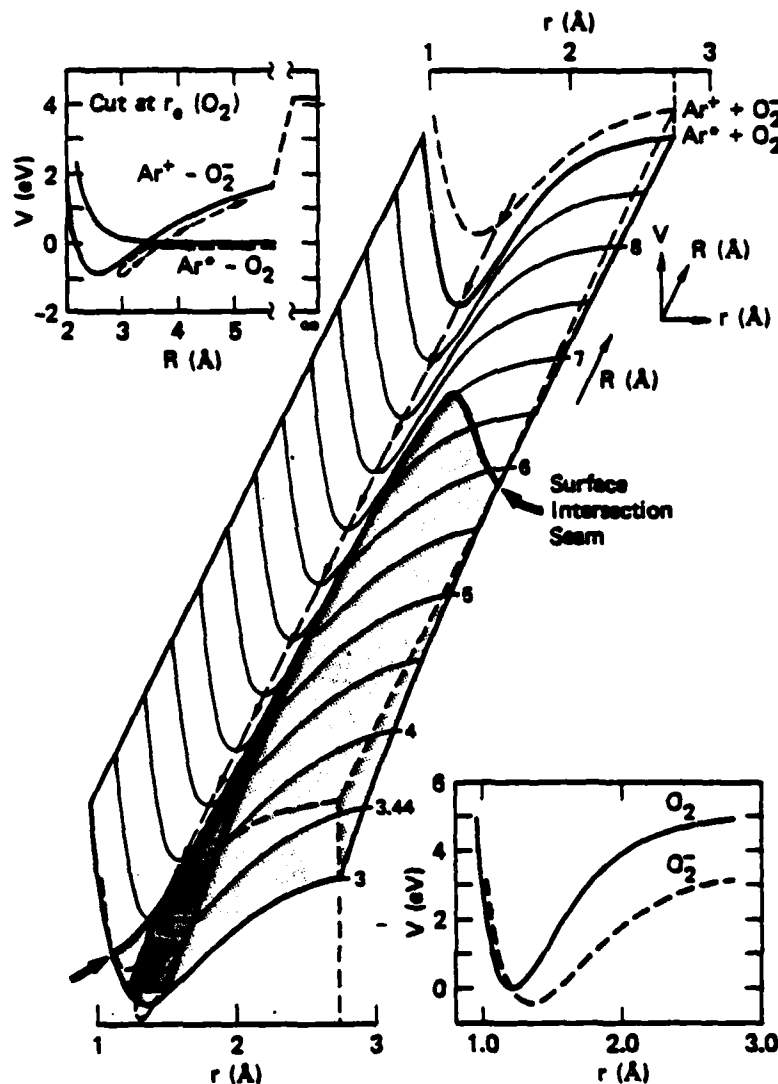
Figure 4. Schematic representation of the $Ar^* + O_2$ potential surface intersecting the coulombic $Ar^+ + O_2^-$ surface: Only the lower surface is shown [covalent at large $Ar-O_2$ separation R, coulombic (shaded) at small R], although dashed lines partially outline the upper surface. A dashed trajectory is shown entering along the valley from top right to bottom left (at fixed O-O separation r), crossing the surface intersection seam, then expanding in the r direction and vibrating as it heads back to large R and a second seam crossing. The upper insert is a cut through the surface at $r = r_e$ $(O_2)$, showing an ionic trajectory to ion-pair products. The lower insert shows, the $O_2$ and $O_2^-$ potential curves; the vertical energy separation between the curves $(EA_v)$ depends strongly on r.

## Orientational Rainbows

For $Ar^* + I_2$ collisions we have noted that the peak at larger angles in the angular distribution for ion-pair formation is a rainbow associated with "ionic trajectories" that travel along the coulombic surface inside $R_c$. The second peak at lower angles is dominated by contributions from the alternative "covalent trajectories." Surprisingly, the $K + O_2$ and $Ar^* + O_2$ trajectory calculations indicate a very large contribution to the low angle peak from ionic trajectories. An example is shown in Figure 5, in which the calculated differential cross section is partitioned into its contributions from the two possible paths to ion-pair products. The new and unusual feature is associated with "ionic" trajectories having impact parameters slightly smaller than those responsible for the principal rainbow peak, where in the analogous atom-atom case, there is a zero in the deflection function (with attractive and repulsive forces just balancing). For these trajectories in the atom-molecule case, the attractive and repulsive forces are nearly balanced, but in general the orientation of the target molecule removes the balance and produces a deflection function[18] with a (non-zero) minimum deflection angle.

Figure 6 shows calculated deflection functions for $Ar^* + O_2$ collisions for two molecular orientations. In each case, the dashed portion and the solid portion are the covalent branch and the ionic branch of the deflection function, respectively. For the light curves (a special case), the deflection functions go through zero at the transition from attractive (large b) to repulsive (smaller b) interactions. In the more general orientation (heavy curves), there is a minimum in the deflection function; we have named this minimum the orientational rainbow (OR). Even after averaging over all orientations, the calculations yield a peak in the ion-pair formation
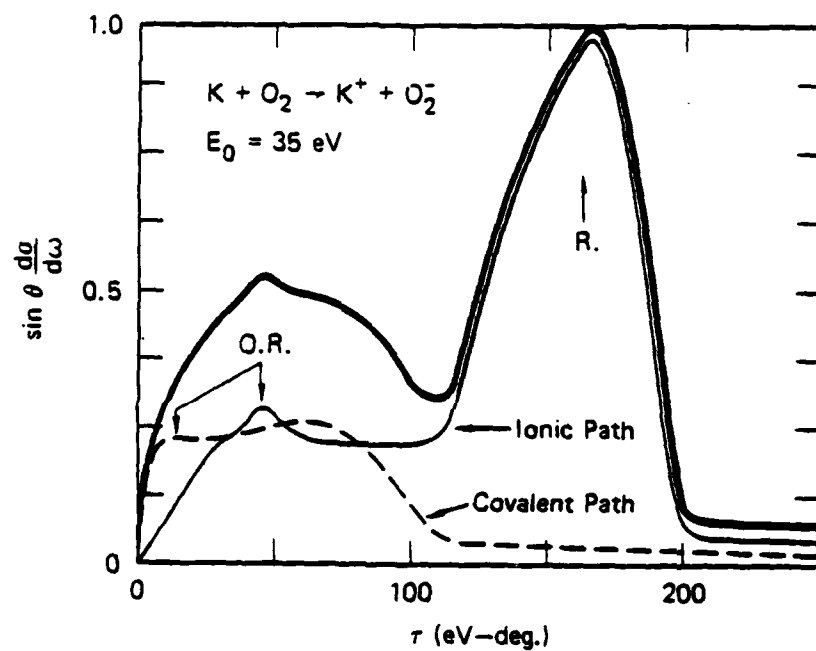
Figure 5. Calculated ion-pair formation differential cross sections for K + $O_2$ at $E_0 = 35$ eV. Shown also are the separated contribution for the ionic and covalent paths. The main rainbow is marked R; the orientational rainbows are denoted OR.
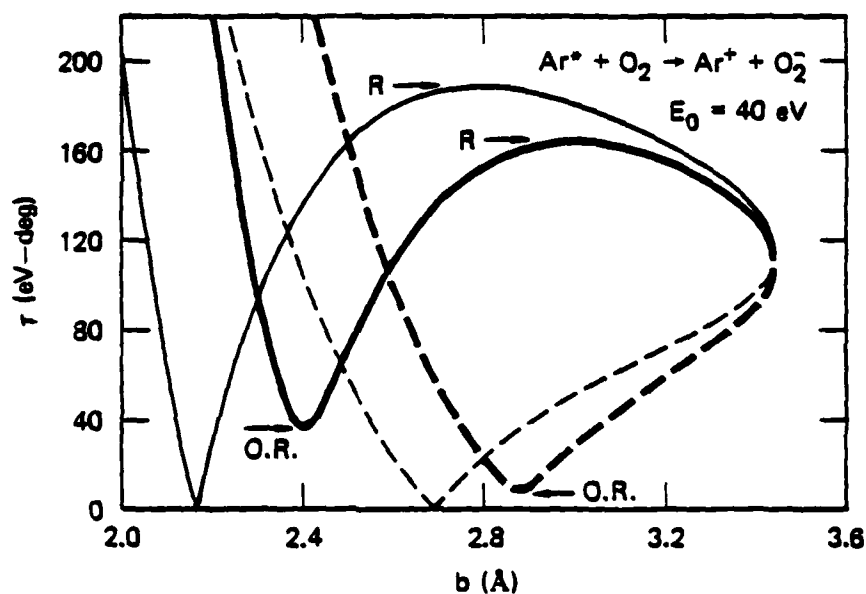
Figure 6. Calculated deflection functions for ion-pair formation in $Ar^* + O_2$ assuming two different orientations of the $O_2$ target. The covalent branch of each curve is dashed. R indicates the classical rainbow, and OR locates the two orientational rainbows observed for one of the $O_2$ orientations.

cross section consistent with this effect.  In fact, a second orientational
rainbow, associated with the covalent path, is also indicated by Figures 5 and
6.

Our trajectory calculations for ion-pair formation in $K + O_2$ and $\cdot\ ^* + O_2$
yield another surprising and interesting result:  a strong energy dependence
in the ratio of the two major peaks in the differential cross section for ion-
pair production.  As the collision energy is lowered, there is a dramatic jump
in the relative intensity of the low angle peak.  This jump is caused by a
rapid increase in the ionic orientational rainbow peak and can be understood
by examining a vibrational timing diagram (Figure 7, cf. discussion of Figure
4 in Appendix D).

The impact parameters contributing to the orientational rainbow are
confined to a small range between $\sim$ 2.3 and 2.6 A.  At high energies (e.g., 90
eV), the ionic trajectories reach the second surface crossing after less than
a single $O_2^-$ vibration, and the compressed $O_2^-$ of relatively small electron
affinity yields a significant reneutralization and concomitant loss of the
ions contributing to the OR feature.  As the energy is lowered, these
trajectories evolve more slowly relative to the $O_2^-$ vibrational period; at low
enough energies (e.g., 40 eV for b = 2.5 A in Figure 7), the $O_2^-$ goes through
more than one vibration before the second surface crossing.  The crossing then
occurs with an expanded $O_2^-$ of large $EA_v$, and a much larger fraction of the
initial ion-pairs pass through the crossing without reneutralizing.

Figure 8 shows the calculated ion-pair peak ratios for $Ar^* + O_2$ and
$K + O_2$ over a beam energy range from 30 eV to 90 eV.  Also shown in Figure 8
are the comparable data for $K + O_2$ (Figure 2) and $Ar^* + O_2$ (Figure 1) over a
slightly larger energy range.  There is evidently a very good qualitative
correspondence between the data and the calculation.  The slight shift in the

19
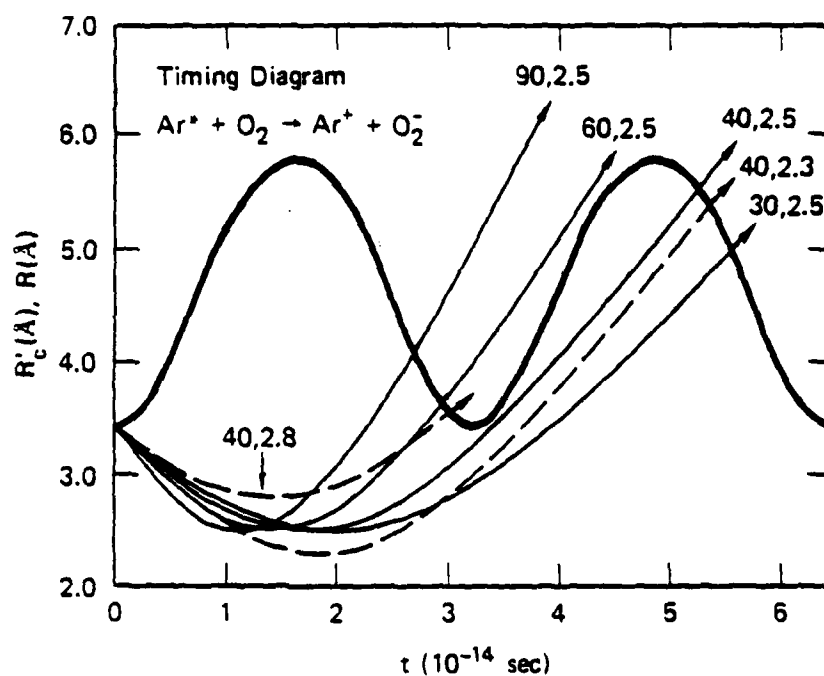
Figure 7. Timing diagram for $Ar^* + O_2$. The zero of the time scale represents the instant of $O_2^-$ formation as the incoming system crosses to the ionic surface. At this instant, the $O_2^-$ begins vibrating, causing synchronous oscillations in the vertical electron affinity and the crossing distance $R_c'$; $R_c'(t)$ is shown by the heavy periodic curve. The light curves, marked first by their energies (in eV) and second by their impact parameters (in A), show various illustrative trajectories by plotting the $Ar^+-O_2^-$ distance, $R(t)$.

20
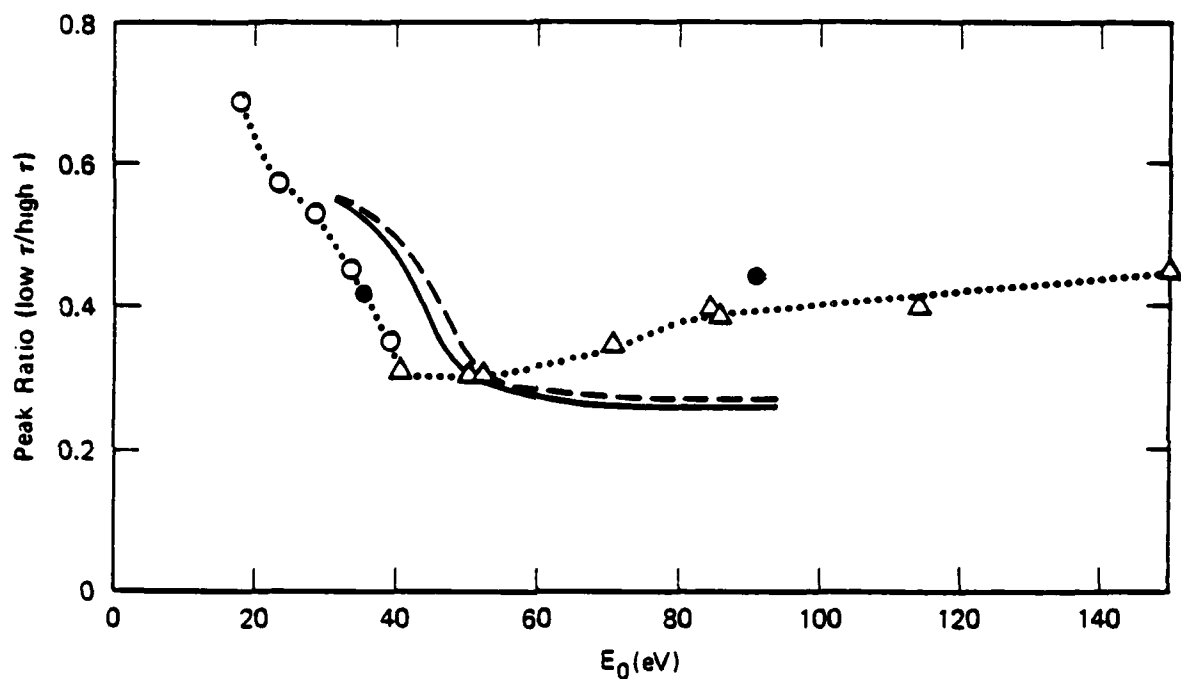
Figure 8. dσ/dω sinθ peak ratios: low angle (covalent) region/ionic rainbow region plotted vs. beam energy.

Solid line: $K + O_2$ calculations

Dashed line: $Ar^* + O_2$ calculations, no continuum depletion

Triangles: $Ar^* + O_2$ data

Open circles: $K + O_2$ data (Argonne)

Closed circles: $K + O_2$ data (FCM).

critical transition energy indicates that the $O_2^-$ vibrational motion may be delayed or slowed[19] in the field of the positive ion relative to the motion expected for an isolated $O_2^-$.

The unusual effect shown by Figure 8 had not been observed previously and, although complicated, can be described in a purely classical framework. This process is an energy-dependent, vibrationally clocked, orientationally derived, rainbow feature in an electronically inelastic transition, and it represents a coupling of electronic, vibrational, rotational, and translational motions! Recent trajectory calculations by G. Parlant (unpublished) on more realistic potential energy surfaces have confirmed our observations, which are being prepared for publication.

## $He^* + O_2$

Appendix F describes[20] our development of a modification of neutralization-reionization spectroscopy that allowed simultaneous and independent measurements of differential cross sections for the ion-pair formation reactions of the two metastable states of He with $O_2$,

$$He^*(2^1S) + O_2 \rightarrow He^+ + O_2^- \tag{12}$$

and

$$He^*(2^3S) + O_2 \rightarrow He^+ + O_2^-. \tag{13}$$
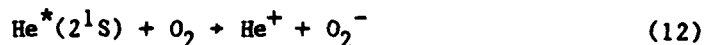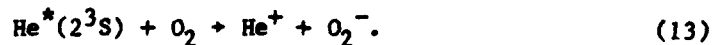
Charge transfer of $He^+$ in Rb y.e. ied a mixture of the two metastables; the $He^*(2^1S)$ formed directly in the charge transfer and the $He^*$ $(2^3S)$ formed

only after ~ascade from a $He^*(2^3P)$ precursor.[21]  After the subsequent ion-pair

formation, the $He^+$ from reaction (13) was lower in energy than the $He^+$ from

reaction (12) by an amount equal to that of the $He(2^3P \rightarrow 2^3S)$ transition.

Since the product energy distributions were reasonably sharp, the two reac-

tions were easily resolvable.  As a check, we placed Na in the charge transfer

cell to produce and react a beam of pure $He^*(2^3S)$.  The results[20] were in

excellent agreement with the distributions for reaction (13) obtained using Rb

charge transfer vapor.

Figure 9 shows time-of-flight measurement of the $He^*$ beam produced by Rb

and by Na charge transfer.  Figure 10 shows representative $He^+$ product energy

distributions at various laboratory scattering angles for a mixed beam of

$He^*(2^3S)$ and $He^*(2^1S)$ formed in Rb.  In each spectrum, the peak at lower

energy is from reaction (13).

The measured differential cross sections for the two ion-pair formation

reactions are shown over a large energy range in Figures 11 and 12.  An expla-

nation for the observed structure and the remarkable differences between the

two reactions is given in Appendix F.  The $He^*(2^1S) + O_2$ reaction shows strong

evidence for trajectories that couple three potential surfaces in a single

trajectory leading to ion-pair products.  These trajectories (hdfdc in Figure

3 of Appendix F) were also the first observed collisions in which three

separate elect.on jumps could be inferred.

Attempts to model these reactions with classical trajectory calculations

required an extension of the program to include three coupled states.  Figures

13 and 14 compare the resulting calculations with experimental differential

cross section data at a beam energy of 70 eV.  The results are only qualita-

tively comparable.  Since the matrix elements coupling the surfaces are

comparable in size to the splitting between the two incoming covalent surfaces
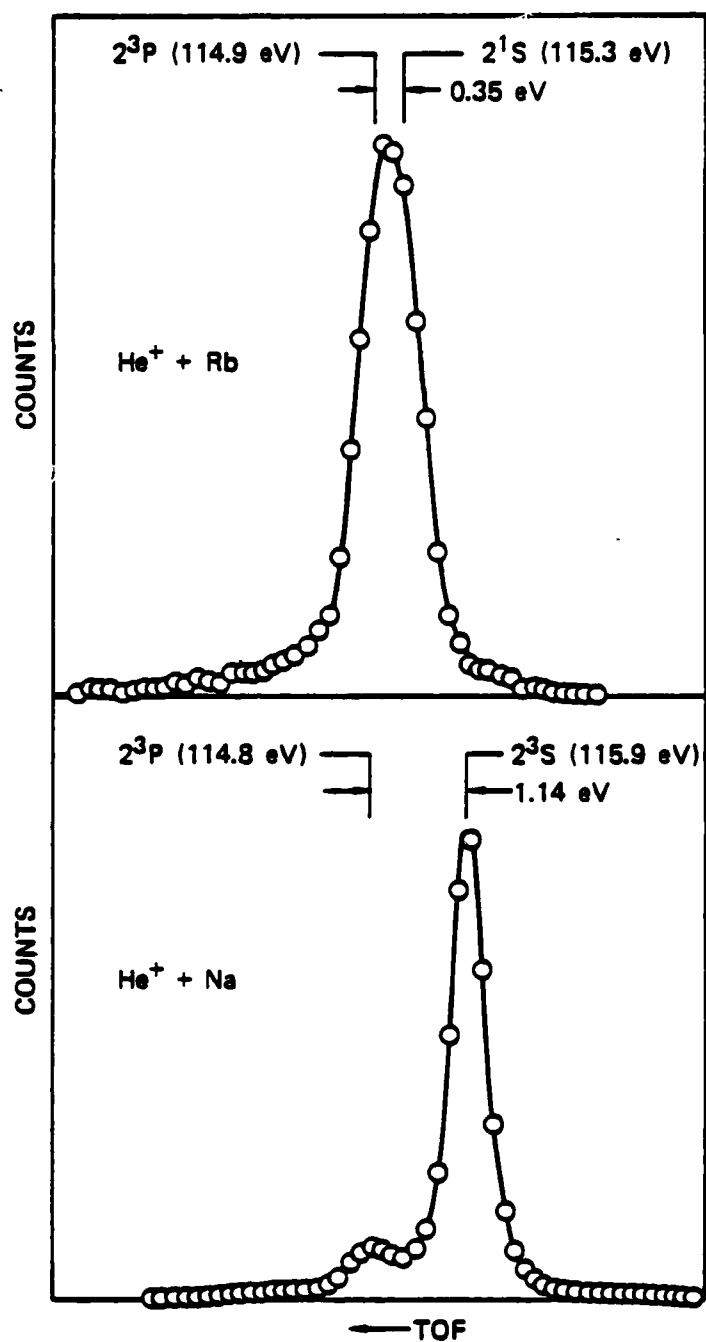
Figure 9. Time-of-flight measurements of He* beam composition from He+ charge transfer in Rb and Na. The two states in Rb are not resolved here, but have been in M. Barat's laboratory.
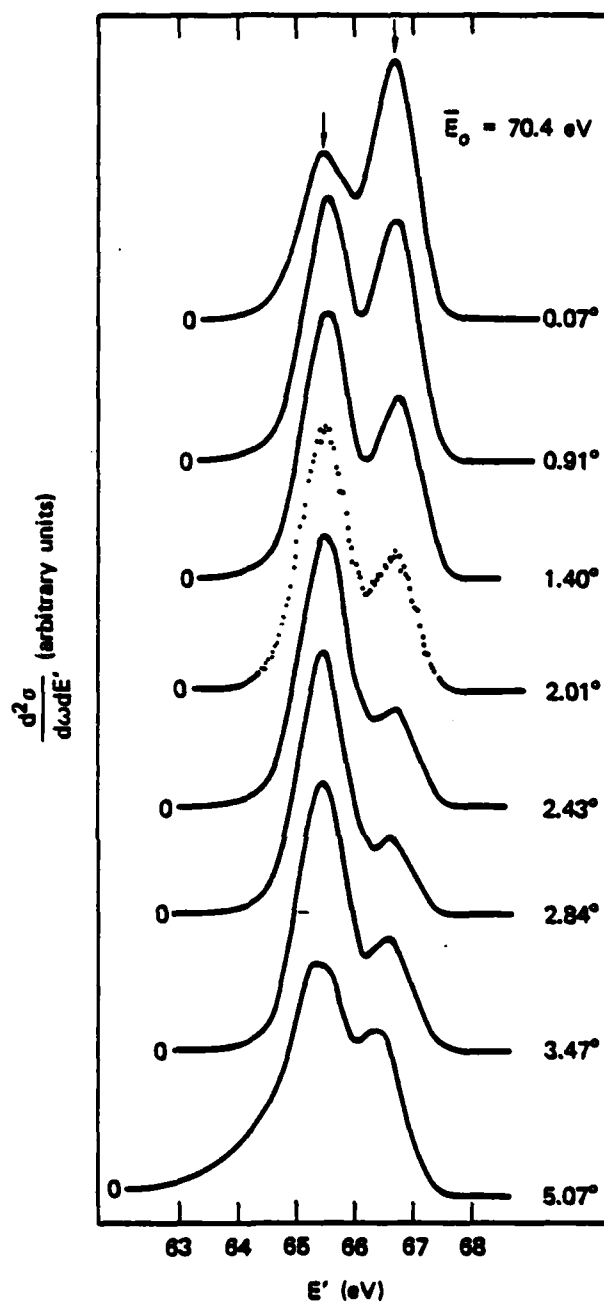
Figure 10. Ion-pair formation double differential cross sections for He* + O₂
collisions at a beam energy of 70.6 eV (2¹S state) and 70.2 eV (2³S
state). At each laboratory scattering angle (marked at right of
each spectrum), the lower energy peak is from reaction (13), the
higher peak from reaction (12). Spectra are all normalized to the
same intensity at their peaks; relative intensities can be obtained
from Figures 13 and 14.

25
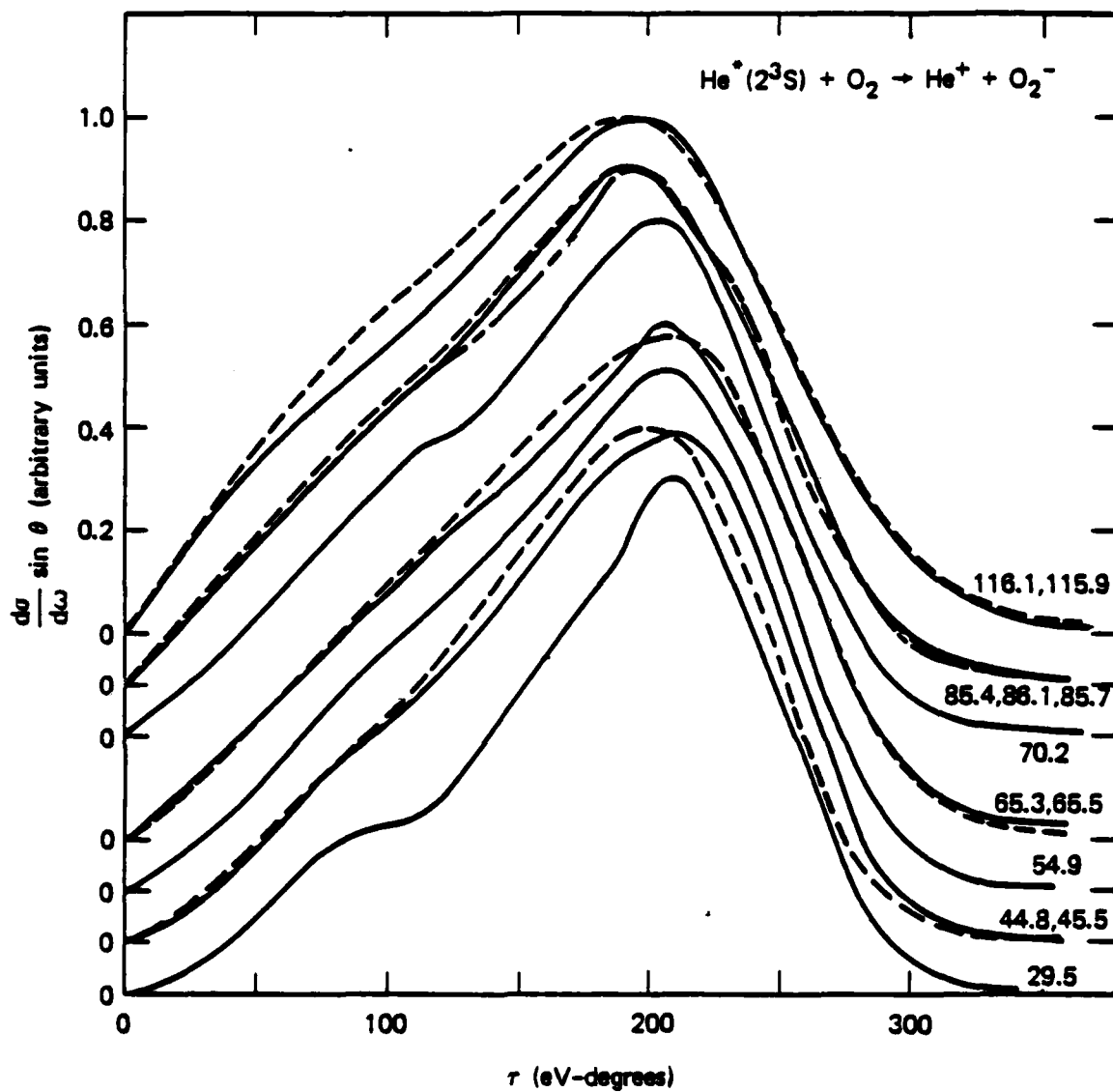
Figure 11. Differential cross section results for reaction (13) plotted vs. the reduced scattering angle $\tau$ ( $=E_o\theta$). Beam energies ($E_o$) are indicated for each curve.
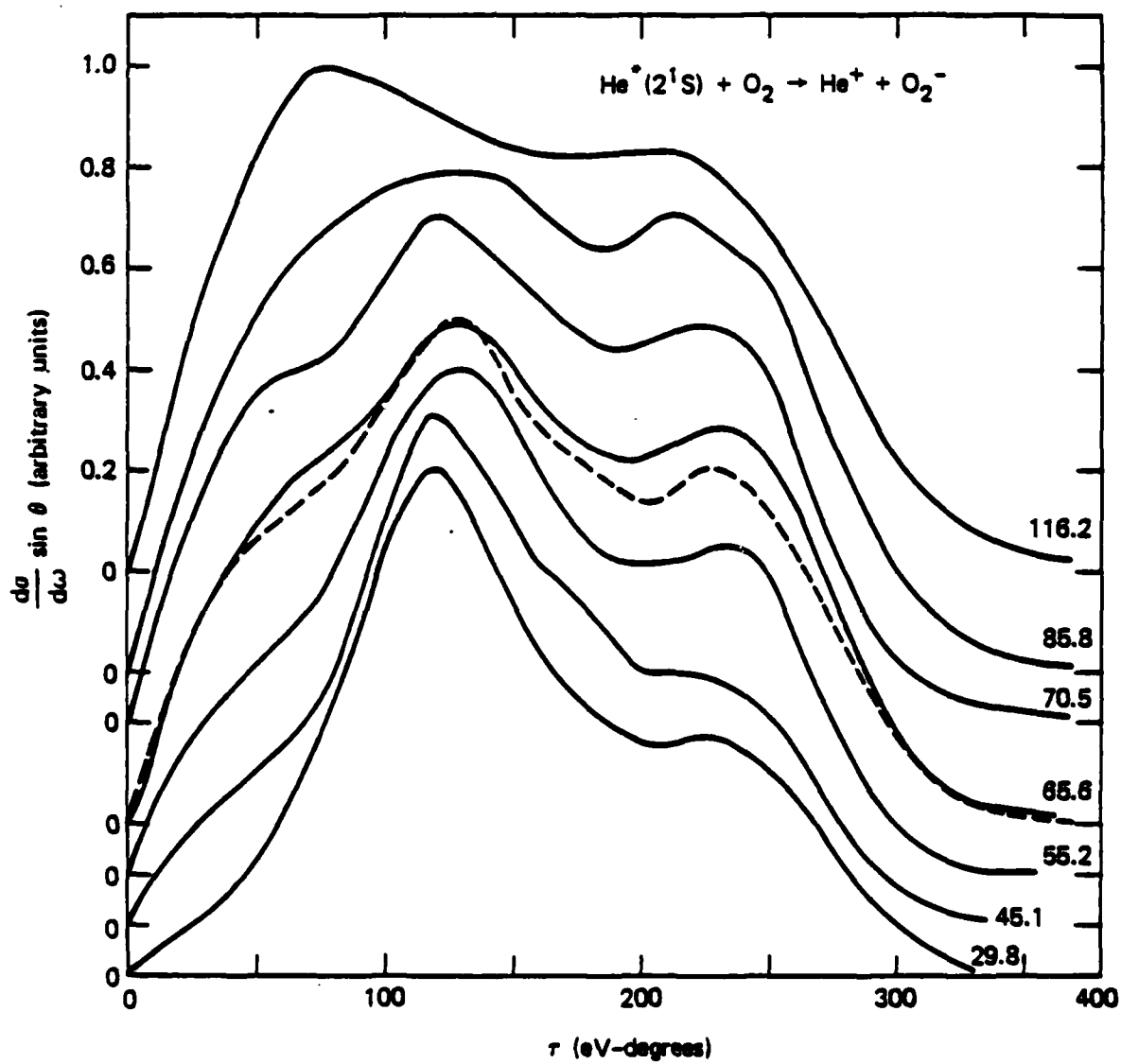
Figure 12. Data for reaction (12). See Legend for Figure 11.
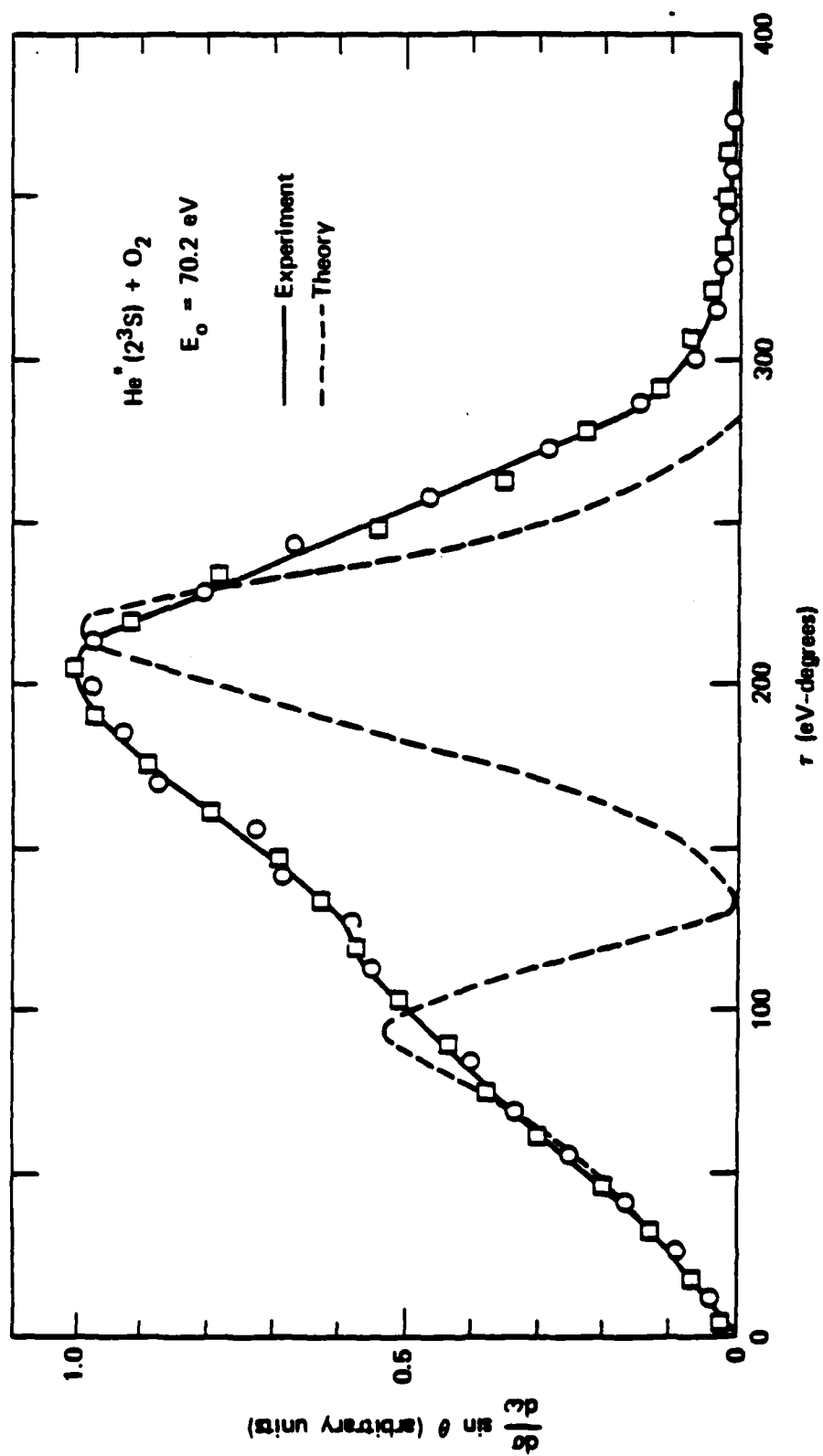
Figure 13. A comparison of calculation and experiment for reaction (13) at $E_o = 70.2$ eV.
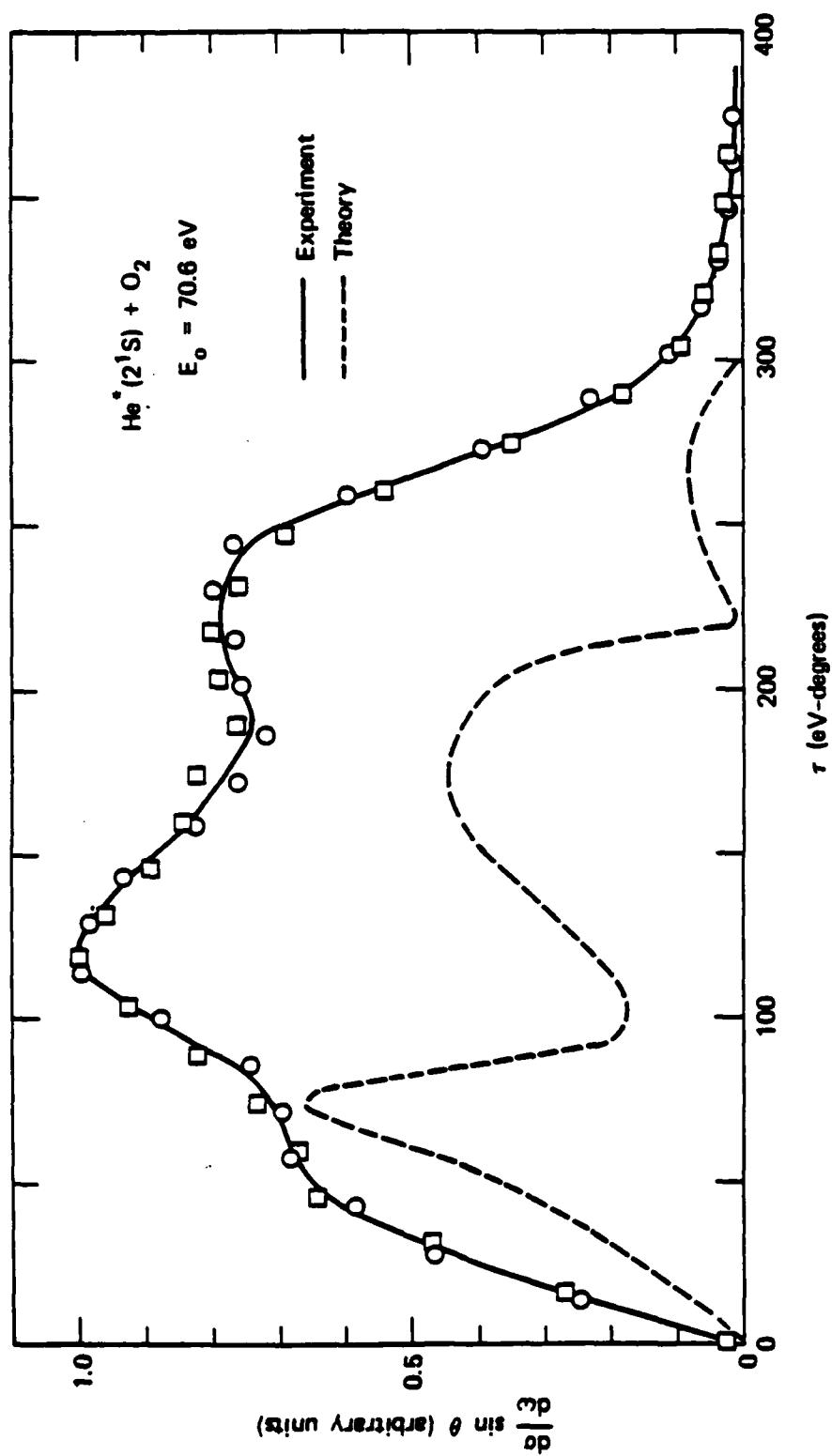
Figure 14. A comparison of calculation and experiment for reaction (12) at $E_o$ = 70.6 eV.

(shown in Figure 3 of Appendix F), our use of a calculation that assumes isolated crossings and calculates deflections using diabatic potentials is obviously inadequate. In particular, if we modified our trajectory calculations to use adiabatic potential surfaces, we anticipate that the central peak in Figure 14 would shift to significantly lower angles. If we also increased the repulsion in the various calculated potential surfaces, we could then probably achieve reasonable agreement in angular position between the calculations and the experiments.

However, the disagreement in relative peak intensities is a much more difficult problem because the individual intensities can depend strongly on their respective depletion by competing continuum channels,

$$He^* + O_2 \rightarrow He + O_2^+ + e^-. \tag{14}$$
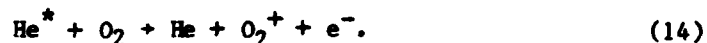
In this case, the large $He^*$ excitation energies (19.8 and 20.6 eV for the $2^3S$ and $2^1S$ states, respectively) cause the interacting discrete potential surfaces (shown schematically in Figure 3 of Appendix F) to be nearly resonant with several different $O_2^+$ electronic states in the continuum channel [Equation (14)]. This would suggest a large, perhaps dominant, role of the Penning process in these systems. In fact, comparison of our attenuation measurement of total $He^*$ destruction with our measured yields of fast positive ($He^+$) and slow positive ($O_2^+$, $O^+$) and negative ($O_2^-$, $O^-$, $e^-$) products indicates that the ion-pair channel is only $\sim 10\%$ of the total destruction cross section at collision energies near 100 eV. The Penning channel dominates in this energy range. Results at higher energies from another laboratory are in agreement with this conclusion.[22]

In addition, for a recent thermal energy investigation[23] of reaction (14), product electron energy distributions were interpreted by assuming a significant continuum depletion of reactants while they were on the ionic $He^+$ + $O_2^-$ surface. If this is true, our modeling in the trajectory calculations of the depletion by continuum processes would need separate estimates of the continuum widths for each of the three surfaces explored in the ion-pair process. Although we could attempt this by, for example, treating the continuum equivalently for all three surfaces, we find this hard to justify in light of our earlier assumption[6] in the $Ar^*$ + $I_2$ system that there was no continuum coupling from the ion-pair surface. Clearly, additional experimental information on the continuum interaction is sorely needed for any attempt to model the rich and complex $He^*$ + $O_2$ interaction.

Ion-pair formation has also been investigated briefly for the interactions of $He^*(2^3S)$ and $He^*(2^1S)$ with NO, $NO_2$, and $N_2$. The neutralization-reionization procedure appears from these reactions to be of general utility in studying $He^*(2^3S)$ and $He^*(2^1S)$ simultaneously, but separately.

The qualitative results for NO targets are similar to those for $O_2$, as was anticipated from the predicted similarities of the shapes of the interacting potential surfaces. With $N_2$ target gas, the cross section is quite small because the negative electron affinity of $N_2$ implies a very small crossing distance $R_c$ between the incoming covalent surface and the product ion-pair surface $He^+$ + $N_2^-$. In contrast, $NO_2$ has a large positive electron affinity and a very large cross section for ion-pair formation.

In analogy with $O_2$ targets, we expect that the Penning processes are more important than ion-pair formation in all of these systems. For this reason,

31

detailed investigation of ion-pair formation in these systems was abandoned in favor of an attempt to develop techniques for examining the continuum processes directly.

## Direct Continuum Channel Measurements

In this work, we have made several significant contributions to the understanding of the ion-pair formation process and the inelastic processes that involve the ion-pair surface as a transient intermediate. In contrast, the competing continuum channel (Penning ionization) has only grudgingly yielded a small amount of information.

The differential cross section comparisons between $Ar^*$ and K for $I_2$ and $O_2$ targets showed only small differences, and the calculations show that these distributions are not very sensitive to variations in the competing channels. For the $He^*$ interactions, we have demonstrated the ability to control the beam composition and investigate $He^*(2^1S)$ and $He^*(2^3S)$ interactions independently. Although this gives us the flexibility for each molecular target to investigate reactions on a coupled set of interacting potential surfaces starting from two separate and well-characterized input channels, it still does not yield any information on the Penning channel that we infer to be the dominant inelastic process.

Any attempt to measure differential cross sections for either the atomic or ionic products of the Penning reaction is hampered by a major experimental difficulty. Consider reaction (14) as an example. If we try to detect the scattered He atom product (possible at energies above ~ 100 eV where the

32

secondary electron ejection coefficient becomes reasonably large), we must contend with a very large background of elastically and inelastically scattered $He^*$,

$$He^* + O_2 \rightarrow He^* + O_2^{(*)}, \qquad (15)$$

interfering with, and probably swamping, the intended measurement. In contrast, to determine differential cross sections for the ionic product(s) that are produced with near-thermal energies, we must expend tremendous efforts in eliminating contact potentials, keeping surfaces clean and uncharged, and transporting and analyzing the products without distorting the nascent distributions. Only one group, working on thermal energy Penning reactions, has achieved any success[24] measuring the distributions of these slow ions. We have developed an alternative approach, suitable at higher energies, that separates the He from the $He^*$.

The key to our technique is the observation that the fundamental marker for the continuum process is the formation of a positive ion from the target species. Hence, if this ion can be extracted from the collision zone and counted, its appearance can be used to validate the detection of He atoms from reaction (14) and discriminate against $He^*$ from reaction (15). The two products of reaction (14) are detected in delayed coincidence on two separate detectors.

A fast $He^*(2^3S)$ beam, produced by charge transfer of $He^+$ in Na vapor, crosses a beam of $O_2$ effusing from a multicapillary array. Grids surrounding the interaction zone are used to extract slow positive product ions to a Channeltron detector near the intersection zone. A second Channeltron can be positioned at different angles around the intersection zone to detect

33

scattered fast neutral products (He and He$^*$). The signal from the first Channeltron, after amplification, starts a time-to-amplitude converter (TAC). The stop input of the TAC receives amplified pulses from the second Channeltron. If a stop pulse is received within the time window of the TAC, an output pulse (amplitude proportional to the measured time difference) from the TAC passes through an analog-to-digital converter to a multichannel analyzer (MCA) used as a pulse-height analyzer. In this way, the MCA produces a spectrum of the time-correlation of delayed coincidences between the two detectors.

Our grid geometry and acceleration techniques for extracting the slow positive ions are designed to minimize the time spread (for a given ion mass) associated with the product ion and also to compensate for the time spreads due to the variation in location of product formation across the beam intersection zone. Then the measured time differences for reaction (14) can be directly correlated with the flight times, and hence the velocities, of the coincident He atoms. He$^*$ from process (15) is not correlated in time with product ions and therefore contributes only a uniform background rate to the coincidence spectra. The very large signal (especially at small scattering angles) from elastic scattering is discriminated against by spreading it uniformly over the time axis; most of the He$^*$ does not even appear within the small TAC time windows selected by the initiating ion-detection pulse.

Figure 15 is a typical coincidence spectrum, taken directly from the MCA without analysis or smoothing, for the He$^*(2^3S)$ + $O_2$ Penning ionization reaction. The beam energy was 296 eV, and the He product was detected at a laboratory scattering angle of 1.3°. Rising above a uniform background from uncorrelated processes are two peaks identified with the Penning processes,
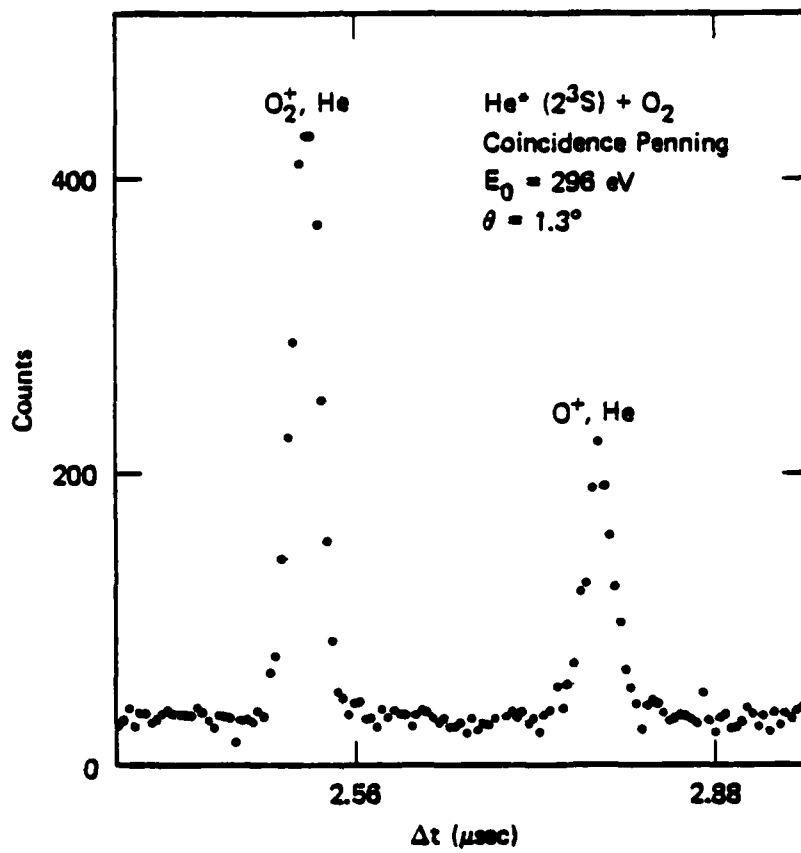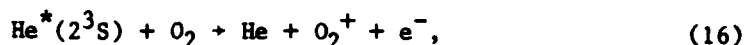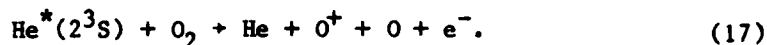
Figure 15. Experimental delayed coincidence spectrum between extracted slow positive ions and scattered fast neutrals in $He^*(2^3S) + O_2$ collisions.

$$He^*(2^3S) + O_2 \rightarrow He + O_2^+ + e^-, \qquad (16)$$

and

$$He^*(2^3S) + O_2 \rightarrow He + O^+ + O + e^-. \qquad (17)$$

The lighter $O^+$ ions, from Penning formation of dissociative or predissociated $O_2^+$ states, are extracted more rapidly than the $O_2^+$ ions and therefore imply a larger time delay before detection of correlated He atoms. It is evident from Figure 15 that we are able to adjust the extraction and timing conditions so that we can examine reactions (16) and (17) simultaneously.

Coincidence spectra for various scattering angles of the He product are given in Figure 16. The simple, single-peak, timing spectra evident at small angles for reactions (16) and (17) become more complex as the scattering angle increases. For both reactions, approximate exothermicity (0) values are indicated above the spectra. Although the main peak is nearly thermoneutral (with the electron carrying away the excess energy separating the initial and final potential surfaces), the second feature indicates an 18-20 eV conversion of translational energy either to internal energy or to an increase in the product electron energy. Very little information now exists concerning $O_2^+$ states 18-20 eV above the initial $He^*(2^3S)$ level, and no obvious explanation can be found for the importance of this peak.

Figure 17 gives reduced $\rho \left\lfloor = \theta \sin\theta \frac{d\sigma}{d\omega} \right\rfloor$ vs. $\tau \left\lfloor = \theta E_0 \right\rfloor$ plots of the angular distributions of the He atoms from reactions (16) and (17). Each point is an integral over the product velocity distribution in the time-of-flight spectrum at the appropriate angle. Clearly, the dissociative channel, reaction (17) is a significant fraction of the total Penning channel; this result is not surprising when one observes that the $He^*(2^3S)$ internal energy is greater than the energy required to dissociatively ionize $O_2$.

He* ($2^3S$) + $O_2$
Coincidence Penning
$E_0$ = 296 eV

$O_2^+$, He          $O^+$, He

Q ≈ 0     -18      0     -20

(a)     -8.1°

(b)     -6.1°

(c)     -4.8°

(d)     2.4°

$\Delta t$ ($\mu$sec) →
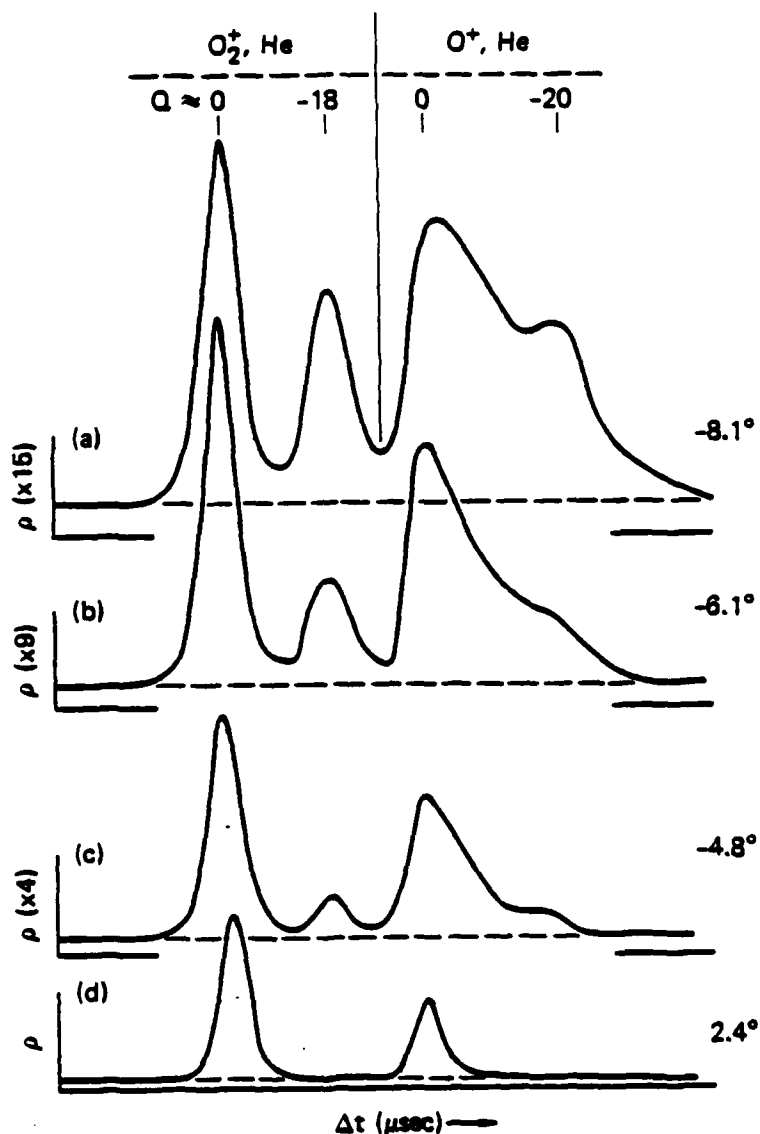
Figure 16. Experimental delayed coincidence for He*($2^3S$) + $O_2$ collisions. The vertical line dividing the spectra separates the contributions from reactions (16) and (17). Exothermicity values (Q) are indicated at the top for each reaction. The laboratory scattering angle for each spectrum is shown at the right. Approximate relative intensities are shown by the scaling factors for ρ on the left.

37

He, O₂⁺ → $He, O_2^+$

He, O⁺ + O → $He, O^+ + O$

$$He^* + O_2 \rightarrow He + O_2^+ + e^-$$
$$\rightarrow He + O^+ + O + e^-$$

$\rho$ (arbitrary units)

10

1

$10^2$

$10^3$

$\tau$ (eV—deg.)

JA-5389-5
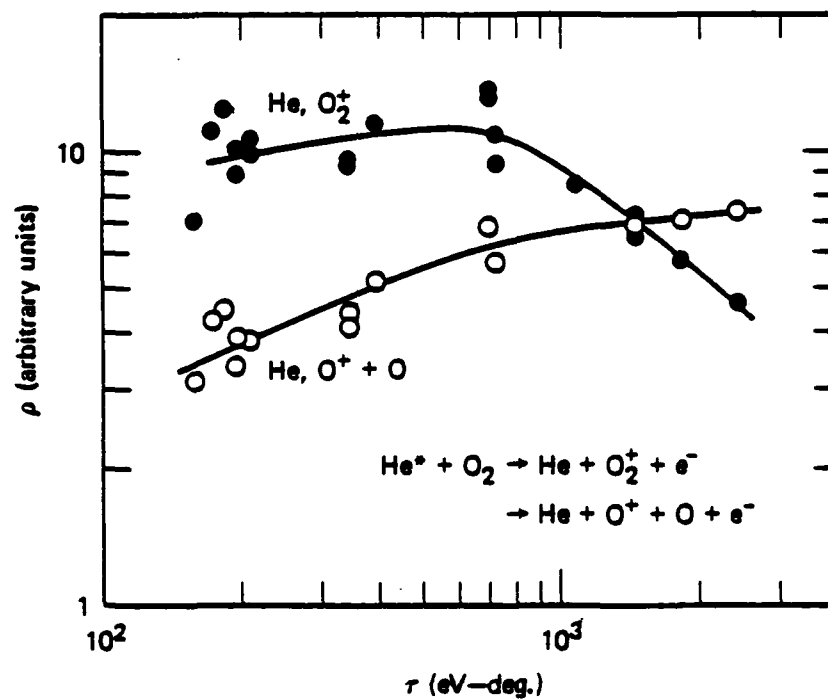
Figure 17. Reduced ($\rho$–$\tau$) differential cross section data for reactions (16) and (17) at $E_0$ = 296 eV.

38

The low angle thresholds for the Penning processes are at smaller angles than those investigated. Measurements at these smaller angles were impossible because the unscattered $He^*$ beam overwhelmed the He detector. A better collimation of the $He^*$ beam would allow measurements to be made closer to the beam. The decrease in beam intensity accompanying a tighter collimation would present no real problem because the coincidence signal levels are very large at small angles. For example, Figure 15 was generated in ~ 6 minutes; satisfactory spectra at half that angle can now be measured in ~ 1 minute. In fact, since we attempt to collect a large fraction of the product ions, we have already been required in these measurements to reduce the beam intensity substantially to avoid very high count rates on the ion detector. The efficient collection of the product ions makes data accumulation much faster in these experiments than in most other two-particle coincidence measurement techniques.

Our results are the first differential cross section measurements for Penning ionization at energies above the thermal range. They are to our knowledge the only double-differential cross section measurements at any energy for an ionization continuum channel in a neutral triatomic system. Although these measurements are preliminary and should be extended to smaller and larger scattering angles, they indicate the success of our newly developed technique and demonstrate its unique capabilities for rapid and direct examination of the Penning channel in collisions at moderate energies.

## ACKNOWLEDGEMENT

# REFERENCES

1.  R. Morgenstern, D. C. Lorents, J. R. Peterson, and R. E. Olson, Phys. Rev. A $8$, 2372 (1973); K. T. Gillen, Tenth International Conference on the Physics of Electronic and Atomic Collisions (X ICPEAC), Invited Lectures and Progress Reports, Paris (1977), p. 473.

2.  Faraday Discussions, Molecular Beam Scattering, Vol. $55$ (1973); M.A.D. Fluendy, Contemp. Physics $16$, 147 (1975).

3   V. Sidis, IX ICPEAC, Invited Lectures, Review Papers and Progress Report, Seattle (1975), p. 295; V. Kempter, ibid., p. 327; R. Morgenstern, ibid., p. 345; M. Barat, VIII ICPEAC, Invited Lectures and Progress Reports, Beograd (1973), p. 43; R. McCarroll, ibid., p. 71.

4.  J. Los, X ICPEAC, Invited Lectures and Progress Reports, Paris (1977), p. 617.

5.  K. T. Gillen, T. D. Gaily, and D. C. Lorents, Chem. Phys. Letters $57$, 192 (1978).

6.  A. P. Hickman and K. T. Gillen, J. Chem. Phys. $73$, 3672 (1980).

7.  A. W. Kleyn and K. T. Gillen, XII ICPEAC, Invited Papers, Gatlinburg, (1981) p. 369.

8.  D. R. Herschbach, Adv. Chem. Phys. $10$, 319 (1966).

9.  E. E. Muschlitz, Science $159$, 599 (1968); J. J. Ewing and C. A. Brau, Phys. Rev. A $12$, 129 (1975); M. F. Golde and B. A. Thrush, Chem. Phys. Letters, $29$, 486 (1974).

10. J. Los and A. W. Kleyn, "Ion-Pair Formation" in Alkali Halide Vapors, P. Davidovits and D. L. McFadden, Eds. (Academic Press, New York, 1979), p. 275.

11. K. T. Gillen and A. P. Hickman, Chem Phys. $\underline{53}$, 383 (1980).

12. A. W. Kleyn, V. N. Khromov, and J. Los, Chem. Phys. $\underline{52}$, 65 (1980).

13. C. E. Young, C. M. Sholeen, A. F. Wagner, A. E. Proctor, L. G. Pobo, and S. Wexler, J. Chem. Phys. $\underline{74}$, 1770 (1981).

14. W. H. Miller and H. Morgner, J. Chem. Phys. $\underline{67}$, 4923 (1977).

15. K. T. Gillen and T. M. Miller, Phys. Rev. Lett. $\underline{45}$, 624 (1980).

16. A. W. Kleyn, E. A. Gislason, and J. Los, Chem. Phys. $\underline{52}$, 81 (1980).

17. A. W. Kleyn, E. A. Gislason, and J. Los, Chem. Phys. $\underline{60}$, 11 (1980).

18. C. F. Giese and W. R. Gentry, Phys. Rev. A $\underline{10}$, 2156 (1974).

19. U. C. Klomp, M. R. Spalburg, and J. Los (manuscript in preparation).

20. T. M. Miller and K. T. Gillen, Phys. Rev. Lett. $\underline{44}$, 776 (1980).

21. C. Reynaud, J. Pommier, V. N. Tuan, and M. Barat, Phys. Rev. Lett. $\underline{43}$, 579 (1979).

22. V. Kempter (private communication).

23. O. Leisin, H. Morgner, and W. Muller, Z. Phys. A $\underline{304}$, 23 (1982).

24. M. T. Leu and P. E. Siska, J. Chem. Phys. $\underline{60}$, 2179, 4082 (1974).

# APPENDIX A

## ION-PAIR FORMATION IN FAST COLLISIONS OF METASTABLE ARGON WITH IODINE [‡]

Keith T. GILLEN, T. Dean GAILY [*] and Donald C. LORENTS

*Molecular Physics Laboratory, SRI International, Menlo Park, California 94025, USA*

Differential ion-pair production cross sections for $Ar^*-I_2$ collisions at center of mass energies of 25–133 eV are quite similar to analogous alkali–$I_2$ results despite the addition of competing channels (Penning ionization and excitation transfer) and possible multiple electronic surface crossings.

## 1. Introduction

The formation of ion pairs from the collision of fast atoms with various target molecules has been investigated extensively over the past several years [1,2]. Detailed differential cross section information only exists, however, for a few prototype systems [3–10], all involving collision partners in their lowest electronic states. Here we describe the first differential cross section measurements of collisional ion-pair formation for electronically excited reactants, a study of the reaction of metastable argon $(Ar^*)$ with $I_2$. This system is unique in that both the incoming covalent potential surfaces $Ar^* + I_2$ and the product ionic surfaces $Ar^+ + I_2^-$ are imbedded in the continuum $Ar + I_2^+ + e^-$. Hence, Penning ionization,

$$Ar^* + I_2 \rightarrow Ar + I_2^+ + e^- , \qquad (1)$$

can compete with the ion-pair channel

$$Ar^* + I_2 \rightarrow Ar^+ + I_2^- . \qquad (2)$$

## 2. Experimental

The apparatus is a modification of one previously described [11] and will be discussed only briefly. An $Ar^+$ parent ion beam produced in a discharge source

is converted to $Ar^*$ by near-resonant charge transfer in Rb vapor [12]. The product fast neutral beam, after decay of radiative excited states, is a mixture of the two metastable states $^3P_0$ and $^3P_2$ and the $^1S_0$ ground state. After deflection of the unneutralized ions this neutral beam enters a collision cell of length 1.3 cm filled with $I_2$ vapor at 300 K and at low density $(<10^{13}/cm^3)$. Product ions are energy analyzed and counted as a function of scattering angle by a $127°$ analyzer and channeltron detector that rotate around the collision cell.

The energy analyzer can be floated at various potentials to analyze parent or product ions with high or low resolution and to determine the separate contributions to any measured energy width due to the ion energy distribution and the energy analyzer transmission function. The energy analyzer has a measured resolution (fwhm) of 2.8% of the analysis energy. A typical value for the energy spread (fwhm) of the parent ion beam is 0.7 eV.

The energy of the $Ar^*$ beam differs from that of the parent $Ar^+$ by a contact potential due to the Rb-coated charge transfer oven and a small energy defect in the charge transfer. We determine the $Ar^*$ beam energy by a pulsed time-of-flight technique [11] using another channeltron detector. The measured angular width of the cylindrically collimated $Ar^*$ beam is typically 0.5° fwhm in the plane of motion of the detector and is probably of similar magnitude perpendicular to this plane. The estimated laboratory angular acceptance of the ion detector is ±0.1° full width (fw) in

192

the plane of its motion and $\pm 0.4°$ (fw) perpendicular to that plane.

## 3. Results

The differential cross section for ion-pair formation is presented in fig. 1 for four center-of-mass (c.m.) collision energies $E_{c.m.}$. For each curve the laboratory angular distributions weighted by $\sin \theta$ are plotted versus the reduced scattering angle $\tau = E_{c.m.}\theta$. These angular distributions were measured with the energy analyzer adjusted to transmit the peak of the product energy distribution at each scattering angle. The observed scattering was confined to low laboratory angles ($<10°$), and the measured product energy profiles appeared to be almost independent of scattering angle.

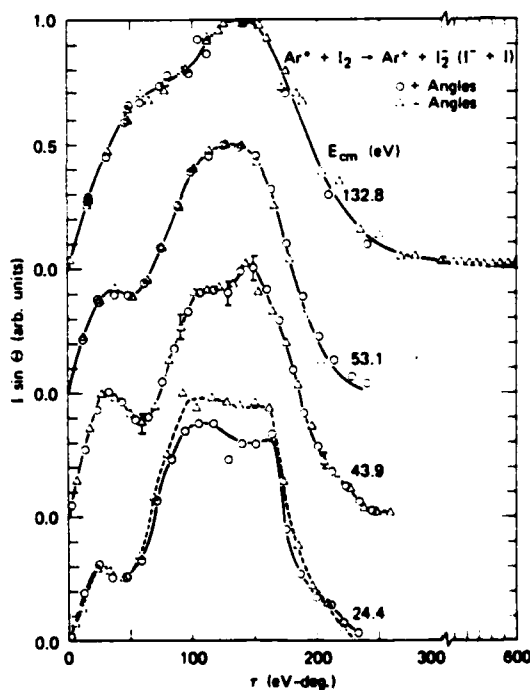At several widely spaced angles, the entire product energy distribution was measured. In every case, a single narrow peak was observed with a width (fwhm) of $\lesssim 0.8$ eV. The measured endothermicities, $\Delta E$, were $2.6 \pm 0.4$ eV. Since the product energy distributions did not vary significantly with scattering angle, the measured angular distributions at fixed $\Delta E$ plotted in fig. 1 are an accurate representation of the total product ion angular distributions. However, predominant small angle scattering of the $Ar^+$ product ions combined with the apparatus angular resolution of $>0.5°$ fwhm implies a significant amount of angular smearing at angles below $\approx 1°$. This smearing is quite significant at the highest energy studied.

## 4. Discussion

A useful framework for discussing reactive encounters involving rare gas metastable ($Rg^*$) projectiles is based on the observation [13—19] of the similarities between $Rg^*$ atoms and alkali atoms M due to the importance in both species of the single loosely bound (4—5 eV) outer s electron. The availability of a large body of detailed collision data, both experimental and theoretical, involving alkali atoms [1, 20—22] often provides a starting point for predicting important features of $Rg^*$ interactions.

For the venerable alkali reaction with a halogen molecule ($X_2$)

$$M + X_2 \rightarrow MX + X, \tag{3}$$

it is well established [20] that the reaction dynamics at thermal energies are dominated by a single potential surface crossing, at a large internuclear separation, between ...e relatively flat $M + X_2$ diabatic surface and an attractive coulombic $M^+ + X_2^-$ surface. At the crossing distance, $r_c$, an electron is said to jump from M to $X_2$, forming $X_2^-$ on its repulsive inner wall in a compressed configuration that dissociates in the field of the positive ion as the ionic MX bond forms.

At collision energies significantly above thermal, dissociation along the coulombic surface becomes energetically accessible and can yield either $M^+ + X^- + X$ or $M^+ + X_2^-$ products. This ion-pair formation channel [1,2] can still be most simply understood in terms of the effect of crossings between the two important potential surfaces, if proper account is taken of $X_2^-$



Fig. 1. Angular distributions of product $Ar^+$ ions from collision of $Ar^*$ with $I_2$ at four center-of-mass energies $E_{c.m.}$. The measured differential cross sections have been weighted by $\sin \theta_{c.m.}$ and plotted against the reduced angle $\tau = E_{c.m.}\theta_{c.m.}$. Successive curves have been displaced vertically by 0.5 units for clarity.

193

bond-stretching during the collision [23,10].

The corresponding ion-pair formation reactions of $Rg^*$ with $X_2$ are similarly influenced by intersections of covalent $Rg^* + X_2$ and coulombic $Rg^+ + X_2^-$ surfaces whose shapes and properties at large $r$ are very similar to the relevant $M-X_2$ surfaces. However, the inner-shell vacancy in $Rg^*$ gives it unique properties and interaction mechanisms potentially more complex than those of alkali atoms. First there are competing channels such as Penning ionization, reaction (1), and electronic energy transfer (e.g., $Ar^* + I_2 \rightarrow Ar + I_2^*$) which may or may not perturb the ion-pair results, depending on the relative importance of the mechanisms. Second, the $Ar^*$ beam contains an unknown mixture of two metastable states ($^3P_2$ and $^3P_0$) separated by 0.17 eV [24] with symmetry and degeneracy properties quite distinct from the M atom ($^2S$). There is a similar distinction between the $Ar^+$ ion with two states split by 0.17 eV ($^2P_{3/2}$ and $^2P_{1/2}$) and the $M^+$ ion ($^1S$). Although the expected low probability of core rearrangement interactions strongly suggests that electron transfer will involve predominantly the $Ar^*(^3P_2) \rightarrow Ar^+(^2P_{3/2})$ and $Ar^*(^3P_0) \rightarrow Ar^+(^2P_{1/2})$ transitions, an additional complication arises from the various distinct potential surfaces that derive from interactions of each of these four atomic states with the diatomic ($I_2$ or $I_2^-$). All of these covalent and coulombic surfaces may not deviate significantly in shape from the corresponding alkali surfaces, except at small $r$, but the transition rates at the surface crossings (at large $r$) could be quite different due to either the altered symmetry properties or the interactions between a number of closely spaced surfaces. Thus, it would not be surprising to observe some significant deviations from analogous alkali results in the features of reaction (2).

If a value of 2.6 eV is used [25] for the adiabatic electron affinity of $I_2$ a minimum endothermicity $\Delta E$ of $\approx 1.6$ eV is necessary to produce ion pairs with the product $I_2^-$ in the lowest vibrational level of its ground electronic state ($^2\Sigma_u^+$). Higher $\Delta E$ values would correspond to production of $I_2^-$ with internal excitation. A translational energy loss of $\approx 2.7$ eV is needed to produce $Ar^+ + I^-$ ($^1S$) $+ I(^2P_{3/2})$ products, and $\Delta E = 3.6$ eV is required [24] before the $Ar^+ + I^- + I^*(^2P_{1/2})$ final state can be reached. If the $I_2^-$ internal energy is equal to the energy generated by a vertical transition from $I_2$ to $I_2^-$ at the $I_2$ equilibrium

bond length (2.67 Å), the predicted $\Delta E$ value would be 2.5 eV using the appropriate (vertical) electron affinity $EA_v$ of 1.7 eV determined by Hubers et al. [26].

The measured energy loss of $2.6 \pm 0.4$ eV implies a near vertical transition ($I_2 \rightarrow I_2^-$) at the crossing of the $Ar^* + I_2$ covalent surface with $Ar^+ + I_2^-(^2\Sigma_u^+)$. It also implies that there is little likelihood of any excited $I^*(^2P_{1/2})$ product. The majority of collisions must therefore yield very highly vibrationally excited $I_2^-$ in the $^2\Sigma_u^+$ ground electronic state, but the range of measured exothermicities allows for the production of some dissociated $I^- + I$ products as well [26].

In the simplest approximation the crossing between the "coulombic" ionic and "flat" covalent surfaces occurs at an $Ar^*-I_2$ distance

$$r_c = 14.4 \text{ Å}/(\text{IP} - \text{EA}),$$

where IP = 4.21 eV (the ionization potential of $Ar^*$), and EA is the electron affinity of $I_2$. Using $EA_v \approx$ 1.7 eV, $r_c$ is approximately 5.7 Å; at such large $r$ values, a coulombic approximation for the $AR^+ + I_2^-$ interaction and an assumption of negligible interaction between $Ar^* + I_2$ are both reasonable. As indicated schematically in fig. 2, there are two distinct paths (a and b) leading to ion products. Since path b (the ionic path) involves significantly more attractive interaction than path a (the covalent path), it should produce $Ar^+$ scattering at larger angles. At the higher energies shown in fig. 1, there are indeed two major peaks in the angular distribution. The $\tau$ values of these peaks are very similar to those found [7,8] in $K + I_2$, the most closely related $M + I_2$ system investigated. As the collision energy is lowered, the ionic peak in fig. 1 broadens, develops secondary structure, and increases in intensity relative to the accompanying covalent peak. These results are again strikingly similar to the published results for $K + I_2$, and the interpretation given below is quite analogous to recent conclusions of Los and co-workers [2,7,23] for $M + X_2$.

A simple Landau–Zener description of the crossing region incorrectly predicts that the two major peaks have comparable total intensities. The reason that the ionic path has a higher yield of product ions can be understood by examining the nature of trajectories that explore the ionic surface inside the initial crossing $r = 5.7$ Å. As indicated in the simplified picture in fig. 2, the electron jump occurs to an $I_2$ molecule near
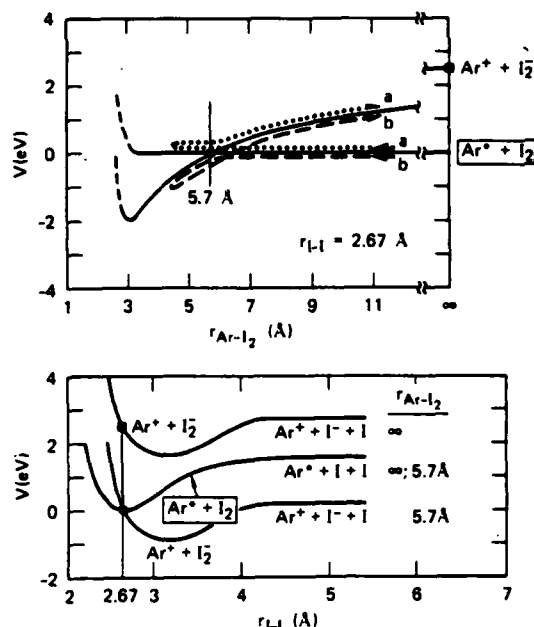
Fig. 2. Sections through an idealized Ar–I–I potential surface. Upper: potential as a function of Ar–$I_2$ distance at an I–I distance (2.67A) corresponding to the equilibrium $I_2$ bond separation. This is a one-dimensional representation of the ion-pair formation channel and shows two different paths through the crossing at 5.7 A leading to ion-pair products. Lower: potential as a function of I–I distance at Ar–$I_2$ distances of ∞ and 5.7 A. The coulombic $Ar^+ + I_2^-$ curve drops in energy as $r_{Ar-I_2}$ decreases; at $r_{Ar-I_2}$ = 5.7 A, transfer from $I_2$ to $I_2^-$ can occur, producing the compressed $I_2^-$.

its equilibrium internuclear distance, forming an $I_2^-$ molecule on its repulsive inner wall. As the $Ar^+$ continues to approach, reaches the turning point, and then recedes from the $I_2^-$, the $I_2^-$ bond is stretching. At the second crossing of the ionic and covalent surfaces, the $I_2^-$ bond is larger, implying a larger effective electron affinity, a larger crossing distance, and a more diabatic crossing [27]. At high collision velocities, the bond length changes little between the two crossings; as the collision velocity is lowered, the first crossing becomes more and more adiabatic and bond stretching yields larger diabatic probabilities (and hence enhanced ion-pair formation) on the return passage.

The additional structure observed at low energies in the ionic channel is more difficult to interpret [28].

A recent model calculation of Aten and Los [10] for K + $Br_2$ suggests that this structure is at least partially due to prestretching of the $X_2$ bond before the reactants reach the crossing seam at $r_c$.

There is no clear evidence of any significant observable effect on the scattering patterns in the ion-pair chancel (2) by the competing Penning or excitation transfer channels. This is evident from the similarity of the $Ar^* + I_2$ scattering to both the K + $I_2$ results and the most recent model calculations [10,28] for M + $X_2$. Further evidence is provided by our preliminary observation that the total destruction cross sections of $Ar^*$ in $I_2$ are near 100 $A^2$, well above the expected Penning cross sections for this energy range [29,30]. Basically the most important contributions to the charge transfer reaction occur at such large impact parameters that they are not significantly altered by processes occurring only at shorter range.

### Acknowledgement

### References

[1] A.P.M. Baede, Advan. Chem. Phys. 30 (1975) 463.
[2] J. Los, in: Proceedings of the Tenth International Conference on the Physics of Electronic and Atomic Collisions, Invited Papers and Progress Reports, ed. G. Watel (North-Holland, Amsterdam, 1978) p. 617.
[3] G.A.L. Delvigne and J. Los, Physica 59 (1972) 61.
[4] C.E. Young, R.J. Beuhler and S. Wexler, J. Chem. Phys. 61 (1974) 174.
[5] T. Mochizuki and K. Lacmann, J. Chem. Phys. 65 (1976) 3257.
[6] M. Kimura and K. Lacmann, Chem. Phys. Letters 51 (1977) 585.
[7] J.A. Aten, G.E.H. Lanting and J. Los, Chem. Phys. 19 (1977) 241.
[8] J.A. Aten, G.E.H. Lanting and J. Los, Chem. Phys. 22 (1977) 333.
[9] J.A. Aten, C.W.A. Evers, A.E. de Vries and J. Los, Chem. Phys. 23 (1977) 125.
[10] J.A. Aten and J. Los, Chem. Phys., to be published.

195

[11] R. Morgenstern, D.C. Lorents, J.R. Peterson and R.E. Olson, Phys. Rev. A 8 (1973) 2372.

[12] J.R. Peterson and D.C. Lorents, Phys. Rev. 182 (1969) 152.

[13] E.E. Muschlitz, Science 159 (1968) 599.

[14] E.W. Rothe, R.H. Neynaber and S.M. Trujillo, J. Chem. Phys. 42 (1965) 3310.

[15] M.F. Golde and B.A. Thrush, Chem. Phys. Letters 29 (1974) 486.

[16] J.J. Ewing and C.A. Brau, Phys. Rev. A 12 (1975) 129.

[27] D.H. Winicur, J.L. Fraites and F.A. Stackhouse, Chem. Phys. Letters 23 (1973) 123.

[18] C.H. Chen, H. Haberland and Y.T. Lee, J. Chem. Phys. 61 (1974) 3095.

[19] D.H. Winicur, J.L. Fraites and J. Bentley, J. Chem. Phys. 64 (1976) 1757.

[20] D.R. Herschbach, Advan. Chem. Phys. 10 (1966) 319.

[21] J.L. Kinsey, MTP Intern. Rev. Sci. 9 (1972) 173.

[22] R. Grice, Advan. Chem. Phys. 30 (1975) 247.

[23] J.A. Aten, M.M. Hubers, A.W. Kleyn and J. Los, Chem. Phys. 18 (1976) 311.

[24] C.E. Moore, Atomic Energy Levels, NBS Circular 467, Vol. 1 (1949); Vol. 3 (1958).

[25] J.L. Franklin and P.W. Harland, Ann. Rev. Phys. Chem. 25 (1974) 485.

[26] M.M. Hubers, A.W. Kleyn and J. Los, Chem. Phys. 17 (1976) 303.

[27] R.E. Olson, F.T. Smith and E. Bauer, Appl. Opt. 10 (1971) 1848.

[28] Ch. Evers, Chem. Phys. 21 (1977) 355.

[29] J.T. Moseley, J.R. Peterson, D.C. Lorents and M. Hollstein, Phys. Rev. A 6 (1972) 1025.

[30] R.H. Neynaber and G. Magnuson, Phys. Rev. A 11 (1975) 865; 14 (1976) 961.

A-5

# APPENDIX B

# Comparison of ion pair formation in the systems Ar*+I₂ and K+I₂

### A. P. Hickman and Keith T. Gillen

*Molecular Physics Laboratory, SRI International, Menlo Park, California 94025*

A simple model that has been used extensively by Los and co-workers to treat ion pair formation in collisions of alkali atoms with diatomic molecules is extended to include continuum coupling via a competing Penning ionization channel. This extended model is then used to calculate the differential cross sections for ion pair formation for the system $Ar^* + I_2$ over the energy range 28–154 eV and to compare with a previous treatment of $K + I_2$. In the absence of significant competition from continuum processes, $Ar^*$ is expected to behave in a manner similar to K, since the active electron is an unpaired $4s$ electron in both cases. We perform model calculations for $Ar^* + I_2$ to investigate the effects of varying the potential curves and charge exchange matrix elements and of including a continuum coupling function $\Gamma(R)$. Comparison with previous calculations for $K + I_2$ suggests increased repulsion on the $Ar^*-I_2$ surfaces relative to those of $K-I_2$. The competing mechanisms of excitation transfer and Penning ionization may have a small effect upon the ion pair angular distributions.

## I. INTRODUCTION

The study of a pair of generally similar reactions enables one to isolate subtle effects that arise specifically from the differences between the two systems. Recent measurements of the differential cross section for ion pair formation in collisions between halogen molecules and alkali atoms or metastable rare gas atoms provide such an opportunity. Over the energy range 30–150 eV, all of the major features observed[1] in the angular distribution for the reaction

$$Ar^*(^3P_{2,0}) + I_2 \rightarrow Ar^* + I_2^- \tag{1}$$

can be correlated with those observed[2-4] in the analogous reaction

$$K + I_2 \rightarrow K^* + I_2^- . \tag{2}$$

However, there are differences in the ratios of the intensities of various features and in the position of the rainbow angle. The general similarity is consistent with the fact that both K and $Ar^*(^3P)$ have an active, unpaired $4s$ electron. The observed differences between the two reactions should be related to the inner shell vacancy in $Ar^*$ and to the additional competing channels energetically accessible to the system, including Penning ionization:

$$Ar^* + I_2 \rightarrow Ar + I_2^- + e^- . \tag{3}$$

In this paper we present model calculations designed to elucidate the causes of the observed differences in the scattering data.

Ion pair formation in the alkali–halogen system has been extensively investigated[5-7] both experimentally and theoretically. These reactions have been modeled quite successfully by Los and co-workers[5,6] using classical trajectory surface-hopping techniques[8,9] that demonstrate the essential features of the reaction mechanism leading to ion pair production. Here we have modified and extended those model calculations to include coupling to the continuum [Reaction (3)]. We estimate the autoionization rate $\Gamma(R)$ using a simplified form of a technique proposed recently by Miller and Morgner.[10]

We are therefore able to perform quantitative calculations that examine the effect of competing channels upon the ion pair distributions in Reaction (1).

In Sec. II we present the details of the model calculations and discuss the inclusion of continuum coupling. Our results are presented and discussed in Sec. III, and Sec. IV contains a summary.

## II. THEORY

### A. Summary of the model

We have adopted the theoretical approach developed by Los and co-workers,[2,5,6] which is a classical-trajectory, surface-hopping model[8,9] with the following additional approximations:

1. Simple analytic potentials are constructed from pairwise interactions for the covalent electronic state $K + I_2$ and for the ionic state $K^* + I_2^-$.

2. The cross sections are obtained as the average of cross sections for various orientations of the target molecule. The axis of this target is assumed not to rotate during the collision. Molecular vibration, however, is included, as explained below.

3. For each trajectory, the classical vibration of the molecule is calculated numerically assuming Morse potentials, and the deflection of the projectile is obtained analytically using classical perturbation theory.

An essential feature of the model is that the ionic and covalent surfaces cross at an $Ar^*-I_2$ distance $R$ that depends on the vibrational coordinate of the molecule. This fact influences the collision in the following way. The system begins asymptotically on the covalent surface. When the particles reach the location of the crossing with the ionic surface, the Landau–Zener formula[11] is used to compute the probability of switching to the other surface. As shown in Fig. 1, there are two possible paths to ion pair formation. The surface crossing may occur on the inward part of the trajectory (the dashed line) or on the outward part (shown by the dotted
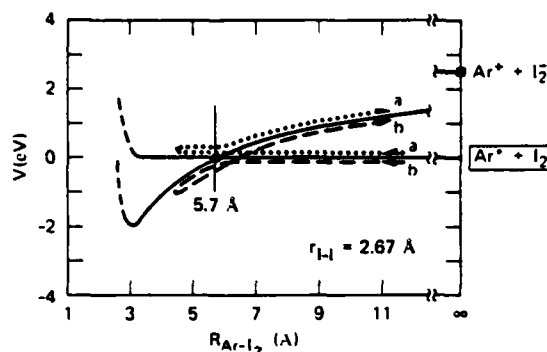
FIG. 1. Two possible paths $a$ and $b$ to ion pair production are schematically indicated. The potential curves represent cuts of the Ar* + I₂ and Ar* + I₂⁻ surfaces at a fixed I₂ separation.

line). A transfer to the ionic surface will initiate an expansion of the $I_2^-$ bond since $I_2^-$ has a larger equilibrium internuclear distance than $I_2$. If this transfer occurs on the incoming trajectory, the resulting $I_2^-$ expansion will yield an effective vertical electron affinity that increases with time. This will increase the radius $R$ at which the second surface crossing is encountered on the outward part of the trajectory. Since the matrix element connecting the two surfaces decreases strongly with increasing $R$, the probability of a diabatic path through the second crossing may be significantly larger than at the first crossing. These effects have already been thoroughly discussed in the literature. [1-6]

The analytic form of the potential surface we have used differs somewhat from the form used in Ref. 2. Ours is defined in terms of Fig. 2 to be

$$V_{00} = V(R_1) + V(R_2) + v_0(r) , \qquad (4)$$

$$V_{11} = V(R_1) - \frac{0.5}{R_1} + V(R_2) - \frac{0.5}{R_2} + v_1(r) . \qquad (5)$$

$v_0(r)$ and $v_1(r)$ are Morse potentials for $I_2$ and $I_2^-$, respectively. The same Morse parameters were used as in Ref. 2, namely, $D = 1.54$ eV, $\beta = 1.87$ Å⁻¹, and $r_e = 2.67$ Å for $I_2$, and $D' = 1.02$ eV, $\beta' = 1.23$ Å⁻¹, and $r_e' = 3.20$ Å for $I_2^-$. $V(R_i)$ is a repulsive term of the Born–Mayer form, [12]

$$V(R_i) = A e^{-BR_i} , \qquad (6)$$

where, following Ref. 2, we initially use $A = 6.4 \times 10^4$ eV and $B = 4.762$ Å⁻¹. Note that for simplicity the same constants $A$ and $B$ are used here for the ionic and covalent terms. The potentials we use are much simpler than those of Ref. 2. Since ab initio calculations are not available, we choose to use potentials with as few adjustable parameters as possible.

The potential surfaces defined by Eqs. (4) and (5) do not reflect the multiplicity of states arising from the inner shell vacancy in Ar*. Our simplified model is equivalent to assuming that all of the covalent surfaces are degenerate, and that all of the ionic surfaces are degenerate. This assumption appears reasonable at large values of $R$, where the surfaces cross. In this region we expect no inner shell rearrangement processes. The core electrons should have only a minor

influence on the potential shapes and coupling matrix elements. This fact is indeed the major reason for the strong analogy to alkali reactions and the justification for our use of the single surface crossing and the coupling matrix element angular dependence [13] [$\cos\alpha$ in Eq. (7) below] that are appropriate to alkali systems. The inner shell vacancy in Ar* would, however, be expected to influence surface parameters at much smaller $R$ values and thereby could affect the shape of the differential cross sections. We will return to this point later.

We use the same form for the coupling matrix element as in Ref. 2:

$$V_{12}(R, r, \theta) = c_1 [I E.A. (r)]^{1/2} R^* e^{-c_2 R^*} \cos\alpha , \qquad (7)$$

where

$$R^* = (R/\sqrt{2})[I^{1/2} + E.A. (r)^{1/2}]. \qquad (8)$$

$I$ is the ionization potential of the projectile and E.A. $(r)$ is the vertical electron affinity of the molecule as a function of the separation $r$. Note that the diagonal terms $V_{00}$ and $V_{11}$ are orientation dependent because they are defined in terms of $R_1$ and $R_2$. Note also that the angular dependence of $V_{12}$ forces it to be zero at the angles required by symmetry. [13] Initially the constants $c_1 = 0.28$ a.u. and $c_2 = 0.65$ a.u. were used [2] for both Reaction (1) and Reaction (2).

For each orientation of the target (in a space-fixed frame), we wish to calculate the two branches of the classical deflection function. These two branches give the scattering angle as a function of impact parameter for trajectories in which the surface crossing occurs on the inward or outward part of the trajectory. (If the crossing occurs twice, or not at all, ion pair formation does not occur and the trajectory is not counted.) For each impact parameter, the scattering angles are therefore calculated for two sequences of events. In both cases, the $I_2$ molecule begins at rest on the neutral potential curve $v_0(r)$ at the equilibrium distance $r_e$, and the projectile follows a straight-line path with constant velocity throughout the collision. For the ionic branch of the deflection function, the system is assumed to switch to the ionic potential at the first crossing. Then the $I_2^-$ molecule begins to move classically on the potential $v_1(r)$, beginning at rest at $r = r_e$ (I₂). The location of the second crossing is determined numerically by monitoring the oscillatory motion of the target and the rectilinear motion of the projectile. For the covalent branch of the deflection function, the molecule does not begin to vibrate until the crossing is encountered a second time,
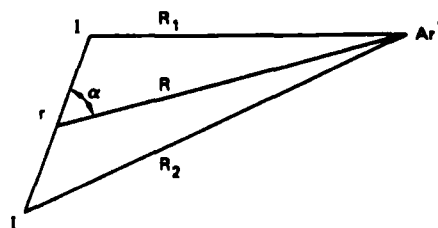


FIG. 2. Illustration of the coordinate system used to define the potential functions.

J. Chem. Phys., Vol. 73, No. 8, 15 October 1980

B-2

so that the first and second crossings occur at the same intermolecular separation $R$. For both branches of the deflection function, the orientation angle $\alpha$ is computed at both crossings. The orientation influences the transition probability through the factor $\cos\alpha$ in Eq. (7).

The preceding discussion shows how the appropriate potential is determined at each point along a given trajectory. The scattering angle is then determined by integrating the cumulative momentum transfer perpendicular to the rectilinear motion, according to standard formulas[14] of classical perturbation theory. The deflection is easily calculated analytically because the functions in Eqs. (4) and (5) are written as sums of two-body potentials.

In order to obtain the cross section, it is also necessary to calculate the probability that the system will follow a given trajectory. This is done using the Landau–Zener formula.[15] The total probability for a given sequence of surface crossings or avoided crossings is the product of the probabilities for each event separately. This is easily calculated once the locations of the two crossing points are known. The result for the cross section (for a particular orientation of the molecule) can be summarized in the following formula:

$$\frac{d\sigma}{d\Omega}\sin\theta = \sum_j \frac{2\pi b_j P^{\text{ion}}(b_j)}{|d\theta^{\text{ion}}/db|} + \sum_{j'} \frac{2\pi b_{j'} P^{\text{cov}}(b_{j'})}{|d\theta^{\text{cov}}/db|} . \qquad (9)$$

$P^{\text{ion}}(P^{\text{cov}})$ is the overall probability of following an ionic (covalent) trajectory for a particular impact parameter $b$. The sums are understood to be over all impact parameters that lead to the scattering angles $\theta$ or $-\theta$. Although Eq. (9) presents the formal definition of the cross section, we found it useful in practice to use a conventional histogram procedure.

## B. The Penning ionization channel

### 1. Estimating $\Gamma(R)$ for molecular systems

$\Gamma(R)/\hbar$ is the rate at which particles are lost from an initial channel into the ionization channel via the reaction (3). $\Gamma$ is given by[16,17]

$$\Gamma = 2\pi\rho |H_{fi}|^2 \qquad (10)$$

$$= 2\pi\rho |\langle \Phi_{final} |H| \Phi_{initial} \rangle|^2 , \qquad (11)$$

where $H$ is the Hamiltonian, $\Phi_{initial}$ is the initial bound state wave function (Ar* + I$_2$), $\Phi_{final}$ is the continuum configuration (Ar + I$_2^+$ + e$^-$), and $\rho$ is the density of continuum states. If the continuum wave function is normalized to unit amplitude asymptotically, then

$$2\pi\rho = 4/k , \qquad (12)$$

where the kinetic energy of the ejected electron is, in atomic units, $E = 1/2\,k^2$.

Miller and Morgner[10] have suggested that the matrix element $H_{fi}$ can be written as the product of an overlap factor and a charge exchange factor. Specializing to our case, Ar* + I$_2$, this would be the product

$$H_{fi} \cong S_{fi} \times H_{fi}^{(0)} \qquad (13)$$

where $S_{fi}$ is the overlap between the valence electron orbital on Ar* and the final state continuum orbital, and

$H_{fi}^{(0)}$ is the matrix element for the one-electron process

$$\text{Ar* + I}_2 \to \text{Ar + I}_2^+ . \qquad (14)$$

Miller and Morgner[10] pointed out that $H_{fi}^{(0)}$ can be estimated using the semiempirical correlation formula of Olson et al.[18]:

$$|H_{fi}^{(0)}| \cong GR\, e^{-R/C} , \qquad (15)$$

where $R$ is the internuclear separation in a.u., and

$$1/C = \frac{1}{\sqrt{2}} (I_{I_2}^{1/2} + I_{Ar}^{1/2}) , \qquad (16)$$

$$G = (I_{I_2} I_{Ar})^{1/2}/C , \qquad (17)$$

where $I_{I_2}$ and $I_{Ar}$ are the ionization potentials of I$_2$ and Ar in a.u., respectively. $|H_{fi}|$ is then given also in a.u.

Based on past experience[19] calculating continuum overlap factors $S_{fi}$, we have simplified the Miller–Morgner formula by setting $S_{fi} \approx 1$. This approximation enables us to evaluate $H_{fi}$ without numerical integration. Furthermore, since the potential surfaces are not in general known, we calculate the density of states $2\pi\rho$ from the energy of the ejected electron as $R \to \infty$. This information is available from spectroscopic data.

Miller and Morgner[10] estimate that their formula is reliable within a factor of 3–5. We expect that our additional approximations will degrade the accuracy somewhat, but the result should certainly still be a reasonable order-of-magnitude estimate.

### 2. Ionization probability as a function of impact parameter

The autoionization rate obtained in the previous section has the form $\Gamma(R) \propto R^2 e^{-\lambda R}$. However, we have found that over the important range of $R$ probed in the collisions, the numerical values of $\Gamma$ can be well fit ($\sim 10\%$) by the simpler form

$$\Gamma(R) = a_1 e^{-a_2 R} . \qquad (18)$$

This is the form of $\Gamma$ that has been assumed in many previous semiempirical studies.[20,21]

We have found that for a $\Gamma$ of the form of Eq. (18), a very simple formula can be obtained, in the perturbation limit, for the ionization probability as a function of impact parameter. Since the translational motion is already treated using classical perturbation theory, a perturbation assumption for the continuum coupling is consistent with the rest of the model.

Let $b$ be the impact parameter. Then the survival probability $P(b)$ that ionization does not occur on a trajectory of impact parameter $b$ is

$$P(b) = \exp[-2F(b)] , \qquad (19)$$

where in the perturbation limit

$$F(b) = \int_b^\infty \frac{\Gamma(R)\,dR}{\hbar v_0 \sqrt{1-(b^2/R^2)}} , \qquad (20)$$

and $v_0$ is the incident velocity.

Substituting Eq. (18) into Eq. (20), integrating by

J. Chem. Phys., Vol. 73, No. 8, 15 October 1980

B-3

parts, and substituting $x = R/b$, we obtain

$$F(b) = \frac{a_1 a_2 b^2}{\hbar v_0} \int_1^\infty \sqrt{x^2 - 1} \; e^{-a_2 bx} \, dx \; . \qquad (21)$$

The integral can be represented in terms of the modified Bessel function $K_1$. Then

$$F(b) = \frac{a_1 b}{\hbar v_0} K_1(a_2 b) \; . \qquad (22)$$

Further simplification is possible because of the relation

$$x K_1(x) \approx 2.076 \, e^{-0.932 x} \qquad (23)$$

which is valid to about 10% for $2 \leq x \leq 12$. The final result is

$$F(b) \cong \frac{2.076 a_1}{a_2 \hbar v_0} \, e^{-0.932 a_2 b} \; . \qquad (24)$$

Formulas (19) and (24) may now be incorporated into the model in the following way. For each orientation, a deflection function is calculated that gives the angular scattering as a function of impact parameter. When the cross section is calculated from a particular branch of the deflection function, a factor is first included to represent the probability that the particles follow the correct sequence of curve crossings. The result is then multiplied by $P(b)$, which gives the probability that the trajectory is completed without loss to ionization.

## III. RESULTS AND DISCUSSION

### A. K + I₂

This reaction has already been treated in detail.[2-4] Here we demonstrate that the use of the potentials defined in Sec. II A leads also to satisfactory agreement with experiment. In Fig. 3, we compare the calculated and experimental values at a lab energy ($E_0$) of 60 eV. The agreement is not surprising since our potentials are nearly the same as those fitted to the data in Ref. 2. The major difference is that we have neglected the small van der Waals term.

### B. Ar* + I₂: General approach

Gillen et al.[1] pointed out that their results for Ar* + I₂ were similar to those of Aten et al.[2] for K + I₂. The important differences are that the covalent peak is relatively somewhat smaller for Ar* + I₂ than for K + I₂ and that the rainbow in the ionic peak occurs at smaller angles. The first difference could be caused by the continuum coupling in the metastable system or by differences in the potentials and charge exchange matrix elements. The second difference should be associated with a difference in the shape of the potential surfaces.

In this and the following subsections we describe our quantitative calculations to investigate possible causes for the experimental differences. With only a qualitative knowledge of the Ar* + I₂ potential surfaces, we do not expect to determine uniquely the coupling parameters in this system. Hence, our approach to Ar* + I₂ ion pair formation calculations is to start with the K + I₂ parameters and determine the changes in the distributions caused by individually altering the continuum width ($\Gamma = 0$ initially), the surface coupling parameters, and the
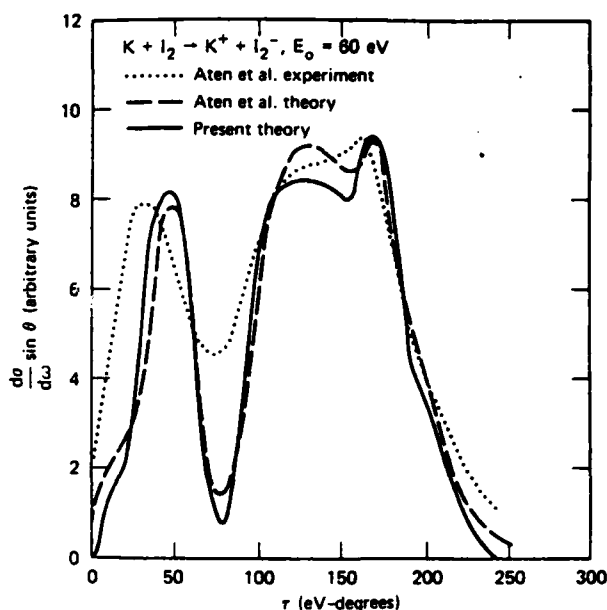


FIG. 3. Comparison of previous calculations and experimental data (Ref. 2) on the system K + I₂ with the present calculation, which uses slightly different interaction potentials.

interaction potentials. The results should yield insight into the possible causes of the differences observed between Ar* + I₂ and K + I₂ in the ion pair channel.

We initially performed trial calculations for Ar* + I₂ assuming $\Gamma = 0$, and using the same potential parameters as for K + I₂. The crossing point differs slightly for this system because the ionization potential of Ar* is slightly smaller than that for K. This change increases $R_c$ somewhat, and thereby decreases $V_{12}$ slightly, but the effect on the calculations was quite small. The calculated peak ratios and the position of the rainbow angle were essentially the same as those calculated for K + I₂, and these values did not agree with the data for Ar* + I₂.

### C. Ar* + I₂: The continuum channel

We then examined the effect of including continuum coupling. It should be noted that $\Gamma(R)$ is assumed to affect only the covalent potential. This is consistent with the conclusions of Hultsch et al.[22] on similar systems. One argues that Penning ionization of the covalent electronic state is initiated by a one-electron process, namely, the "exchange" process, in which an electron from the ground state atom jumps into the hole of the excited atom. There is then a large overlap between the valence electron of the excited atom and the continuum orbital. In contrast for a system on the Ar° + I₂⁻ surface, continuum coupling necessitates a simultaneous two-electron rearrangement; such a process would be expected to have a much lower probability.

For the ground electron state of I₂⁻, which is 9.3 eV above I₂, we follow the prescription of Sec. II B and obtain (for $\Gamma$ and $R$ in atomic units)

$$\Gamma(R) = 1.752 R^2 \, e^{-1.902 R} \; . \qquad (25)$$
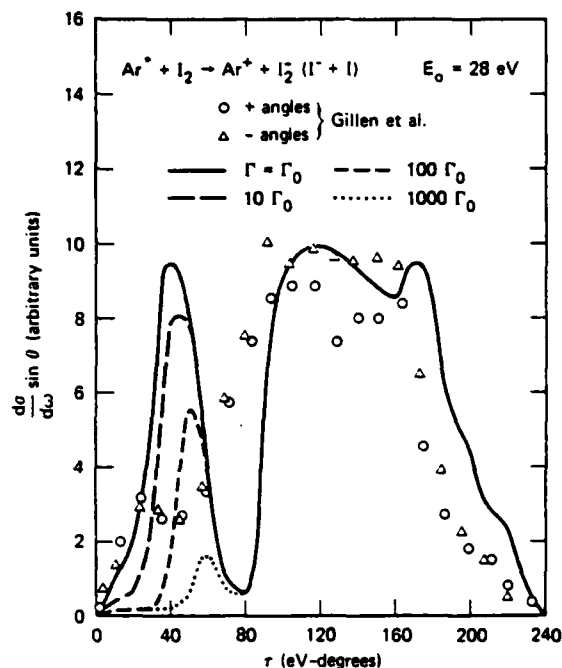
J. Chem. Phys., Vol. 73, No. 8, 15 October 1980

B-4

FIG. 4. Calculation of the differential cross section for ion pair formation in $Ar^* + I_2$ compared with the data of Ref. 1. The effect of different autoionization rates $\Gamma(R)$ in the covalent channel is illustrated. $\Gamma_0$ is the function estimated using the method discussed in Sec. II.B.1, and given by Eq. (26). Successively larger values of $\Gamma(R)$ reduce the covalent peak by larger fractions.

For $R$ in the range $4 - 12a_0$, this is well fit by the form

$$\Gamma_0(R) \cong 11.16\, e^{-1.614R} \text{ a. u.} \tag{26}$$

We performed calculations using this form of $\Gamma(R)$ and keeping the other potential parameters the same. The result is that the continuum coupling is not large enough to cause a significant effect on the ion pair distributions.

The charge transfer matrix element estimated from Eq. (15) is a one-electron matrix element. In fact, $\Gamma(R)$ should be larger than $\Gamma_0(R)$ to account for the two equivalent electrons in the $^2\pi_{3/2,g}$ orbital. Moreover, the $I_2$ molecule has a valence configuration $(\sigma_g 5p)^2 (\pi_{1/2,u} 5p)^2 (\pi_{3/2,u} 5p)^2 (\pi_{1/2,g} 5p)^2 (\pi_{3/2,g} 5p)^2$, and these ten electrons have vertical ionization potentials[23] between 9.3 and 13.0 eV. In the spirit of our one-electron estimate of $\Gamma_0$, we should also calculate approximate continuum coupling widths for the other electrons.

Although the ionization potential for electrons in the lowest two of these orbitals is larger than the $Ar^*$ excitation energy, Miller and Morgner[10] have shown that the electronic energy transfer to a pseudocontinuum Rydberg state,

$$Ar^* + I_2 \rightarrow Ar + I_2^{**} \tag{27}$$

(core excited in this case) can be treated in an equivalent way to a true continuum interaction. The details of the formula are slightly different; however, the calculated coupling widths are found to be quite similar to those

for states whose ionization potentials are lower than the excitation energy of the incoming state. Assuming the contributions for all ten electrons can be added (a reasonable first approximation), we obtain a resultant $\Gamma(R)$ that is 10–15 times larger than $\Gamma_0(R)$ for $R$ values between 5 and 11 a. u.

The effects of various coupling functions $\Gamma(R)$ on the calculated angular distribution for Reaction (1) at 28 eV are shown in Fig. 4. Continuum effects are generally more pronounced at lower energies, and $E_0 = 28$ eV is the lowest energy studied. Clearly $\Gamma = 10\,\Gamma_0$, which approximates the summed ten electron continuum coupling estimated above, yields a noticeable depletion of the covalent peak. However, $\Gamma > 100\,\Gamma_0$ seems required before the intensity ratios of the covalent and ionic peaks are in reasonable agreement with experiment. Since our approximate estimates of $\Gamma$ are relatively crude, it is possible that $\Gamma$ is indeed an order of magnitude larger than estimated. Hence, the continuum coupling effect could make some contribution to the attenuation of the covalent peak in Reaction (1). However, the larger $\Gamma$ values ($100\,\Gamma_0$, $1000\,\Gamma_0$) give covalent peaks that are strongly attenuated at low $\tau$ values; the angular positions of the calculated peaks then disagree considerably with the data.

### D. $Ar^* + I_2$: Sensitivity to the coupling matrix element $V_{12}$

Another possible cause for the smaller covalent peak in $Ar^* + I_2$ could be a larger coupling matrix element $V_{12}$. We have performed calculations in which $\Gamma = 0$ and the constant $c_1$ of $V_{12}$ is varied [see Eq. (7)]. We find that a significant change in $V_{12}$ from the value for $K + I_2$ is needed to cause the desired change in $Ar^* + I_2$ peak ratios. Figure 5 shows the experimental angular distribution at $E_0 = 51$ eV, compared with three calculations assuming $V_{12}$ multiplied by factors of 1.0, 2.5, and 5.0 relative to $K + I_2$. Even though the peak ratios are accurately matched by scaling $V_{12}$ by approximately 2.5, we feel that this is an unreasonable change considering the expected similarities between K and $Ar^*$. Although the potential surfaces for the two reactions have quite different symmetries, these differences are associated with the symmetry of the $Ar^*$ core. At the very large crossing radius (~5.7 Å) between the ionic and covalent surfaces, the properties of the core should play a minor role in the electron transfer process and the outer $Ar^*$ electron should behave like a $4s$ electron in K.

### E. $Ar^* + I_2$: Sensitivity to $V_{22}$

It is obvious from Fig. 5 that the calculated rainbow angle is not in good agreement with the experimental data. None of the modifications detailed above has altered the calculated rainbow position. Since its position is most sensitive to the well depth in the ionic channel, we investigated modifications to the potential parameters necessary for achieving a match to the experimental rainbow angle. In our model, the well depth is controlled by the choice of the parameters $A$ and $B$ in Eq. (6). We found that varying these parameters to decrease the well depth caused the rainbow to shift to smaller angles, as expected. Another effect of this change was
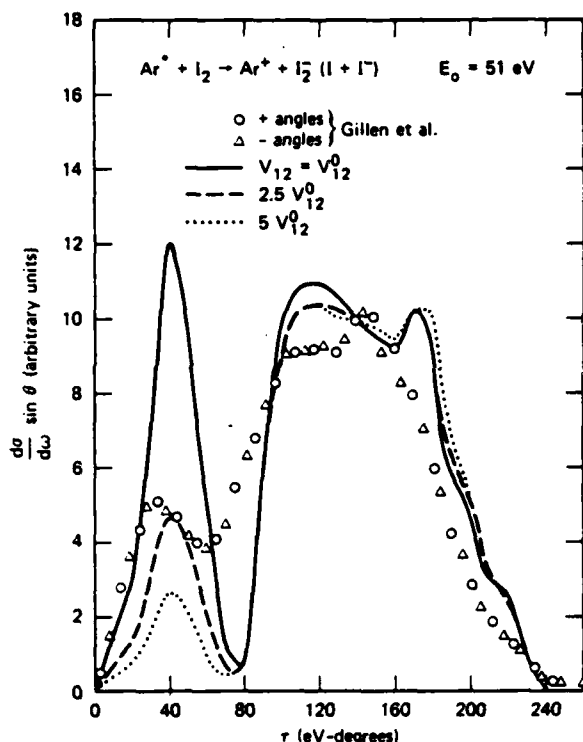
J. Chem. Phys., Vol. 73, No. 8, 15 October 1980

B-5

FIG. 5. Calculation of the differential cross section for ion pair formation in Ar* + I₂ compared with the data of Ref. 1. The effect of different coupling matrix elements $V_{12}$ is illustrated. $\Gamma(R)$ is set to zero in all cases. $V_{12}^0$ is the form given by Eq. (7) with $c_1 = 0.28$ and $c_2 = 0.65$, the same parameters used in Ref. 2 for K + I₂. The scaled values of $V_{12}$ correspond to changing $c_1$ to 0.7 and 1.4.

a reduction in the size of the covalent peak relative to the ionic peak. Figure 6 shows the effect of changes in the potential parameters upon the ion pair distributions. The modification that gave a reasonable fit to the ionic rainbow angle corresponds to an Ar*–I₂ "well depth" that is ~0.5 eV shallower than that of K* + I₂ (at the same I–I internuclear separation).

For comparison, there are good *ab initio* calculations for the diatomic potentials in ArF, KrF, and the Xe halides.[24] For each of these systems the well depths of the various ion pair states are between 0.3 and 0.7 eV shallower than those of the analogous alkali halide molecule. With spin–orbit coupling included, the three ion pair states calculated for each rare-gas halide pair differ by less than ~0.2 eV in well depth and 0.1 Å in $R_e$ from each other. If a similar result obtained for the triatomic systems, our method of treating the Ar* + I₂ system by a single (average) ion pair surface intersecting a single covalent surface would be a reasonable approximation to the average scattering on the relevant surfaces and our resultant 0.5 eV difference in Ar*–I₂ and K*–I₂ well depths would appear to be reasonable.

### F. Ar* + I₂: Conclusions

Our calculations clearly indicate that the ion pair angular distributions for Reaction (1) depend quite sensi-

tively on the shapes of the interaction potentials, the surface coupling matrix elements, and the amount of depletion from competing continuum coupling and excitation transfer channels. With only crude model potentials and order-of-magnitude estimates for the continuum coupling and excitation transfer effects, it does not seem justified to vary parameters to achieve a fit to the data that would be both model dependent and nonunique. However, an estimate of the probable causes for the differences from Reaction (2) can be useful in suggesting directions for further experimental or theoretical effort on this system.

The shift of the ionic rainbow for Reaction (1), to lower $\tau$ values than that for Reaction (2), seems to be consistent with a shallower well in the Ar* + I₂ interaction (see Fig. 6). This change also lowers the magnitude of the covalent peak relative to the ionic peak. In fact all other modifications combined would only need to lower the covalent peak by an additional 30%–40% to achieve a good agreement with the experimental data at $E_0 = 51$ eV.[25]

Combined with the change in the ionic potential described in Sec. E, an increase of $c_1$ by ~40% over the K + I₂ value (0.28) would achieve a reasonable match to the experimental data. However, such a change in $V_{12}$ still seems rather large. As evidence for this assertion, we note that Hubers *et al.*[26] present a reduced matrix element formula that is slightly modified from Eq. (7) and correlates with all alkali–halogen systems to an accuracy of better than 10%. The modification of the
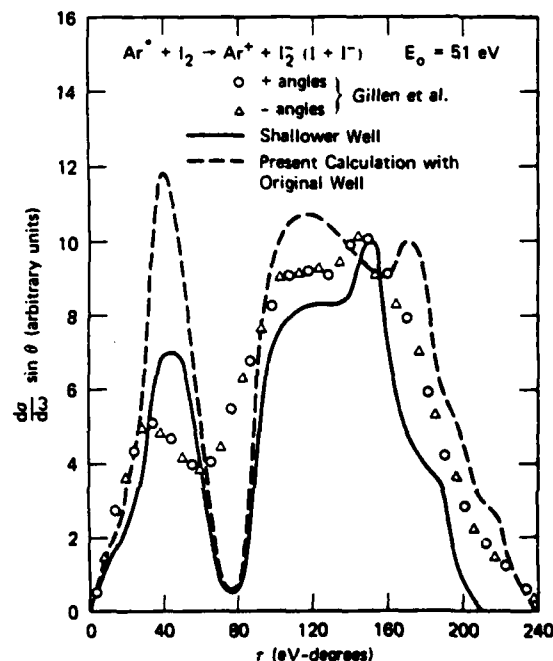


FIG. 6. Calculation of the differential cross section for ion pair formation in Ar* + I₂ compared with the data of Ref. 1. The potential parameters, defined in Eqs. (4)–(6), are $A = 6.4 \times 10^4$ eV and $B = 4.762$ Å⁻¹ for the original well, and $A = 1.35 \times 10^4$ eV and $B = 3.781$ Å⁻¹ for the shallower well.

J. Chem. Phys., Vol. 73, No. 8, 15 October 1980

B-6

Ar* + I₂ matrix element postulated here would deviate by 40% from the prediction[26] based on the alkali data and would then suggest some real differences of Ar* from alkalilike properties at distances of $R_c \approx 5.7$ Å. It is difficult to understand such a large effect at that distance caused by a vacancy in the ion core.

Alternatively, a continuum coupling width of ~200 $\Gamma_0$ could be combined with the shallower ionic potential to match the peak ratios adequately. This width is somewhat larger than the rough estimate (10–15 $\Gamma_0$) based on the Miller–Morgner[10] arguments, and the attenuated covalent peak would be located at larger $\tau$ values than the data would allow. Yet our estimate of $\Gamma$ is subject to considerable uncertainty and could be significantly in error. Also, the covalent peak position and shape are sensitively dependent on the potential functions used. This has been demonstrated[4] in K + Br₂ by a comparison of calculations on diabatic and adiabatic surfaces. Hence, continuum coupling (3) and excitation transfer (27) reactions involving the ten valence I₂ electrons could be responsible for all or part of the remaining 30%–40% depletion of the covalent peak.

Finally, we note that making the potentials more repulsive tends to decrease the size of the covalent peak relative to the ionic peak. For simplicity, we have constrained our calculations so that the repulsive Born–Mayer terms are identical on the ionic and covalent surfaces. Although this is a reasonable first approximation, one could decrease the covalent peak by relaxing this constraint and allowing more repulsion in the covalent potential. If such a difference were responsible for the smaller covalent peak in (1) relative to (2), it would necessarily imply differences between the two systems in the repulsive region. This is easier to accept than large differences (40%) in the coupling matrix elements at the much larger distances associated with the surface crossings.

## IV. SUMMARY

The small differences between the differential cross sections for ion pair formation in the Ar* + I₂ and K + I₂ system can be explained, in part, by a more repulsive wall in the ionic Ar* + I₂⁻ surface relative to K⁺ + I₂⁻. This yields a smaller ionic well depth (by ~0.5 eV at $r_e$ of I₂) and a correspondingly smaller ionic rainbow angle that is in agreement with the data. If the covalent surfaces Ar* + I₂ and K + I₂ have repulsive terms similar to those on their ionic counterparts, the calculated ratio for the intensity of the covalent peak to the ionic peak in Reaction (1) is too large by a factor of ~1.4.

This ratio can be improved by one or more of the following: a relative increase in the repulsion on the Ar* + I₂ covalent surface; a depletion of the covalent peak by competing Penning (3) and excitation transfer (27) reactions; and an increase in the coupling matrix element at the surface crossing between the ionic and covalent surfaces. The third possibility seems least likely since it requires effects from the Ar* core vacancy to be important at large R (~5.7 Å).

Since the potential surfaces have only been estimated in a crude way and since the continuum coupling width is

only known very approximately, we feel that no claim to a unique fit can be made. Continuum coupling and excitation transfer processes may indeed cause observable, but small, depletions of the covalent peak in the ion pair process (1).

[1]K. T. Gillen, T. D. Gaily, and D. C. Lorents, Chem. Phys. Lett. 57, 192 (1978).

[2]J. A. Aten, G. E. H. Lanting, and J. Los, Chem. Phys. 19, 241 (1977).

[3]J. A. Aten, G. E. H. Lanting, and J. Los, Chem. Phys. 22, 333 (1977).

[4]J. A. Aten and J. Los, Chem. Phys. 25, 47 (1977).

[5]J. Los, in Proceedings of the Tenth International Conference on the Physics of Electronic and Atomic Collisions, Invited Papers and Progress Reports, edited by G. Watel (North-Holland, Amsterdam, 1978), p. 617.

[6]J. Los and A. W. Kleyn, in Alkali Halide Vapors, edited by P. Davidovits and D. L. McFadden (Academic, New York, 1979), p. 275.

[7]S. Wexler and E. K. Parks, Ann. Rev. Phys. Chem. 30, 179 (1979).

[8]J. C. Tully and R. K. Preston, J. Chem. Phys. 55, 562 (1971).

[9]R. K. Preston and R. J. Cross, J. Chem. Phys. 59, 3616 (1973).

[10]W. H. Miller and H. Morgner, J. Chem. Phys. 67, 4923 (1977).

[11]N. F. Mott and H. S. W. Massey, The Theory of Atomic Collisions (Clarendon, Oxford, 1965), 3rd ed., p. 353.

[12]M. Born and J. E. Mayer, Z. Phys. 75, 1 (1932).

[13]E. A. Gislason and J. G. Sachs, J. Chem. Phys. 62, 2678 (1975).

[14]L. D. Landau and E. M. Lifshitz, Mechanics (Pergamon, Oxford, 1969), 2nd ed., pp. 55–56.

[15]L. D. Landau, J. Phys. (USSR) 2, 46 (1932), C. Zener, Proc. R. Soc. London Ser. A 137, 696 (1932).

[16]W. H. Miller, Chem. Phys. Lett. 4, 627 (1970).

[17]W. H. Miller, J. Chem. Phys. 52, 3563 (1970).

[18]R. E. Olson, F. T. Smith, and E. Bauer, Appl. Opt. 10, 1848 (1971).

[19]A. P. Hickman, A. D. Isaacson, and W. H. Miller, J. Chem. Phys. 66, 1483 (1977).

[20]A. P. Hickman and H. Morgner, J. Phys. B 9, 1765 (1976).

[21]Z. F. Wang, A. P. Hickman, K. Shobatake, and Y. T. Lee, J. Chem. Phys. 65, 1250 (1976).

[22]W. Hultzsch, W. Kronast, A. Niehaus, and M. W. Ruf, J. Phys. B 12, 1821 (1979).

[23]D. C. Frost, C. A. McDowell, and D. A. Vroom, J. Chem. Phys. 46, 4255 (1967); A. B. Cornford, D. C. Frost, C. A. McDowell, J. L. Ragle, and I. A. Stenhouse, J. Chem. Phys. 54, 2651 (1971).

[24]T. H. Dunning, Jr. and P. J. Hay, J. Chem. Phys. 69, 134 (1978); P. J. Hay and T. J. Dunning, Jr., J. Chem. Phys. 69, 2209 (1978).

[25]That experiment is considered the most reliable, since the signal levels were much smaller at lower energies ($E_0$ = 28 eV) and the angular resolution was much lower at higher energies.

[26]M. M. Hubers, A. W. Kleyn, and J. Los, Chem. Phys. 17, 303 (1976).

J. Chem. Phys., Vol. 73, No. 8, 15 October 1980

B-7

# APPENDIX C

## SCHEMATIC MODEL FOR THE DIFFERENTIAL CROSS SECTION IN ION-PAIR FORMATION

Keith T. GILLEN and A.P. HICKMAN
*Molecular Physics Laboratory, SRI International, Menlo Park, California 94025, USA*

An analytic approximation to the differential cross section is derived for ion-pair formation in a model two-state ("turned-on Coulomb") system. The result gives insight into the structure observed in recent experiments.

## 1. Introduction

Ion-pair formation differential cross sections have been measured recently for fast collisions of alkali atoms [1] and metastable rare gas atoms [2] with various targets. The results usually have similar basic features that result from a crossing between the incoming covalent potential surface and a strongly attractive ion-pair surface. The ion-pair product angular distribution generally exhibits two peaks, the "ionic" and the "covalent" peaks, resulting from trajectories that, at internuclear separations smaller than the surface crossing distance, travel along the ionic and covalent surfaces, respectively. The ionic peak, located at larger angles, often has a single secondary maximum or shoulder on its low-angle side. This secondary structure is observed with many molecular targets [1,2], but also appears in the simple two-body reaction $Na + I \rightarrow Na^+ + I^-$ [3]. In this paper we present a very simple model that highlights the origin of this secondary maximum and suggests why it appears in *some systems but not in others*.

## 2. Model

In this section we derive an analytic approximation to the differential cross section for ion-pair formation under idealized assumptions about the two electronic potentials involved. We find, a posteriori, that the trajectories that contribute to the secondary maximum only probe the potentials in a range where our approximations are reasonably accurate.

Consider the model potentials shown in fig. 1. We assume that the ionic potential is given by the pure Coulomb form $V_1(R) = -1/R$. Let $\Delta E$ be the energy difference between the neutral (covalent) and ion-pair channels. Then if the zero of energy is defined to be the asymptote of the ionic potential, the covalent curve is approximated by the constant value $V_0(R) =$
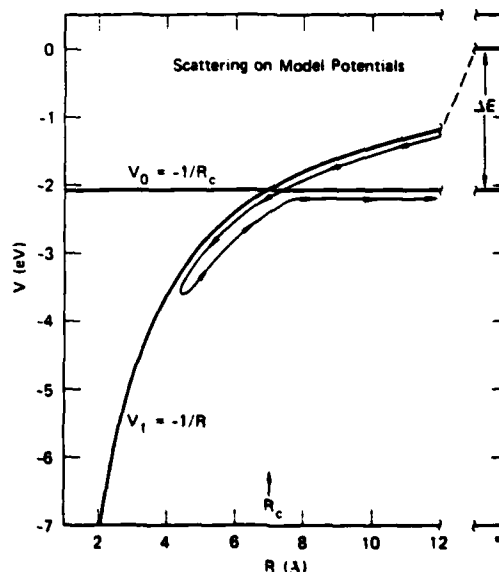


Fig. 1. Model potentials and curve crossing sequence for the time-reversed ionic trajectory that converts ion-pair reactants to neutral products.

$-\Delta E = -1/R_c$, where $R_c$ is the crossing point of $V_0(R)$ and $V_1(R)$. (Atomic units are used throughout this section unless otherwise indicated.) For these idealized potentials, the deflection function (scattering angle versus impact parameter) can be determined analytically for trajectories that begin asymptotically on $V_0$ and end up on $V_1$ after a curve crossing at $R_c$. The deflection function has two branches, corresponding to trajectories that make the crossing on the inward or outward part of the classical motion.

It is convenient to begin by considering the time-reversed trajectory shown by the arrows in fig. 1. Let $E$ and $b$ denote the c.m. collision energy and impact parameter relative to the ionic asymptote. We denote by $E'$ and $b'$ the corresponding quantities relative to the covalent asymptote. Clearly $E' = E + \Delta E$; the relation between $b$ and $b'$ is obtained by invoking the fact that the angular momentum must be the same at $t = +\infty$ and $t = -\infty$. The result is

$$b' = b[1 - (\Delta E)/E']^{1/2}. \tag{1}$$

Using the potentials shown in fig. 1, the c.m. scattering angle $\theta$ for an impact parameter $b$ is given by [4]

$$\theta = \pi - b \int_{R_0}^{\infty} (dR/R^2)(1 - b^2/R^2 + 1/RE)^{-1/2}$$

$$- b \int_{R_0}^{R_c} (dR/R^2)(1 - b^2/R^2 + 1/RE)^{-1/2}$$

$$- b \int_{R_c}^{\infty} (dR/R^2)(1 - b^2/R^2 + 1/R_cE)^{-1/2}. \tag{2}$$

The turning point $R_0$, which depends on $b$, is obtained from the relation

$$1 - b^2/R_0^2 + 1/R_0E = 0, \tag{3}$$

and $b \leqslant (R_c^2 + R_c/E)^{1/2}$ is necessary to reach $R_c$. After some algebraic and trigonometric manipulation, eq. (2) can be solved exactly for the deflection function

$$\theta = -\arcsin Y - \arcsin[Y(1 - b^2U)^{1/2}], \tag{4}$$

where

$$Y = (1 + 4b^2E^2)^{-1/2} \tag{5}$$

and

$$U = (R_c^2 + R_c/E)^{-1}. \tag{6}$$

The first term in eq. (4) is exactly half the Rutherford deflection angle $\theta_R$ for pure coulombic scattering

$$\theta_R = -2 \arcsin Y = -2 \arctan(1/2BE). \tag{7}$$

The alternative covalent path, which involves a transfer from the coulombic to the flat potential on the inward portion of the trajectory, has a deflection angle $\theta'$ given by

$$\theta' = \theta_R - \theta, \tag{8}$$

so that the covalent and ionic branches of the deflection function yield scattering angles at every $b$ that add up to $\theta_R$ for the same $b$. Considering the limiting case where the two branches of the deflection function meet for a turning point $R_0(b^*) = R_c$, one obtains from eq. (3)

$$b^* = U^{-1/2}$$

and the second term in eq. (4) vanishes, implying that

$$\theta^* = -\arcsin Y = \tfrac{1}{2}\theta_R. \tag{9}$$

Alternatively, eq. (8) and the requirement that $\theta' = \theta$ yield the same result. Using eq. (3) this can be reduced to

$$\theta^* = -\arcsin[1/(1 + 2R_cE)]. \tag{10}$$

One can show that this result is in agreement with a formula given by Young et al. [5] for the same limiting angle.

A single approximation, the small-angle approximation $\tan \theta \approx \theta$, is all that is required to invert the deflection function and obtain the differential cross section. Eq. (4) becomes

$$\theta = -(1/2bE)[1 + (1 - b^2U)^{1/2}], \tag{11}$$

and the differential cross section for the inverse of ion pair formation $(d\sigma_{01}/d\omega) \sin \theta$ is given by

$$(d\sigma/d\omega) \sin \theta = |b \, db/d\theta|$$

$$= |16E^2\theta(U - 4E^2\theta^2)/(4E^2\theta^2 + U)^3|. \tag{12}$$

Surprisingly the identical eq. (12) is obtained for the covalent branch of the deflection function. Note that as $R_c \to \infty$, the limit of purely coulombic scattering, eq. (12) would yield

$$(d\sigma/d\omega) \sin \theta \to 1/E^2\theta^3, \tag{13}$$

C-2

which agrees with the Rutherford result under the same small angle approximation $\theta \approx \tan \theta \approx \sin \theta$.

Eqs. (12) and (1) can be used to obtain the differential cross section for the ion-pair formation process (which will be called "turned-on Coulomb scattering")

$$(d\sigma_{10}/d\omega) \sin \theta = |b' \, db'/d\theta| \tag{14}$$

$$= (1 - \Delta E/E')[16E^2\theta/(4E^2\theta^2 + U)^3]|U - 4E^2\theta^2|.$$

Differentiation shows that this function has two peaks at reduced deflection angles

$$\tau_1 \equiv E'\theta = 0.181E'U^{1/2}/E \tag{15}$$

and

$$\tau_2 = 0.796E'U^{1/2}/E. \tag{16}$$

The function drops to zero between these peaks when $|U - 4E^2\theta^2| = 0$ and

$$\tau_{min} = 0.5E'U^{1/2}/E. \tag{17}$$

Eq. (17) is an alternative small angle approximation to eq. (10), and locates the minimum in the differential cross section between the ionic and covalent branches. The peak $\tau_1$ will be seen to approximate the position of the covalent peak, while $\tau_2$ gives a simple first approximation to the position of the secondary maximum. Clearly, the ionic rainbow [1] maximum cannot be obtained in our simple model that neglects repulsive forces entirely.

By solving eq. (11) for $b$, one can demonstrate that the coulombic impact parameter $b_2$ that corresponds to the peak in the differential cross section at $\tau_2$ is

$$b_2 = 0.901U^{-1/2}. \tag{18}$$

Then the corresponding impact parameter along the flat asymptote is

$$b_2' = 0.901R_c. \tag{19}$$

The analogous result for the covalent peak is

$$b_1' = 0.641R_c. \tag{20}$$

## 3. Example: Na + I

Delvigne and Los [3] have measured differential cross sections for the reaction

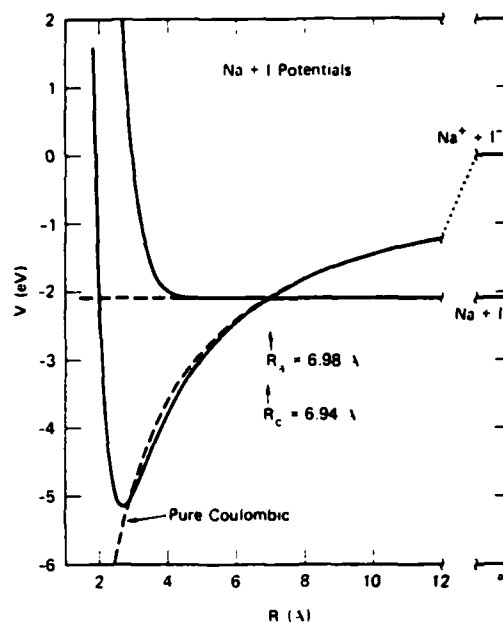$$Na + I \rightarrow Na^+ + I^- \tag{21}$$



Fig. 2. NaI potentials of Delvigne and Los (————) compared to our model potentials (– – –) for the same system.

and have calculated deflection functions for this system us..g a multi-term potential function. Their potentials are shown in fig. 2 along with idealized curves consistent with our model developed in section 2. The major differences in the realistic potentials are, of course, the repulsive terms in both the ionic and covalent curves, but there are $R^{-4}, R^{-6}$, and $R^{-7}$ attractive terms in their Rittner $Na^+ + I^-$ potential that cause it to be more attractive for $R \gtrsim 3$ Å and move the curve crossing out to $R_a = 6.98$ Å compared to the coulombic $R_c = 6.94$ Å for the simpler approximation.

Fig. 3 shows deflection functions for reaction (21) at $E_c = 13.1$ eV. Results of Delvigne and Los are compared to our calculations using eqs. (4) and (8). The coulombic case [from eq. (7)] is also shown for comparison. Here our results deviate from those of Delvigne and Los in ways that are easily associated with the differences in the potentials shown in fig. 2.

The measured differential cross sections for reaction (21) at two energies are shown in fig. 4 along with our curves calculated from eq. (14). The Ruther-
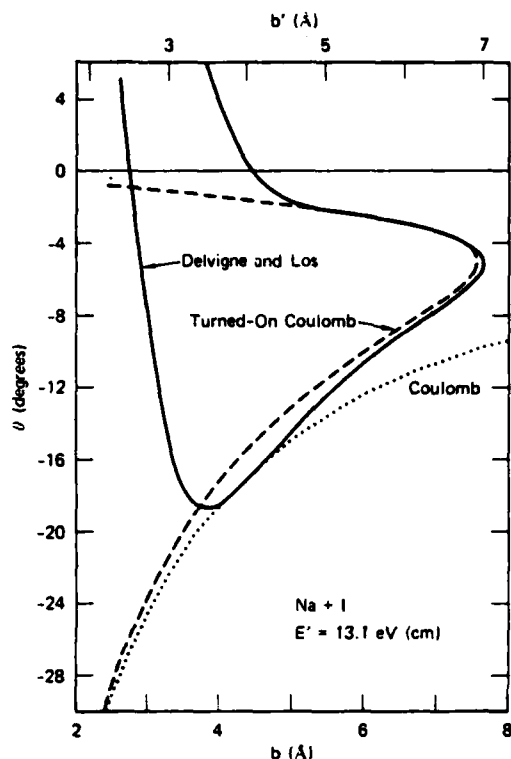
Fig. 3. Deflection functions for reaction (21) at $E' = 13.1$ eV. The results of Delvigne and Los (——) are plotted versus the covalent impact parameter $b'$. Our results from eqs. (4) and (8) (– – –) have impact parameters $b'$ and $b$ at large distances along the flat and coulombic potentials, respectively. Shown for comparison is a pure coulombic deflection function plotted versus $b$ from eq. (7) (··········) for $R_c \to \infty$, $E' \to E$.
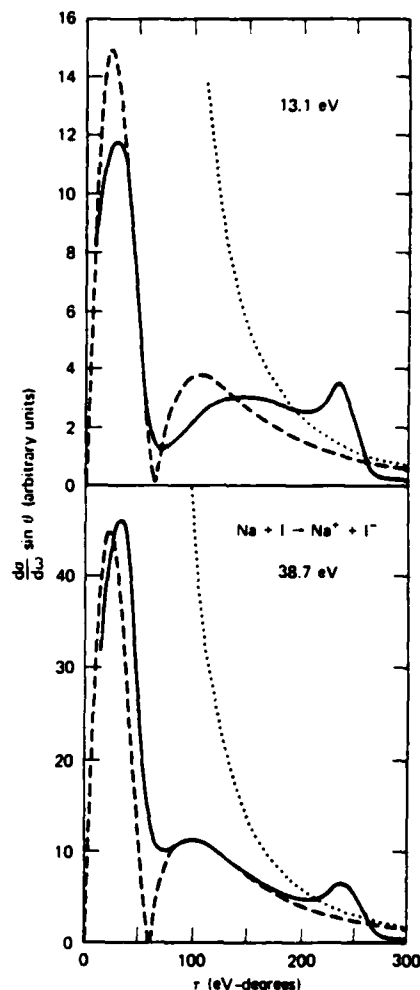


Fig. 4. Smoothed differential cross section measurements for reaction (21) from Delvigne and Los (——) compared to our turned-on Coulomb calculations (– – –) and purely coulombic (Rutherford) results (··········) under the small angle approximation $\theta \approx \sin \theta \approx \tan \theta$. The calculations have not been smoothed to account for apparatus resolution parameters. The abscissa $\tau$ is the product of the collision energy and the scattering angle.

ford cross sections derived from eq. (13) are also shown for comparison. Clearly the turned-on Coulomb calculation cannot produce the ionic branch rainbow at $\tau \approx 240$ eV deg since repulsive terms are not included. Yet the calculation at 38.7 eV matches all other major features of the experimental results, in particular the shape and position of the intermediate secondary peak. This may seem surprising, since the calculation does not take into account the probability $P(b')$ for crossing from one curve to another at the point $R_c$. This neglect is in effect equivalent to an assumption that the probability of following either path, $P(1 - P)$ or $(1 - P)P$, is nearly constant for all $b'$

values contributing to the intermediate peak region of the differential cross section. Coincidentally, this seems to be the case [3] at $E' \approx 39$ eV.

At the lower energy $E' = 13$ eV, the calculation does not match the position of the experimental inter-

mediate peak. In this case the diabatic probability is significantly less than 0.5, and $(1 - P)P$, the overall branching probability for following the ionic path, decreases strongly as $b'$ increases toward $R_c$. This decreases the low-angle side of the intermediate peak and causes the experimental peak position to shift to larger $\tau$ values.

Better agreement with the experimental data at 13 eV could obviously be achieved by using estimates of the coupling matrix elements to weight the differential cross sections by Landau–Zener curve-crossing probabilities $P(1 - P)$ as a function of $b$. An even better fit would be achieved by using improved potentials in the crossing region [6]. However, the point of the present example is that the *existence* of the intermediate peak in the angular distribution can be explained without invoking these complications. Variation of $P$ with $b$ and adiabatic corrections to the potential can be viewed as secondary effects that do not cause the intermediate peak, but merely modify its shape and position.

In addition, bond stretching of the molecular ion on the ion-pair surface can dramatically modify branching ratios [7]. Orientation effects are also important, since coupling matrix elements can have strong dependences on collision geometry [8]. Finally, adiabatic prestretching can yield ion-pair products for impact parameters larger than the nominal $R_c$ value [9]. These molecular effects taken together can shift, modify, enhance, or mask the intermediate peak. Other more detailed, theoretical treatments [7,9,10], relying heavily on numerical calculation, have been used to investigate these molecular effects. We have no reason to add these complications to our very simple model.

Our primary goal in this paper has been the development of a simplified, analytic model that illuminates the basic cause for the secondary peak sometimes observed in ion-pair formation differential cross sections. Knowledge of the simplest framework for describing this peak should aid in the application and interpretation of more sophisticated calculations.

## 4. Discussion

The example in the preceding section clearly is a good system for applying our simple model. The fact that the surface crossing distance $R_c$ is much larger than the region where repulsive terms become important implies a reasonable separation between the secondary peak and the ionic rainbow. This separation is evident from a comparison of the impact parameters corresponding to the secondary peak $[b_2 \approx 6.3 \text{ Å}$ from eq. (19)] with the impact parameters important in the rainbow region (see fig. 3). The large value of $R_c$ also implies that our idealized potentials are reasonable approximations to the true potentials for distances important in the secondary peak region. Finally, reaction (21) does not have any of the complications associated with molecular targets.

In other systems where the crossing distance $R_c$ is closer to the minimum in the ion-pair potential, the secondary peak and the ionic rainbow peak will be closer together. In some cases they may coalesce into one single unresolved peak. Likewise, the covalent peak may also be attenuated by repulsive interactions that spread the scattering over a wider angular range.

Molecular targets [1] indeed have much lower vertical electron affinities than I atoms and the surface crossings are located at much smaller distances.

## References

[1] J. Los and A.W. Kleyn, in: Alkali halide vapors, structure, spectra, and reaction dynamics, eds. P. Davidovits and D.L. McFadden (Academic Press, New York, 1979) p. 275.

[2] K.T. Gillen, T.D. Gaily and D.C. Lorents, Chem. Phys. Letters 57 (1978) 192.

[3] G.A.L. Delvigne and J. Los, Physica 67 (1973) 166.

[4] L.D. Landau and E.M. Lifshitz, Mechanics (Addison-Wesley, Reading, 1969) pp. 48–57.

[5] C.E. Young, R.J. Beuhler and S. Wexler, J. Chem. Phys. 61 (1974) 174.

[6] M.B. Faist and R.D. Levine, J. Chem. Phys. 64 (1976) 2953.

[7] M.M. Hubers, A.W. Kleyn and J. Los, Chem. Phys. 17 (1976) 303;
J.A. Aten, G.E.H. Lanting and J. Los, Chem. Phys. 19 (1977) 241.

[8] E.A. Gislason and J.G. Sachs, J. Chem. Phys. 62 (1975) 2678.

[9] J.A. Aten and J. Los, Chem. Phys. 25 (1977) 47.

[10] Ch. Evers, Chem. Phys. 21 (1977) 355.

## Collisional Excitation of Ar* + O₂ Mediated by Ion-Pair Formation

Keith T. Gillen

*Molecular Physics Laboratory, SRI International, Menlo Park, California 94025*

and

Thomas M. Miller

*Molecular Physics Laboratory, SRI International, Menlo Park, California 94025, and Physics Department,*
*University of Oklahoma, Norman, Oklahoma 73019*[a]

For Ar* + O₂ collisions at ≈ 100 eV energies an intense rainbow peak has been observed in the neutral-product angular distribution. The surprisingly large inelasticities (1–2 eV) and the absence of elastic scattering in this small-angle feature are explained by a charge-transfer model involving transient formation of an $Ar^+ + O_2^-$ intermediate. Large product inelasticities are understood by examing the relative timing of the projectile motion and the $O_2^-$ vibration on the intermediate surface.

We describe detailed double-differential cross-section measurements for the interaction of a metastable-argon beam with O₂ target molecules. Ion-pair surfaces $(Ar^+ + O_2^-)$ play a key role in this system and indeed we find that Ar⁺ ions are an important reaction product. Here we present dramatic evidence that the ion-pair surface also acts as an intermediate state in an important inelastic energy transfer process yielding *neutral* products. This process yields unexpectedly large values of translational- to internal-energy transfer for interactions occurring at relatively large impact parameters. The large inelasticities and the apparent absence of elastic scattering for these ion-pair–mediated collisions will be explained here using a very simple model that compares the timing of the relative translational motion to that of the vibrational motion of the transient $O_2^-$ intermediate ion. In this work, we are probing the crucial energy range where the collisional time and vibrational period are of comparable size.

Our apparatus[1] and techniques[2] have been described previously. Briefly, an $Ar^*(^3P_{0,2})$ beam, produced by near-resonant charge transfer of Ar⁺ in Rb vapor, enters a collision cell filled with O₂. The angular-energy distribution of Ar⁺ product ions from

$$Ar^* + O_2 \rightarrow Ar^+ + O_2^- \qquad (1)$$

is measured by a rotatable Channeltron mounted behind a 127° electrostatic energy analyzer. A second rotatable Channeltron detector is used to determine the angular distribution of scattered neutral products. Time-of-flight (TOF) techniques are used to measure velocity distributions and determine inelasticities for these scattered neutrals.

The angular distribution of Ar⁺ product ions seen in Fig. 1(a) has a single peak at 1.4°, an intense rainbow feature caused by the potential well of the $Ar^+ + O_2^-$ surface [see Fig. 2(a)] for trajectories that transfer to the ion-pair surface on the initial inward passage through the surface crossing.

We observe a similar rainbow peak at a nearly identical angle in measurements of the neutral-product angular distribution [Fig. 1(b)]. This rainbow must also result from trajectories that sampled the ionic potential well during the collision, since purely repulsive scattering on the upper covalent potential would yield a monotonic, nearly flat, ρ vs θ distribution. A second, nearly flat, underlying contribution evident in Fig. 1(b) can be associated with these purely repulsive interactions.

TOF measurements give additional evidence for the two separate major pathways to neutral products. Figure 3 shows a typical Ar* TOF distribution at an angle in the rainbow region. The distribution can be characterized by its nominal c.m. exothermicity value Q (~ − 0.73 eV) and its energy width W [~ 3.0 eV full width at half maximum (FWHM)]. When measured values of W and Q are plotted vs θ in Figs. 1(c) and 1(d), it is evident that the rainbow region has anomalously large values of inelasticity and inelastic widths compared to the distributions at wider angles. The underlying covalent repulsive scattering has a gradually increasing inelasticity (and a slightly increasing width) as the angle increases. This is consistent with a simple momentum-transfer
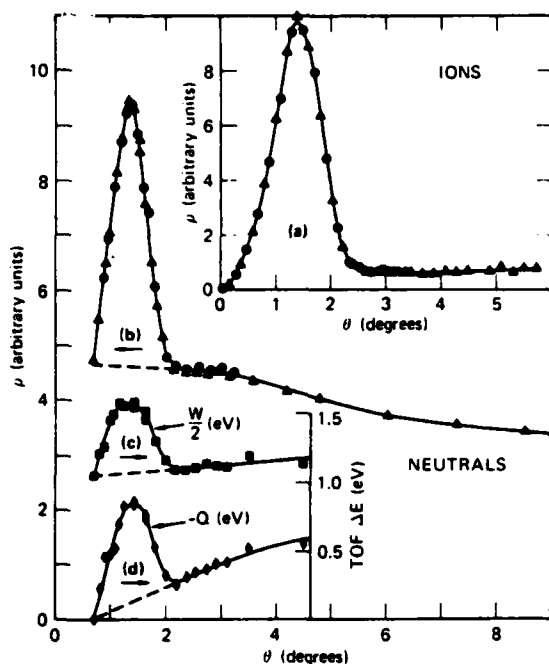
FIG. 1. Data for $Ar^* + O_2$ collisions at a beam energy $E_0 = 114$ eV. (a) Product $Ar^+$ laboratory angular distribution; plotted is $\rho = \theta\sin\theta\, d\sigma/d\omega$. (b) Scattered $Ar^*$ angular distribution. (c) Half-width of the $Ar^*$ energy distribution vs $\theta$. (d) $Ar^*$ c.m. energy loss vs laboratory $\theta$.



FIG. 2. Cuts through the two (idealized) potential surfaces. (a) A cut at the $O_2$ equilibrium separation $r = r_e$, showing the initial surface crossing at $R = R_c = 3.44$ Å. $R$ is the distance from the atom to the center of the molecule. (b) Cuts at fixed $R$. At the initial idealized crossing ($R = R_c = 3.44$ Å) the $O_2^-$ is formed compressed; as it vibrates (changes of $r$ along horizontal line in $O_2^-$ potential well), the surface crossing distance at the second crossing $R_c'$ also varies ($3.44$ Å $\leq R_c' \leq 5.78$ Å). The $Ar^* + O_2$ curve is essentially unchanged for $3.44$ Å $\leq R \leq 5.78$ Å, while the $Ar^+ + O_2^-$ curve moves vertically $\propto -1/R$.

process at small $R$. The width, average $Q$ value, and fractional contribution of the covalent component can readily be extrapolated into the rainbow region, as shown by the dashed lines in Fig. 1. This allows one to estimate and remove the covalent contribution from TOF distributions measured in the rainbow region and to obtain the resultant, highly inelastic, contribution from the ion-pair–mediated process (see, e.g., Fig. 3),

$$Ar^* + O_2 \to [Ar^+ \cdot O_2^-] \to Ar^* + O_2 + Q. \tag{2}$$

Similar large inelasticities are obtained at other angles in the rainbow region for process (2). At lower energies ($E_0 \sim 70$–$90$ eV), this inelasticity decreases slightly; otherwise the results are quite similar to those shown here. Clearly process (2) yields very little elastic ($Q = 0$) scattering. The true elastic contribution is even smaller than it appears in Fig. 3, since the TOF distributions have not been corrected for experimental resolution (an apparatus resolution FWHM, estimated from TOF beam profiles, is shown in Fig. 3).
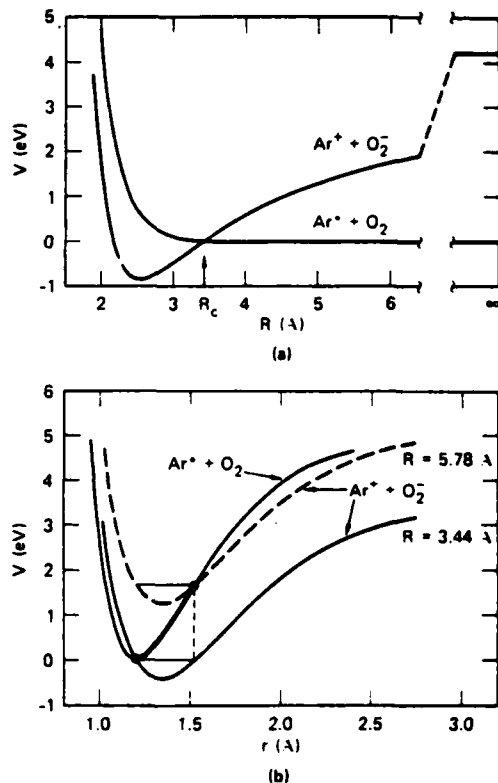
We believe that the large inelasticities and negligible elastic scattering for process (2) in the rainbow region can be understood as a simple consequence of the timing of $O_2^-$ bond stretching (and subsequent vibration) between the two surface crossings on the incoming and outgoing portion of the trajectory. Vibrational timing[3] has indeed been invoked[4] to explain oscillations in the energy dependence of total cross sections for ion-pair formation in the similar Cs and K $+O_2$ systems. The effects of $O_2^-$ vibrational timing have also been observed quite recently in the product angular[5] and energy[6] distributions for these related systems.
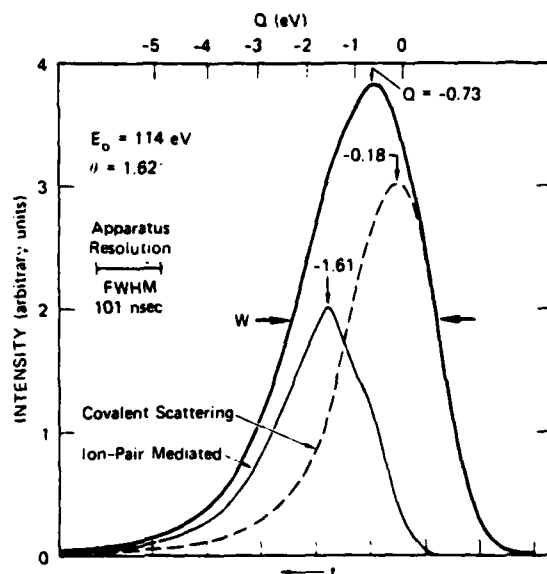
FIG. 3. Typical Ar* TOF (and energy-loss) spectrum in the rainbow region. The observed spectrum (heavy line) has contributions from (a) pure covalent scattering (dashed curve) and (b) ion-pair–mediated inelastic scattering (light solid line). The dashed curve is estimated from TOF distributions obtained just beyond the rainbow region, shifted to the energy loss at 1.62° indicated by the dashed portion of Fig. 1(d), and normalized to give branching ratios consistent with the partitioning in Fig. 1(b). The light solid curve is obtained by subtraction.

We use a simplified classical picture to illuminate the basic physics underlying the mechanism. Assume that the $O_2^-$ and $O_2$ potential curves are not perturbed by $Ar^+$ and $Ar^*$, respectively, at distances $R > R_c = 3.44$ Å, that the Coulombic term $-1/R$ dominates the ion-pair interaction at these distances, that the $O_2$ begins at rest at the bottom of its well at $r_e(O_2)$, that transitions between diabatic electronic states occur vertically (with $r$ unchanged) and only at the surface crossing seam, that electron transfer (at $t = 0$) initiates a vibration (initially an expansion) of $O_2^-$, and that the motions along $r$ and $R$ on the ion-pair surface evolve independently. Figure 2(b) shows the $Ar^*$ $+O_2$ and $Ar^+ +O_2^-$ surfaces at $R = 3.44$ Å, the distance ($R = R_c$) corresponding to the initial transition to the ionic surface. In our simple picture, the $O_2^-$ is produced with a particular internal energy (shown by the horizontal line going to the right from the intersection point). As $R$ decreases to its minimum value (at the turning point) and
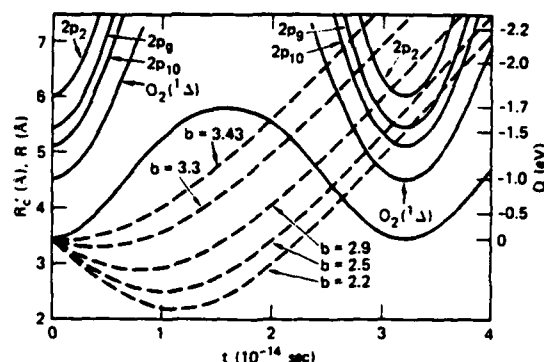


FIG. 4. Dependence of $R_c'$ (solid lines) and $R$ (dashed lines) on time $t$ after the initial transfer to the ion-pair surface. $R_c'$ is shown (unlabeled) for the incoming neutral electronic states and (labeled) for several higher neutral states of Ar or $O_2$. $R(t,b,E_0)$ is shown for several $b$ (in Å) and for $E_0 = 114$ eV.

then increases, the $O_2^-$ vibrates. A knowledge of the shapes of the $O_2$ and $O_2^-$ curves allows an estimate[4] of the time dependence of the surface crossing radius $R_c'(t)$ to be made from the classical vibrational timing, $r(t)$, of the $O_2^-$. $R_c'(t)$ depends on the $Ar^*$ ionization potential, $\varphi_{IP}$, and the time-dependent vertical electron affinity of $O_2$, $\varphi_{EA}(r(t))$, via $R_c'(t) \approx (14.4 \text{ eV Å})/[\varphi_{IP} - \varphi_{EA} \times (r(t))]$. The relative timing of the translational motion and the $O_2^-$ vibration determine the $r$ and $R$ values for the second surface crossing. With proper timing a fully expanded $O_2^-$ (after 0.5 vibrations) could recross to the covalent surface at $R = 5.78$ Å [see Fig. 2(b)], producing an inelastic excitation of $O_2$ by ~1.7 eV.

Figure 4 shows the dependence of $R_c'$ and $R$ on the time $t$ after the initial surface crossing on the incoming trajectory. $R(t)$ was calculated using straight-line trajectories for simplicity. For a given $b$, the intersection of $R(t)$ and $R_c'(t)$ determines the time of the second crossing and the inelasticity of reaction (2), $Q = -14.4(1/R_c - 1/R_c')$, for those collisions returning to the covalent surface at the second crossing. Note that the initial expansion of $R_c'$ is so rapid that trajectories with $b$ values just inside of the crossing at $R = 3.44$ Å cannot overtake it and must meet it later as it contracts. The long time spent on the ionic surface and the resultant significant attractive interactions are responsible for the rainbow feature in the neutral scattering [Fig. 1(b)] occurring at an angle comparable to the rainbow peak angle in the ionic scattering [Fig. 1(a)] of re-

D-3

action (1). Classical deflection function calculations[7] for the ion-pair–mediated process (2) show that the impact-parameter range $2.5 \text{ Å} \le b \le 3.44$ Å contributes to the rainbow feature. Hence, in this simple picture, the rainbow feature of the neutrals would yield inelasticities between $\sim 1.0$ and 1.6 eV.

This simple model explains the lack of elastic scattering in the rainbow region for reaction (2); but it slightly underestimates the average inelastic scattering values. Although relaxing some of our simplifying assumptions might yield a better fit to the data, the basic physics is clearly already contained in the model. One possible route to larger inelasticities involves transfer from the ion-pair intermediate surface to more highly excited neutral surfaces. The crossing radii $R_c'$ between the ion-pair surface and higher neutral surfaces also oscillate with time. A few examples are shown in the upper portion of Fig. 4. Although the larger values of $R_c'$ seem to imply smaller coupling matrix elements and thereby much lower adiabatic crossing probabilities,[3] there may be other factors favoring production of electronically excited states. In fact, the radial motion of the particles $[R(t)]$ relative to that of the *moving* crossing $[R_c'(t)]$ should be the radial velocity appropriate for estimating curve-cross-

ing probabilities. In the extreme case, when the crossing sphere is expanding rapidly and parallel to $R(t)$, e.g., for $b = 2.5$ and the $2p_2$ state of Ar in Fig. 4, the interaction can be profoundly altered. Significant electronic excitation might result.

[a]Present address.

[1]R. Morgenstern, D. C. Lorents, J. R. Peterson, and R. E. Olson, Phys. Rev. A 8, 2372 (1973).

[2]K. T. Gillen, T. D. Gaily, and D. C. Lorents, Chem. Phys. Lett. 57, 192 (1978); T. M. Miller and K. T. Gillen, Phys. Rev. Lett. 44, 776 (1980).

[3]J. Los and A. W. Kleyn, in *Alkali Halide Vapors. Structure, Spectra, and Reaction Dynamics*, edited by P. Davidovits and D. L. McFadden (Academic, New York, 1979), p. 275.

[4]A. W. Kleyn, M. M. Hubers, and J. Los, Chem. Phys. 34, 55 (1978).

[5]A. W. Kleyn, V. N. Khromov, and J. Los, J. Chem. Phys. 72, 5282 (1980).

[6]A. W. Kleyn, E. A. Gislason, and J. Los, unpublished.

[7]K. T. Gillen, A. P. Hickman, and T. M. Miller, unpublished.

# APPENDIX E

PHYSICS OF ELECTRONIC AND ATOMIC COLLISIONS
S. Datz (editor)
© North-Holland Publishing Company, 1982

## SUBPICOSECOND EXPERIMENTS ON MOLECULAR VIBRATION

Aart W. Kleyn[†]
FOM Instituut voor Atoom-en Molecuulfysica, Amsterdam Wgm, The Netherlands
and
Keith T. Gillen[*]
Molecular Physics Laboratory, SRI International
Menlo Park, California 94025

Vibrational motion on the subpicosecond time scale of a transient collision intermediate has been observed through its striking effects upon differential and total cross sections in inelastic and reactive processes in atom- and ion-molecule collisions. Transient charge transfer processes that form a short-lived diatomic ion and then return to the original potential energy surface are shown to be efficient paths to high vibrational excitation of molecular targets. Similar effects should be observable in a large number of collision systems.

## Introduction

A precise knowledge of the potential energy surface for a triatomic system could, in principle, be used to predict the detailed distribution of product states for inelastic or reactive processes, that probe the triatomic surface as a transient intermediate during a collision. In contrast, even when detailed state-to-state rates are available, it is far more difficult to extract quantitative information on the relevant potential surfaces from measurements of inelastic and reactive processes. The critical significance of the collision intermediate justifies strenuous experimental efforts to improve our view of its fleeting existence.

One approach to examining a collision intermediate is to prepare it directly in a well-defined state or energy level and observe its subsequent evolution. Examples using photoexcitation of neutrals and ions are given in the chapters by A. Giusti-Suzor[1] and P. C. Cosby.[2] These "half-collision" experiments can often analyze decay channels and surface couplings with great precision assuming sufficient spectroscopic information is available.

An alternate and quite difficult approach involves the examination of a transient collision intermediate by direct spectroscopic observation of the very short-lived colliding system (see, e.g., chapter by J. Polanyi[3]) or by optical pumping of the system while it is reacting (see, e.g., chapter by A. Gallagher[4]). These experiments, closely related to spectroscopic line broadening, are still in an exploratory stage and must eventually address the difficult problem of determining the dependence of emission line widths upon nuclear coordinates in the transient intermediate.

In contrast, our approach to examining the collision intermediate uses more traditional scattering techniques, but adjusts experimental conditions so that the transient intermediate itself provides an internal clock whose timing can be observed through its profound effects upon the resultant product distributions.

369

E-1

The internal clock is the vibrational motion of a transient ion, formed as part
of the short-lived intermediate. We will demonstrate for a few relatively simple
systems involving charge transfer intermediate states that very detailed informa-
tion about the collision dynamics can be obtained. In some cases vibrations of
the transient intermediate on the subpicosecond time scale can be seen experi-
mentally. The vibrational motion of this transient species yields the most
dramatic results in carefully chosen systems when the collision velocity is
adjusted to make the collision time comparable to the vibrational time.

### Atom-Atom Ion-Pair Formation

Most of the work described in this report will involve neutral atom-molecule col-
lisions that are strongly influenced by charge transfer to ion-pair states during
the collision process. It is therefore useful first to consider a related, but
simpler, atom-atom interaction, that of Na with I. Shown in Figure 1 are the
lowest $^1\Sigma^+$ diabatic covalent and ionic potential curves for NaI. At large dis-
tances R, the ion-pair state is asymptotically higher than the covalent state by
$\Delta E = IP(Na) - EA(I)$, where IP is the ionization potential of Na and EA is the
electron affinity of the I atom. The ion-pair state decreases in energy as R
decreases and crosses the covalent state at $R = R_c$. In the simplest approxima-
tion, considering only the coulombic term of $V_{ion}$, $R_c = 14.4/\Delta E$, with $\Delta E$ in eV
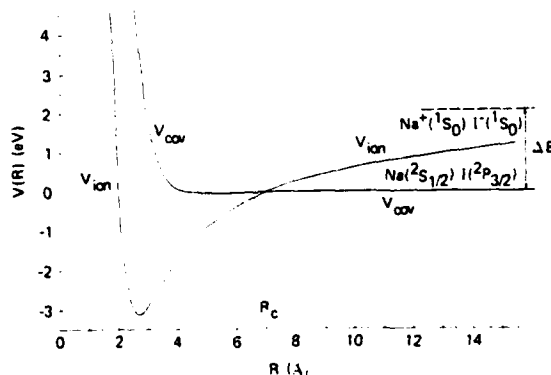and $R_c$ in Å.



Figure 1. Diabatic Na-I potentials.

Since the $^1\Sigma^+$ covalent curve is the same symmetry as the ion-pair curve, there
will be an avoided crossing in the corresponding adiabatic curves at $R = R_c$. For
thermal energy Na and I atoms approaching each other along the $^1\Sigma^+$ curve (1/8
of the collisions statistically), an electron will jump from Na to I in the
vicinity of $R_c$ as the adiabatic state abruptly changes from a covalent to an
ionic character. After the inner ionic region is visited, the outgoing trajec-
tory will once again cross $R_c$ and the electron will return to the Na$^+$.

As one raises the collision energy, one expects eventually that a fraction of the collisions will proceed diabatically through the crossing region at $R_c$ and that for collision energies $E_o > \Delta E$, the ion-pair product channel $Na^+ + I^-$ would be observed. Formation of ions indeed has been observed in both total and differential cross section experiments.[5,6]

The probability for ion-pair formation depends, of course, on the strength of the coupling between the two interacting surfaces. In the simplest Landau-Zener (L-Z) description (see, for example, refs. 7, 8), the probability P for diabatic behavior at a crossing through the sphere of radius $R_c$ is

$$P = \exp\left(-\frac{2\pi H_{12}^2}{v_R |S|}\right), \tag{1}$$

where $H_{12}$ is the coupling matrix element, $v_R$ is the radial velocity at $R = R_c$, and $S = \frac{d}{dR}(V_{cov} - V_{ion})$ evaluated at $R = R_c$. Faist and Levine[9] have obtained excellent fits to the Na + I scattering data by using improved adiabatic potentials and a slight modification of the crossing distance. Nonetheless the simple diabatic L-Z model is a reasonable first approximation to the scattering process.

## Atom-Molecule Systems: $O_2$ Target

Collisions of fast alkali atoms with $O_2$ molecules are influenced in an analogous way to Figure 1 by the crossing between the covalent incoming potential and strongly attractive ionic potentials. Necessarily the three atom system is vastly more complicated by the extra degrees of freedom, and the greater uncertainties in the knowledge of the potential surfaces and their interactions. The simple potential curves of Na + I are replaced by multidimensional potential surfaces in the triatomic system. Nonetheless, a carefully chosen set of physically reasonable simplifications allows us to generate an interesting classical picture of the collision dynamics.

The basic assumption is an uncoupling of the internal motion of the target molecule from the relative translational motion. To apply this assumption, we must exclude impact parameters that explore the inner repulsive core of the interaction potential. This neatly excludes the collisions resulting in the normal impulsive mechanisms for inelastic excitation transfer.

Consider a Cs atom approaching an $O_2$ molecule on a covalent surface. Assume that the O-O distance r is the classical equilibrium separation of $O_2$, $r_e$. At a $Cs-O_2$ distance, $R_c$, corresponding to a crossing with the ionic surface, an electron can jump to form $Cs^+ + O_2^-$. In the spirit of our simple picture, assume a vertical transition, an instantaneous electron jump that forms $O_2^-$ with an unchanged bond length, $r_e$. Clearly then, the crossing distance $R_c$ is given by $R_c = 14.4/[IP(Cs) - EA_v(O_2)]$ where $EA_v$ is the vertical electron affinity of $O_2$ at $r = r_e$. Since the equilibrium internuclear separation of $O_2^-$ is larger than that of $O_2$, the nascent $O_2^-$ begins its existence in a compressed state on its repulsive inner wall (see the $O_2$, $O_2^-$ potentials in Figure 2). As the $Cs^+$ and $O_2^-$ ions explore the attractive region inside $R_c$, the $O_2^-$ starts to expand, thus initiating an $O_2^-$ vibration. It is clear from Figure 2 that as the $O_2^-$ goes through one complete classical vibration, the vertical electron affinity (which depends on the instantaneous value of r) first increases, then decreases with a period identical to that of the $O_2^-$ vibration. Since $R_c$ depends on the instantaneous value of $EA_v(r)$ through

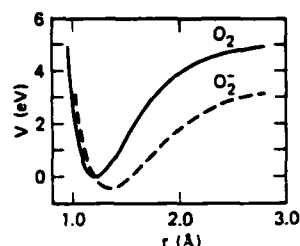$$R_c = 14.4/\{IP(Cs) - EA_v[r_{O_2^-}(t)]\}, \tag{2}$$

Figure 2.  Schematic $O_2$ and $O_2^-$ ground state
potential curves.

this crossing radius must vibrate in and out with the same period as the $O_2^-$.
Hence the position of the second crossing with the covalent surface depends
critically on the relative timing of the translational motion and the $O_2^-$ vibra-
tion.  Since the coupling $H_{12}$ decreases exponentially with $R_c$,[8,10] the branch-
ing probability P at this second crossing is also a very sensitive function of
the relative timing.  Depending on collision velocity and impact parameter, the
transient ion-pair intermediate may have a second crossing with the covalent
surface either in an expanded geometry that favors diabatic behavior or in a
compressed geometry that favors adiabatic behavior in the coupling region.

Figure 3 shows schematically $Cs + O_2$ collisions at $E_o = 35.5$ eV and various
impact parameters.  Each trajectory (drawn as a straight line for simplicity of
presentation) is assumed to convert to $Cs^+ + O_2^-$ ion-pairs at the initial
crossing at $R = R_c$.  At that instant ($t = 0$) the crossing radius $R_c$ starts
vibrating with the $O_2^-$ period in accord with Equation (2).  The calculated radius
$R_c'$ at the second crossing point (a function of b) is indicated in Figure 3.  The
lower trajectories labelled 1, 2, 3 have impact parameters that correspond to
reaching the second crossing after 1, 2, or 3 full vibrations of the $O_2^-$ (and of
$R_c'$).  These trajectories would tend to favor adiabatic passage through the second
crossing region yielding reneutralized products.  In contrast the upper trajec-
tories have impact parameters that would reach the second crossing after ~ 1.5
or 2.5 $O_2^-$ vibrations and would yield larger diabatic probabilities for ion-pair
products.  Clearly the branching ratio would have an impact parameter dependence
that might show up as oscillations in the differential cross sections for this
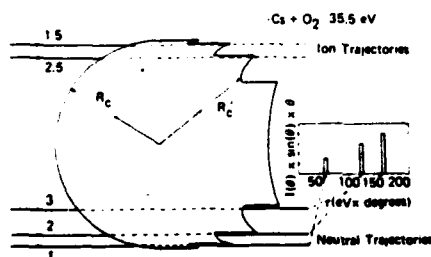system.



Figure 3.  Vibrational timing
effects on $R_c'$ for $Cs + O_2$
collisions.  The straight line
trajectories (at bottom) favor-
ing reneutralization would
suffer quite different attrac-
tive deflections during the time
spent on the ionic intermediate
surface.  The insert at the
right indicates angular posi-
tions and relative intensities
for three reneutralization peaks
predicted from classical trajec-
tory calculations.

Figure 4 shows the angular distribution of neutral scattering in various colli-
sion systems.[11] The 35.5 eV Cs + $O_2$ data indeed has distinct structure that is
consistent with the suggested vibrational timing arguments in Figure 3. This can
be compared to the nearly flat distribution, associated with purely repulsive
potentials, evident for Cs + Ar scattering also in Fig. 4. At higher collision
velocities, the structure for Cs + $O_2$ changes dramatically since the reneutral-
izing trajectories shift to smaller impact parameters and the number of observ-
able vibrational oscillations decreases as the collision time decreases. The
value of $R_c'$ not only influences the branching probability for reneutralization,
but also strongly affects the extent of deflection since $R_c'$ is the distance at
which the coulombic force is "switched off"; its variation implies a related
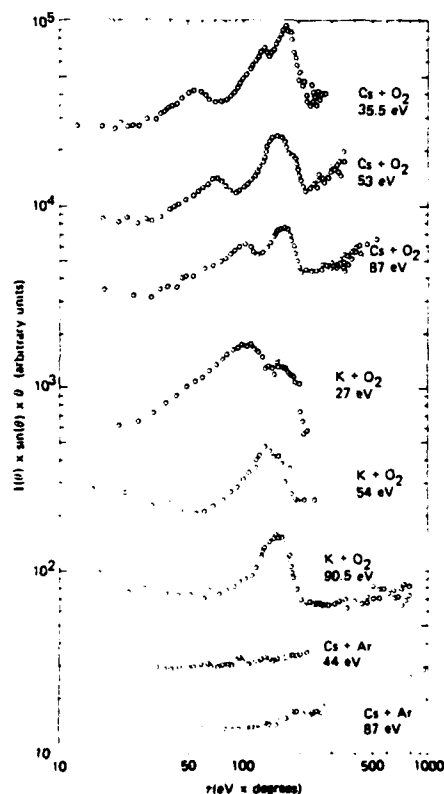variation in the total time that the attractive force operates.



Figure 4. Neutral product angular
distributions plotted vs. reduced
angle $\tau = E\theta$ for several collision
systems at various beam energies.

The energy dependence of the total
cross section for ion-pair formation
in the Cs + $O_2$ system[12] is shown
in Fig. 5. Although integrating the
oscillating ion-pair formation
probability over all impact
parameters at each energy might be
expected to wash out any strong
oscillations in the velocity
dependence of the total cross
section, one still observes these
oscillations. In fact, the inter-
pretation of oscillatory total cross
section data for ion-pair formation
in Cs + $O_2$ and K + $O_2$ collisions[13]
yielded the first dramatic
indication that multiple transient
molecular vibrations could be used
as an internal clock for the
collision intermediate.

Returning to the differential cross
section measurements in Figure 4, we
note that the lighter K atom
explores a higher velocity regime
than Cs in the same energy range.
In fact, the reneutralization
structure simplifies considerably
for K + $O_2$ at 90 eV. In this case
the time spent in the inner ionic
region is somewhat shorter than the
time for one $O_2^-$ vibration for all
impact parameters larger than the
extent of the repulsive inner
core. The single peak is a rainbow
feature in the reneutralization
angular distribution. Figure 6
shows a similar reneutralization
rainbow in the scattering of
metastable Ar atoms by $O_2$ at
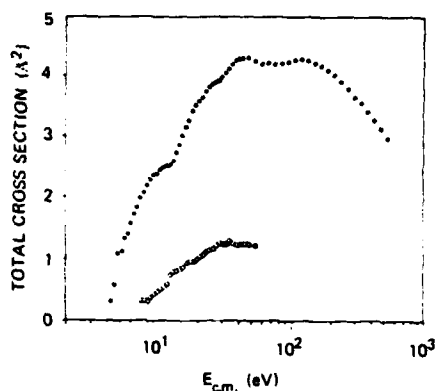
E-5

Figure 5. Total ionization cross section for Cs + $O_2$ collisions. Closed circles show negative ion products; open circles—electrons.
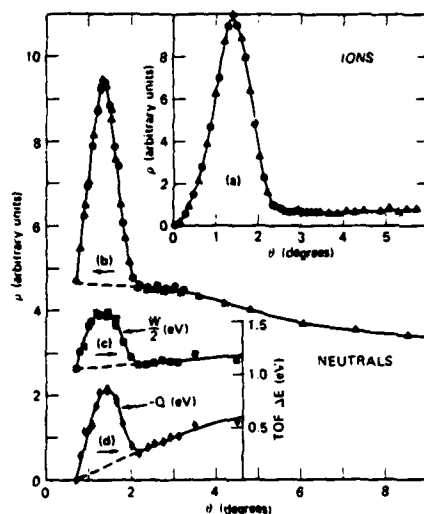


Figure 6. $Ar^* + O_2$ scattering at $E_o$ + 114 eV. (a) Product $Ar^+$ angular distribution $\rho = \theta_* \sin \theta \, d\sigma/d\omega$ vs. $\theta$. (b) $Ar^*$ neutral angular distribution. (c) Half-width of the product $Ar^*$ energy profile vs. $\theta$. (d) Average $Ar^*$ c.m. energy loss vs. laboratory $\theta$.

E = 114 eV,[14] $Ar^* + O_2 \rightarrow Ar^+ + O_2^- + Ar^* + O_2$. The corresponding ion-pair rainbow for $Ar^* + O_2 \rightarrow Ar^+ + O_2^-$ is also shown. The neutral rainbow is located at slightly smaller angles because the coulombic attraction is cut off at $R_c'$ when reneutralization occurs. The similarities of the $Ar^*$ and K reactions with $O_2$ are not surprising and are consistent with many other comparison studies between metastable rare gas and alkali reactions.[15-17]

Another important consequence of the vibrational timing upon the reneutralization products is the very large vibrational excitation of $O_2$ that can result. A stretched $O_2^-$ would reneutralize vertically to a vibrationally excited $O_2$ as can be seen in Figure 2.

E-6

Indeed, large vibrational $O_2$ excitation for scattering at angles in the rainbow region is observed by time-of-flight (TOF) measurements of scattered $Ar^{*}$[14] (and in the analogous $K + O_2$ system[18,19]). When the TOF inelasticity Q and its measured half-width $\frac{1}{2}$ are plotted vs. $\theta$ (Fig. 6), an isolated highly-inelastic feature appears precisely in the rainbow region built upon a second feature whose inelasticity slowly rises with $\theta$. The second feature is associated with the more common impulsive inelastic scattering on the repulsive inner wall of the covalent potential. This covalent contribution can be seen in the nearly flat background that underlies the sharp rainbow peak in the neutral angular distribution.

## Atom-Molecule Systems: Halogen Targets

In a series of experiments at the FOM institute, reported at the Paris ICPEAC[20] and reviewed elsewhere,[8,21] the effects on ion-pair formation of bond stretching in alkali atom halogen molecule collisions were studied. The results have since been confirmed in work by other groups.[22,23] Reactions of alkalis and $Ar^{*}$ with halogens have analogous mechanisms to those described for $O_2$ targets. However, there are great differences in the details of the potential surfaces and the resulting product distributions. First, since the vibration times of the heavy halogen negative ions are a factor of 5-10 larger than that of $O_2^{-}$, the halogen negative ion will only undergo a fraction of a vibration before the second crossing is reached. Second, the larger vertical electron affinity of the halogens and their much more rapid increase with r imply a larger $R_c$ and a very rapidly increasing $R_c(t)$. Hence in many cases, an adiabatic first passage through $R_c$ will yield such a rapid increase with t of $R_c$ that the second crossing will be almost entirely diabatic. Hence the ion-pair rainbow (as in Fig. 6) will have no accompanying neutral rainbow from reneutralization of the second crossing.

Yet strong rainbows in the neutral scattering have been observed and have been attributed to another consequence of bond stretching, vibrationally-induced third crossings. Consider the covalent route to the ionic surface with electron transfer occurring at the second crossing of the sphere of radius $R_c$. As the ions continue to larger distances, the $Br_2^{-}$ bond will start to stretch and $R_c$ will start to follow the departing ions. Since the ultimate increase in $R_c$ for halogens is very large, the expanding crossing radius will soon overtake the outgoing $K^{+}$ ion. This results in a third crossing created by the intramolecular motion of the $Br_2^{-}$. The situation is shown schematically in Fig. 7 for $K + Br_2$ at 20 eV.
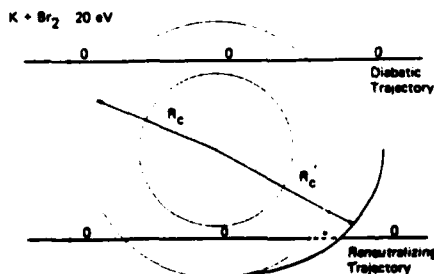
K + Br$_2$  20 eV

Figure 7. Simplified picture of a collision of a fast K atom and a fixed Br$_2$ molecule. The repulsive part of the potential is indicated by the sphere. Two types of trajectories leading to neutral products are shown. Whenever the system is neutral an 0 is inserted in the trajectory; the ionized state is indicated with a +.

If reneutralization occurs, $r > r_e(Br_2)$ and consequently vibrational excitation
will take place. This vibrational excitation indeed has been observed by Kleyn
et al.[24]  Since the coulomb force is only active for a very short time at the
end of the collision the scattering angles are small. Thus the first effect of a
third crossing occurring for covalent reneutralization is that anomalous vibra-
tional excitation can be observed at very small scattering angles. The second
effect of covalent reneutralization is that it leads to a vibrationally induced
rainbow. The origin of this rainbow can be seen by referring to Fig. 7. At
$t = 0$, $R_c'$ starts increasing, eventually overtaking the departing ion. For large
b (near $\bar{R}_c$), the ion trajectory has a very small component in the R direction, is
overtaken quickly by the expanding sphere, and suffers little attractive deflec-
tion. As b decreases, the time spent on the coulombic surface (before the third
reneutralizing crossing) increases. However, the resulting increase in the
attractive interaction with decreasing b is eventually compensated by the fact
that the attractive force has an ever smaller component perpendicular to the
trajectory. Hence a maximum attraction can occur in the deflection function for
impact parameters larger than the repulsive core. This yields a rainbow that is
shaped more by the bond-stretching dynamics than by the R dependence of the ion-
pair potential. This rainbow feature occurs at very small scattering angles. An
example (Fig. 8) is shown for collisions of $Ar^*$ with $I_2$ at 60 eV.[25] The cross
section at angles beyond the rainbow region is flat, and due to underlying
contributions from repulsive scattering. Similar behavior has been found for
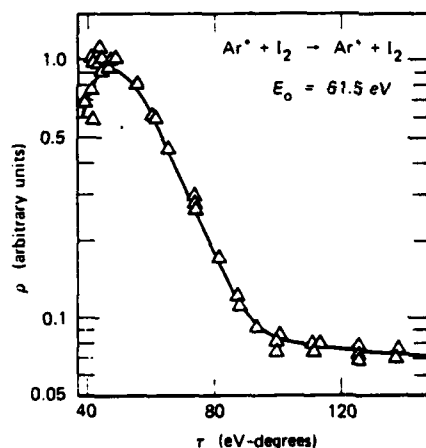$K + Br_2$ collisions.[24]



Figure 8.  Neutral product
angular distribution
$\rho = \theta \sin \theta \frac{d\sigma}{d\omega}$ plotted vs.
reduced angle $\tau = E.\theta$ for
$Ar^* + I_2$ at 61.5 eV.

### Theoretical Models and Extension to Other Systems

The simple pictorial models described here can be made more quantitative by using
classical trajectory surface hopping calculations on diabatic potentials, while
still assuming an uncoupling between the r and R motions on the two potential
surfaces. The calculational techniques and their application to ion-pair forma-
tion in collisions of alkali atoms and $Ar^*$ with halogen molecules have been
described in detail (see, e.g., 8, 17, 24, 25). These calculational techniques

have been extended to the systems considered here, both in their simplest form
and with extensions to simulate adiabatic effects important for impact parameters
near $R_c$. All of the important observed features—structure in the neutral
angular distributions with $O_2$ targets, large $O_2$ excitations mediated by the ion-
pair surface, oscillations in the total ion-pair formation cross section, cova-
lent reneutralization rainbows in the scattering by halogen molecules—appear in
the calculations.

The discussion of vibrational motion so far has been completely classical. This
approach gives satisfactory qualitative explanations for the processes described
above. If one is interested in the description of final vibrational state dis-
tributions obtained using state specific detection, better methods are required.
One method, the moving wavepacket approach introduced by Gislason et al.[27,28]
has been very successful in explaining final vibrational state distributions from
quenching experiments and is similar in spirit to the work discussed so far. In
the moving wavepacket method, the time evolution of the vibrational wavefunction
is represented by the evolution of a wavepacket on the respective potential sur-
faces. When the potential surfaces are assumed additive in R and r the method is
easy to use. The easiest and mathematically most elegant version of the method
employs diabatic potential surfaces and the wavepacket is projected from one
molecular potential to another at each adiabatic passing of a crossing. The
expression for the final vibrational state population can be given in closed
form.

The diabatic model has been used to explain energy-dependent oscillations in the
final vibrational state distribution of $N_2(C^3\Pi_u)$ excited in the quenching of $Ar^*$
by ground state $N_2$.[27,29] *The results are shown in Fig. 9.* The experimental
ratio (v = 1/v = 0) oscillates as a function of energy. The model calculations
show that the oscillations are due to several vibrations of the intermediate $N_2$
molecule, which obtained some $N_2^-$ character from a higher $Ar^+ + N_2^-$ surface. The
molecular vibrations during the collisions are reflected in the oscillatory
motion of the wavepacket in its potential. The adiabatic version of the moving
wavepacket model has been used to explain quenching of excited Na by $N_2$ and CO
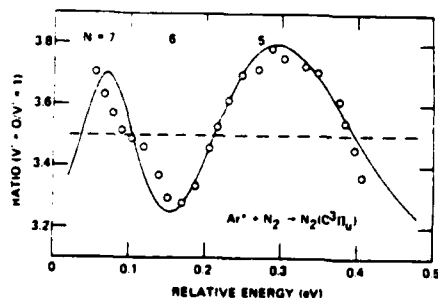and very good agreement between theory and experiments has been obtained.[28]



Figure 9. Population ratio
(v'=0/v'=1) for the $N_2 (C^3\Pi_u)$
product resulting from
quenching of $Ar^*$ by $N_2$ as a
function of energy. The
circles are the experimental
points; the solid line is the
theoretical result. The number
N refers to the number of half
vibrations of the transient $N_2$
molecules.

The moving wavepacket model is an intermediate between the simple classical
approach mainly used to explain this kind of atom-molecule collisions and more
complete quantal studies. Kloep and Los[12] solved the close coupled equations

for some limiting cases and demonstrated the potential importance of non-vertical transitions at low energies. Hickman,[30] using a classical path method and the Magnus approximation, observed oscillations in his calculated cross section for ion-pair formation in Cs + $O_2$ collisions. Recently, Becker and Saxon[31] performed close coupling calculations for inelastic K + $O_2$ collisions involving the ion-pair intermediate. These calculations confirm the simple ideas developed using the classical models. In addition, this kind of calculations gives much more insight into the detailed collision dynamics and serves as a standard with which the classical and semiclassical techniques can be compared and judged.

The effects of vibrational timing in the subpicosecond range have been mainly studied systematically in collisions of alkali or metastable rare gas atoms with simple molecules like halogens, $O_2$ and $N_2$. There is no reason to believe that these effects will not occur in many other collision systems. One obvious extension is to the study of ion-pair mediated effects in alkali collisions with larger molecules. Recently, the importance of "bond-bending" effects in the $NO_2^-$ ion[32] have been discussed in analogy to bond stretching in the halogens. Other recent experiments have indicated the possible involvement of similar vibrationally inelastic effects due to temporary charge transfer from $H^+$ or $H^-$ to $O_2$.[33,34] Collisionally-produced emissions in metastable rare gas-halogen reactions at near thermal energies seem to be similarly unaffected by bond stretching.[35] In addition, these effects should be observable in many excitation transfer or Penning ionization reactions.

## Summary

We have emphasized here the importance in atom-molecule collisions of vibrational excitation that is induced by involvement of another electronic state of the transient intermediate species. In contrast to the direct excitation of a vibrator by repulsive interactions on a single potential surface, this intermediate-induced excitation can yield high internal energies in large impact parameter collisions. Vibrational timing of the intermediate species on a subpicosecond time scale can be observed as structure in measurements of both differential and total cross sections.

There are several general requirements for direct observation of these effects. First, the collision must involve another electronic state of the diatomic molecule having a somewhat different geometry from that of the initial state. In an adiabatic description, the intermediate must access a region of the potential surface, where the molecular bond-strength is drastically modified from that of the isolated molecule. Systems with important low-lying ion-pair states satisfy this requirement. The second requirement for observation of vibrational timing is that the transfer from one diabatic state to the other occurs in a region of the potential surface where the repulsive forces are not important and do not significantly deform the molecular potentials. This is the case for many reactive systems that exhibit "harpooning" behavior, e.g., alkali and metastable rare gas collisions with halogens and $O_2$. This second requirement is a matter of convenience, since the general effects described here should be important even in systems where repulsive forces are significant in the region of electronic state interaction. A third requirement for clear observation of these vibrational effects is the need for the collision time to be not vastly different from the vibrational period of the intermediate diatomic. In general this is the case for collision energies from a fraction of an eV to several hundred eV, depending on the system.

We conclude that vibrational timing in the subpicosecond range is an important and neglected effect, the study of which can reveal the internal motion of transient states and thus provide detailed information on the dynamics of molecular collisions and the potential surfaces involved.

## References

1. A. Giusti-Suzor, XII ICPEAC, Gatlinburg Tenn. Invited Lect., Ed. S. Datz, North-Holland Publ., Amsterdam, 1981.
2. P. C. Cosby, XII ICPEAC, Gatlinburg Tenn., Invited Lect., Ed. S. Datz, North-Holland Publ., Amsterdam, 1981.
3. J. Polanyi, XII ICPEAC, Gatlinburg Tenn., Invited Lect., Ed. S. Datz, North-Holland Publ., Amsterdam, 1981.
4. A. Gallagher, XII ICPEAC, Gatlinburg Tenn., Invited Lect., Ed. S. Datz, North-Holland Publ., Amsterdam, 1981.
5. A.M.C. Moutinho, J. A. Aten, and J. Los, Physica (Utrecht) 53 (1973) 471.
6. G. A. L. Delvigne and J. Los, Physica (Utrecht) 67 (1973) 166.
7. A.P.M. Baede, Adv. Chem. Phys. 30 (1975) 463.
8. J. Los and A. W. Kleyn, in: Alkali Halide Vapors, eds. P. Davidovits and D. L. McFadden (Academic Press, New York, 1979) p. 275.
9. M. B. Faist, B. R. Johnson, and R. D. Levine, Chem. Phys. Lett. 32 (1975) 1; M. B. Faist and R. D. Levine, J. Chem. Phys. 64, (1976) 2953.
10. R. E. Olson, F. T. Smith, and E. Bauer, Appl. Opt. 10 (1971) 1848.
11. A. W. Kleyn, V. N. Khromov, and J. Los, J. Chem. Phys. 52 (1980) 5282; A. W. Kleyn, V. N. Khromov, and J. Los, Chem. Phys. 52 (1980) 65.
12. U. C. Klomp and J. Los, to be published in Chem. Phys.
13. A. W. Kleyn, M. M. Hubers, and J. Los, Chem. Phys. 34 (1978) 55.
14. K. T. Gillen and T. M. Miller, Phys. Rev. Letters 45 (1980) 624.
15. K. T. Gillen, T. D. Gaily, and D. C. Lorents, Chem. Phys. Letters 57 (1978) 192.
16. D. W. Setser, T. D. Dreiling, H. C. Brashears, and J. H. Kolts, Faraday Discussions Chem. Soc. 67 (1978) 1613.
17. A. P. Hickman and K. T. Gillen, J. Chem. Phys. 73 (1980) 3672.
18. A. W. Kleyn, E. A. Gislason, and J. Los, Chem. Phys. 52 (1980) 81.
19. C. E. Young, C. M. Sholeen, A. F. Wagner, A. E. Proctor, L. G. Pobo, and S. Wexler, J. Chem. Phys. 74 (1981) 1770.
20. J. Los, X ICPEAC, Paris, Invited Lect., North Holland Publ., Amsterdam (1977), p. 617.
21. A. W. Kleyn, E. A. Gislason, and J. Los, to be published in Phys. Reports.
22. S. Wexler and E. K. Parks, Ann. Rev. Phys. Chem. 30 (1979) 179.
23. K. Lacmann, Adv. Chem. Phys. 42, (1980) 513.
24. A. W. Kleyn, E. A. Gislason, and J. Los, accepted for publ. in Chem. Phys.
25. K. T. Gillen, unpublished results.
26. J. A. Aten, G.E.H. Lanting, and J. Los, Chem. Phys. 19 (1977) 241.
27. E. A. Gislason, A. W. Kleyn, and J. Los., Chem. Phys. Lett. 67 (1979) 252.
28. E. A. Gislason, A. W. Kleyn, and J. Los, Chem. Phys. 59 (1981) 91.
29. E. R. Cutshall and E. E. Muschlitz, J. Chem. Phys. 70 (1979) 3171.
30. A. P. Hickman, J. Chem. Phys. 73 (1980) 4413.
31. C. H. Becker and R. P. Saxon, accepted for publication in J. Chem. Phys.
32. K. Kimura and K. Lacmann, Chem. Phys. Letters 70 (1980) 41.
33. F. A. Gianturco, Uwe Gierz and J. Peter Toennies, J. Phys. B 14 (1981) 667.

34.  U. Hege and F. Linder, XII ICPEAC, Gatlinburg Tenn., 1981, Abstr. Contr. Papers, Ed. S. Datz, p. 945.
35.  M. S. de Vries and R. M. Martin, XII ICPEAC, Gatlinburg Tenn., 1981, Abstr. Contr. Papers, Ed. S. Datz, p. 949.

# APPENDIX F

## Ion-Beam Neutralization-Reionization Spectroscopy of Ion-Pair Formation in Reactions of He*(2³S) and He*(2¹S) with $O_2$

Thomas M. Miller[a] and Keith T. Gillen

*Molecular Physics Laboratory, SRI International, Menlo Park, California 94025*

(Received 5 February 1980)

For He⁺ beams neutralized in alkali vapors and reionized in $O_2$ gas, information on the intermediate neutral states has been used for the first time to isolate the differential cross sections for ion-pair formation in a pair of reactions occurring simultaneously. The reactions of He*(2³S) and He*(2¹S) with $O_2$ are strongly coupled by a shared Coulombic product channel, and evidence exists for unique three-surface trajectories leading to ion-pair products He⁺ + $O_2^-$.

At ion energies $E_i$ above ~10 eV, metastable rare-gas beams[1] can be produced[2] efficiently by charge-transfer neutralization of the parent ion beam in an alkali vapor. The neutralized beam (after radiative decay of short-lived states) is usually an unknown mixture of the two metastable states (2¹S and 2³S for He*) and the ground state ($^1S_0$). One would generally expect that both measurement and modification of the neutral-beam *composition* would be needed for isolating the contributions of the various neutral-beam components to subsequent scattering experiments. However, we have used only a knowledge of the *states* produced in the neutralization reaction

$$He^+ + Rb \rightarrow He^* + Rb^+ \qquad (1)$$

under conditions in which the beam *composition* is not determined, to resolve and investigate separately the ion-pair reactions

$$He^*(2^3S) + O_2 \rightarrow He^+ + O_2^- \qquad (2)$$

and

$$He^*(2^1S) + O_2 \rightarrow He^+ + O_2^-. \qquad (3)$$
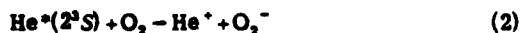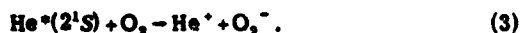
These results are the first in which detailed ion-pair–formation data have been obtained for two separate entrance channels leading to a common exit channel. We will show that Reactions (2) and (3) have remarkably different angular distributions that can nevertheless be understood from qualitative estimates of the deflection functions for the important trajectories leading to ion-pair products. Reaction (3) appears to be the first to show evidence for the coupling of three different potential surfaces in a single trajectory leading to ion-pair products.

Our apparatus and basic techniques have been described in detail.[3,4] Briefly, a He* beam is produced by a near-resonant charge-transfer neutralization of a fast He⁺ beam in Rb or Na vapor. Unreacted ions are swept aside before

the beam enters a collision cell filled with $O_2$. He⁺ product ions from this second collision are detected by a Channeltron mounted behind an 127° electrostatic energy analyzer. This detector system can be rotated around the scattering center to measure the product He⁺ angular distributions. The energy analyzer can be floated at various potentials to analyze product ions with high or low resolution. A separate Channeltron detector was used to measure the He* beam energy ($E_0$) with time-of-flight (TOF) techniques.

For a He⁺ beam neutralized to He*(2¹S) in Reaction (1) and then reionized in Reaction (3), the translational-energy separation $E_L$ between the original He⁺ beam ($E_i$) and the final He⁺ product ($E'$) is given by[5]

$$E_L = E_i - E' = K + I(Rb) - I(He^*(2^1S))$$
$$+ I(He^*(2^1S)) - A_a(O_2) + E_{int}(O_2^-), \qquad (4)$$

where $K$ is the Rb contact potential, $I[X]$ is the ionization potential of $X$, $A_a$ is the adiabatic electron affinity, and $E_{int}(O_2^-)$ is the product $O_2^-$ internal energy. The first three terms on the right-hand side give the energy shift due to neutralization, and the last three terms are for the reionization reaction. The third and fourth terms cancel, implying that, in the absence of radiative cascade, any other intermediate neutral states yielding the same $O_2^-$ internal states in the reionization step would produce He⁺ product ions of identical energy-loss values $E_L$. In contrast, neutralization to a state that radiates before the reionization collision causes the third and fourth terms in Eq. (4) to differ by the energy of the photon(s) radiated.

A recent communication[6] on TOF measurements of excited-He-state populations produced in near-resonant charge transfer of He⁺ with various alkali vapors demonstrates that 100–200-eV charge transfer in Rb (or Cs) yields significant
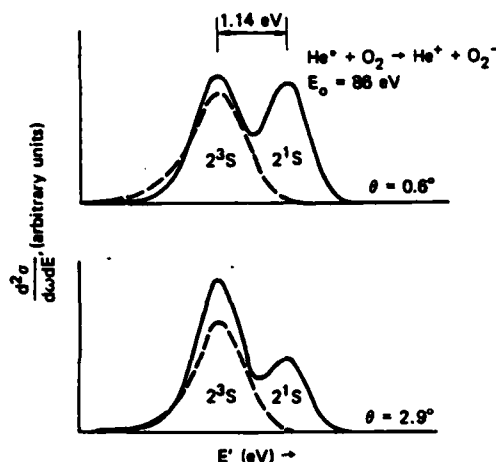
FIG. 1. Representative He$^+$ product energy distributions for He* beams formed by charge transfer in Rb (solid line) and in Na (dashed line).



FIG. 2. Product He$^+$ laboratory angular distributions from reactions of He*($2^1S$) and He*($2^3S$) with $O_2$.

amounts of only two He states: $2^1S$ and $2^3P$. The $2^3S$ metastable component of the beam comes exclusively from rapid radiative decay of the $2^3P$ state. Our TOF measurements over the beam energy range 30–200 eV confirm that no $2^3S$ is produced directly in Reaction (1) in this energy range. Hence, the He$^+$ product ions from Reactions (2) and (3) could be separated by 1.14 eV (the energy of the $2^3P - 2^3S$ photon) in accord with Eq. (4).

Figure 1 presents product He$^+$ laboratory energy distributions at two scattering angles for He*+$O_2$ collisions at He* beam energies of ~85.5 eV. The doubled-peaked He$^+$ distributions result from He* beams produced by charge transfer in Rb; the peak separations are consistent with the predicted shift of the products of Reaction (2) to lower energy due to the $2^3P - 2^3S$ photon. The dashed curves, of slightly lower analyzer resolution, present analogous results for a beam formed in Na where the TOF measurements prove that He*($2^3S$) is the only major beam component. The energy widths of the measured He$^+$ profile for both Reactions (2) and (3) are convolutions of the beam width (typically <0.5 eV full width at half maximum), the detector bandpass (adjustable, but typically 0.5 eV at highest resolution used), and the widths of the product state distributions at the measured angle. Clearly these product state distributions are narrow enough that the two reactions can be easily resolved.
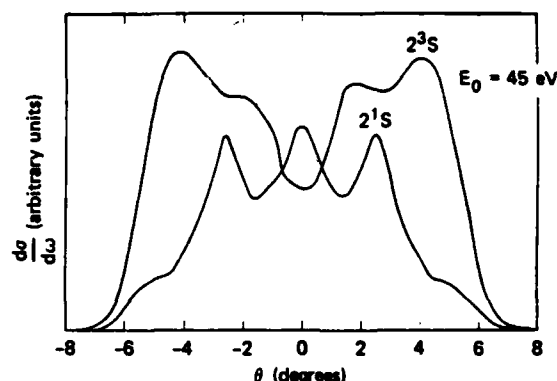
Similar energy scans at other angles demonstrate that these peaks neither broaden nor shift in energy over the angular range in which there is significant scattered intensity. This result suggests a particularly simple approach for measuring the angular distributions of the products of Reactions (2) and (3) quickly and separately. After He* production with Rb charge transfer, separate angular distributions are determined with the energy analyzer at high resolution and set to transmit ions with energies near the peak of the signal for Reaction (2) and for Reaction (3). Reaction (2) can be studied independently for a He*($2^3S$) beam produced in Na, and energy-integrated angular distributions are found to be in excellent agreement with those obtained with the simpler method. The product He$^+$ angular distributions shown in Fig. 2 are typical results that demonstrate dramatic differences between the two reactions.

Analysis of several recent measurements of detailed differential cross sections for ion-pair formation has yielded much insight into the reaction dynamics.[7] The projectile is usually, but not always,[4] a ground-state alkali atom. All these systems[4,7] are strongly influenced by crossings at large internuclear distances (typically 3–7 Å) between an essentially flat incoming covalent surface and a strongly attractive Coulombic surface asymptotically a few electronvolts higher. Transitions can occur as this crossing region is traversed. At collision energies above a few electronvolts, the products can separate as ion pairs with a very large reaction cross section.

In collisions involving metastable rare-gas atoms,[4] the interacting surfaces are often also
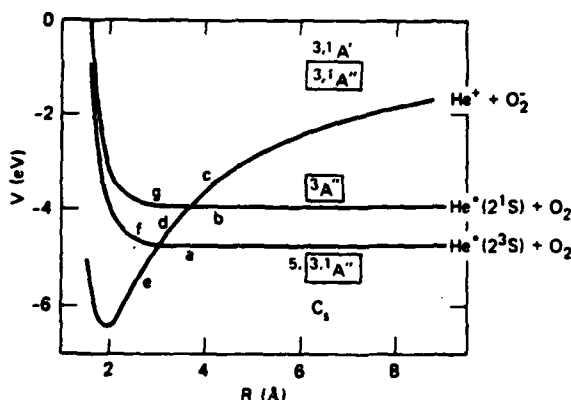
FIG. 3. Schematic He*-$O_2$ potentials, showing all the possible surface symmetries in the lowest symmetry ($C_s$) orientation. All three asymptotic states are coupled by $^3A''$ surfaces.

imbedded with a continuum, and competition from Penning ionization and excitation transfer reactions may influence the ion-pair distributions. An additional and unique feature of Reactions (2) and (3) is their expected direct coupling to each other, as indicated in Fig. 3, which shows the interaction of He* and $O_2$ at a fixed O-O distance (nominally the $O_2$ equilibrium bond length). The symmetries of the various surfaces in $C_s$ geometry are indicated for both incoming reaction pairs and for the ionic product channel. Note that both reactants can couple to the ion-pair channel; note especially that the $^3A''$ surfaces provide a mechanism for coupling of all three asymptotic states.

The angular position of the three distinct peaks (at ≈0°, 2.6°, and ≥5°) evident in Fig. 2 for the $2^1S$ reaction and the two peaks (near 2° and 4.2°) for reaction of He*($2^3S$) can now be understood qualitatively from an examination of the possible trajectories in Fig. 3 that yield ion-pair products. For the He*($2^3S$)+$O_2$ reactants, the two paths "aedc" (called the "ionic" path)[7] and "afdc" (the "covalent" path) are possible. Two prominent peaks would be expected in the angular distribution. The peak at larger angles (from more attractive interactions) would be a rainbow from the portion of the deflection function associated with trajectories following the ionic path. A second maximum at smaller angles is due to the attractive interactions on the outgoing portion of the covalent trajectories. This expectation is based on analogous results for many other ion-pair reactions.[4,7]

The He*($2^1S$)+$O_2$ system, however, is the first one studied in which the reactant channel is not the lowest coupled state asymptotically. In addition to the "ionic" path (bdedc) and the "covalent" path (bgc) to the ion-pair products, there is a three-surface trajectory (bdfdc). The rainbow peak from the ionic trajectory would be expected to be at a larger angle than the corresponding rainbow for the $2^3S$ reaction, since more attraction occurs during the trajectory (an extra traversal of region d). Likewise, the covalent peak from Reaction (3) would be expected at smaller angles than that from Reaction (2). The three-surface trajectory could then be responsible for the prominence of the intermediate peak at ~2.6°. Qualitative estimates of the deflection functions expected for the five different reaction paths are then in good agreement with the measured relative angular positions.

Better estimates of the product distributions require deflection function calculations that attempt to match the data quantitatively by accounting for surface coupling parameters and branching ratios and effects from competition with other channels (including continuum coupling). Classical trajectory calculations confirm and extend the general conclusions presented here; in particular, the three-surface peak at 2.6° is enhanced by trajectories (bdc) that do not nominally reach the second crossing and is modified further by strong deviations from diabatic behavior at the inner crossing. These calculations and the detailed experimental results will be presented elsewhere.[8]

(a)Current address: Physics Department, University of Oklahoma, Norman, Okla. 73019.

[1]K. T. Gillen, in Proceedings of the Tenth International Conference on the Physics of Electronic and Atomic Collisions, Paris, 1977, edited by G. Watel (North-Holland, Amsterdam, 1978), p. 473.

[2]J. R. Peterson and D. C. Lorents, Phys. Rev. 182, 152 (1969).

[3]R. Morgenstern, D. C. Lorents, J. R. Peterson, and R. E. Olson, Phys. Rev. A 8, 2372 (1973).

[4]K. T. Gillen, T. D. Gaily, and D. C. Lorents, Chem. Phys. Lett. 57, 192 (1978).

[5]M. Durup, G. Parlant, J. Appell, J. Durup, and J.-B. Ozenne, Chem. Phys. 25, 245 (1977).

778

[5]C. Reynaud, J. Pommier, V. N. Tuan, and M. Barat, Phys. Rev. Lett. 43, 579 (1979).

[7]Reviewed by J. Los and A. W. Kleyn, in *Alkali Halide Vapors, Structure, Spectra and Reaction Dynamics*, edited by P. Davidovits and D. L. McFadden (Academic, New York, 1979), p. 275.

[8]K. T. Gillen, T. M. Miller, and A. P. Hickman, unpublished.